# A NEW CLASS OF DIRHODIUM COMPOUNDS WITH AN ELECTRON ACCEPTOR LIGAND: ENHANCING CHEMOTHERAPEUTIC PROPERTIES WITH LIGHT

A Dissertation

by

ALFREDO MILTON ANGELES BOZA

Submitted to the Office of Graduate Studies of
Texas A&M University
in partial fulfillment of the requirements for the degree of

DOCTOR OF PHILOSOPHY

May 2007

Major Subject: Chemistry

# A NEW CLASS OF DIRHODIUM COMPOUNDS WITH AN ELECTRON ACCEPTOR LIGAND: ENHANCING CHEMOTHERAPEUTIC PROPERTIES WITH LIGHT

A Dissertation

by

ALFREDO MILTON ANGELES BOZA

Submitted to the Office of Graduate Studies of
Texas A&M University
in partial fulfillment of the requirements for the degree of

DOCTOR OF PHILOSOPHY

Approved by:

Chair of Committee, Kim R. Dunbar
Committee members, Marcetta Y. Darensbourg
Francois P. Gabbai
David P. Giedroc
Head of Department, David H. Russell

May 2007

Major Subject: Chemistry

# ABSTRACT

A New Class of Dirhodium Compounds with an Electron Acceptor Ligand: Enhancing Chemotherapeutic Properties with Light. (May 2007)

Alfredo Milton Angeles Boza, B.S., Pontificia Universidad Católica del Perú

Chair of Advisory Committee: Dr. Kim R. Dunbar

The syntheses and characterization of new dirhodium complexes based on the electron acceptor ligand dipyrido[3,2-a:2´,3´-c]phenazine (dppz) and its derivatives are reported. These complexes have been shown to photocleave pUC18 plasmid *in vitro* under irradiation with visible light which results in the nicked, circular form of DNA. Unlike typical DNA photocleavage agents, the new compounds are capable of photocleaving DNA in the absence of oxygen as well as in the presence of oxygen. The toxicity of the complexes which contain the electron acceptor dppz ligand toward human skin cells increases when the cell cultures are irradiated with visible light. In contrast, the photocytotoxicity of those complexes that do not contain the dppz do not differ from cytotoxicity in the dark.

The chemistry of the newly synthesized dirhodium-dppz complexes with glutathione, which is considered to be an important molecule in the deactivation of metal-based drugs, has also been investigated. The results show that glutathione reversibly reduces $[Rh_2(\mu\text{-}O_2CCH_3)_2(dppz)_2]^{2+}$ (**6**) and $[Rh_2(\mu\text{-}O_2CCH_3)_2(dppz)(bpy)]^{2+}$ (**7**), and that they are easily reoxidized to the original form in air. EPR measurements

and DFT calculations indicate that the additional electron is delocalized in the ligand orbitals.

The molecular characteristics that affect the *in vitro* activity of dirhodium complexes is discussed. The lability of the groups coordinated to the dirhodium complexes is a significant factor that influences the toxicity of the complexes. In addition, the presence of labile solvent molecules and monodentate acetate groups provide potential "open sites" accessible for nucleophilic substitution, as opposed to these sites being occupied by non-labile groups that reduce the reactivity of the complexes.

Finally, the results also demonstrate that the carbonato-bridged complexes of the type $[Rh_2(\mu\text{-}O_2CO)_2(diimine)_2(H_2O)_2]^{2+}$ are useful precursors to access new dirhodium-diimine compounds that are not accessible from the acetate precursors. These compounds react with trifluoroacetamide, 2-pyrrolidinone, and trifluoroacetic acid to form products in which the carbonato ligands are substituted in favor of the new bridging group. This work provides a foundation for the preparation of new series of dirhodium complexes that contain the dppz ligand and bridging ligands other than acetate.

To my parents Alfredo and Niria, my siblings Renzo and Rocío; and my new family Dafhne, Francisco, Aurora.

"Nonostante la visione drammatica delle cose,
ho un fondo di ottimismo che sicuramente mi viene
da quelle prime grandi esperienze d'amore materno"
Dacia Maraini

## ACKNOWLEDGMENTS

The work presented in this dissertation could not have been accomplished without the invaluable support and friendship of several individuals. I am grateful to my advisor, Prof. Kim R. Dunbar, who painstakingly guided me along this five-year journey. Her love for research and different aspects of chemistry acts as never-ending source of energy for all the people that have the luck of working under her tutelage. I would like to thank Prof. Claudia Turro, who has been a splendid collaborator as well as a good friend. I am also grateful to Prof. Pat Woster for his advice on the pharmaceutical arena and for his constant encouragement. My thanks also go to my committee members: Profs. M. Y. Darensbourg, F. P. Gabbai, and D. P. Giedroc.

My family has always supported me in every endeavor I have undertaken in my life, and my graduate studies were no exception. My parents have made several sacrifices for my education, and for this, I will always be thankful. I thank my brother and sister, for every good moment I spent with them. I certainly missed them during these years. My gratitude also goes to my grandparents, whose love filled my childhood with indescribable happiness.

I cannot forget the members of the Dunbar group, whose companionship made my hours in the laboratory special. My thanks go to Drs. Karn Sorasaenee, Jitendra Bera, Hanhua Zhao, and Michael Shatruk, who spent part of their valuable time giving me valuable advice. I would also like to thank Carolina Avendano, Matthew Hilfiger, Ferdi Karadas, Nazario Lopez, and Dr. Eric Schelter for their friendship. I thank the past and

present members of the biogroup, Drs. Helen Chifotides, Sofi bin Salamon, Abdellatif Chouai, and Mijeong Kang, as well as the students, Dafhne Aguirre, Ed Funck, and Benjamin Duffus. My thanks are also extended to the rest of the group members, Brandi Schottel, Eric Reinheimer, Kristen Chambers, Ian Giles, Andrew Prosvirin, Charlene Campbell, Karen Farnsworth, and Mashalle Mooring.

My thanks to Dr. Patty Fu, Dr. Patricia Bradley, and Danny Lutterman, from the Turro group; and to Hemali Amunugama, from the Woster group, for testing the compounds synthesized in this work as well as for their always helpful suggestions. I would also like to thank Dr. Dino Villagrán and Dr. Lisa Pérez for their time and help with the DFT calculations.

Finally, I would like to thank my wife, Dafhne Aguirre, for her love, patience, and, more importantly, for being here with me.

# TABLE OF CONTENTS


CHAPTER Page

I INTRODUCTION……..1

General Principles of Cancer Chemotherapy…….1
Antitumor-Active Metallic Drugs…….…….4
Dirhodium Complexes……...11

II SYNTHESIS, DNA BINDING AND PHOTOCLEAVAGE OF DIRHODIUM(II,II) DPPZ COMPLEXES……30

Introduction……30
Experimental Section…….33
Results and Discussion…….. 42
Concluding Remarks……..77

III EFFECT OF GLUTATHIONE ON THE ACTIVITY OF DIRHODIUM(II,II) DPPZ COMPLEXES……78

Introduction……78
Experimental Section…….82
Results and Discussion…….. 86
Concluding Remarks……..103

IV DIRHODIUM(II,II) DPPZ COMPLEXES: UNDERSTANDING THEIR *IN VITRO* ACTIVITY……...104

Introduction……104
Experimental Section…….106
Results and Discussion…….. 115
Concluding Remarks……..134

V GENERATION OF NEW DIRHODIUM(II,II) DPPZ COMPLEXES…….135

Introduction……135
Experimental Section…….138
Results and Discussion…….. 142
Concluding Remarks……..159

CHAPTER Page

VI CONCLUSIONS……160

REFERENCES……..……..167

VITA……..……178

# LIST OF FIGURES


FIGURE Page

I.1 Schematic representations of Pt compounds that are anticancer active…….6

I.2 Schematic representations of Ru and Ti anticancer active compounds…….8

I.3 Intrastrand crosslinks formed by cisplatin: (a) 1,2-intrastrand, and (b) 1,3-intrastrand…….. 8

I.4 Schematic depictions of metal-based compound binding sites……..10

I.5 Dirhodium complexes with antitumor activity…….. 12

I.6 Schematic representation of the adduct formed between $Rh_2(\mu\text{-}O_2CCH_3)_4$ and 1-methyladenosine…….. 17

I.7 Schematic representation of the adduct formed between $Rh_2(\mu\text{-}O_2CCH_3)_2(\mu\text{-}HNOCCF_3)_2$ and 9-ethylguanine (R = Et)……..17

I.8 Molecular structure of (a) H-T *cis*-[ $Rh_2(\mu\text{-}O_2CCH_3)_2(9\text{-EtGua})_2(CH_3OH)_2$] and (b) H-H *cis*-[ $Rh_2(\mu\text{-}O_2CCH_3)_2(9\text{-EtGua})_2((CH_3)_2CO)(H_2O)]^{2+}$…….. 18

I.9 Molecular structure of H-T *cis*-$[Rh_2(DTolF)_2(9\text{-EtAdeH})_2(CH_3CN)]^{2+}$……19

I.10 Structures of $Rh_2(\mu\text{-}O_2CCH_3)_2(GpG)$ and $Rh_2(\mu\text{-}O_2CCH_3)_2(pGpG)$……. 22

I.11 Structure of $Rh_2(DTolF)_2(GpG)$…… 22

I.12 Denaturating PAGE (5%) of reactions between cisplatin (cis-DDP), $Rh_2(\mu\text{-}O_2CCH_3)_4$ (Rh1), $[Rh_2(\mu\text{-}O_2CCH_3)_2(CH_3CN)_6]^{2+}$ (Rh2), and $Rh_2(\mu\text{-}O_2CCF_3)_4$ (Rh3)…….. 25

I.13 Agarose gel of transcribed mRNA in the presence of *cis*-$[Rh_2(\mu\text{-}O_2CCH_3)_2(phen)_2]^{2+}$ at various complex/[template DNA base] ratios, *R*. Lanes 1-6, *R* = 0.0000, 0.0005, 0.0010, 0.0015, 0.0020, 0.0025…27

II.1 $^1$H-NMR spectrum of the aromatic region of *cis*-$[Rh_2(\mu\text{-}O_2CCH_3)_2(dppz)(\eta^1\text{-}O_2CCH_3)(CH_3OH)](O_2CCH_3)$ (**5**)……..…… 44

FIGURE Page

II.2 Thermal ellipsoid plot at the 50% probability level of the cation in **6a**…… 46

II.3 Thermal ellipsoid plot at the 50% probability level of the cation in **6b**…… 47

II.4 Thermal ellipsoid plot at the 50% probability level of the cation in **7**…….. 54

II.5 Electronic absorption spectra of 5 μM (a) **5** and (b) **6** in 5 mM Tris (pH = 7.5) in water (——) and in the presence of 100 mM calf-thymus DNA (- - - ) and 100 mM PSS (— — ). Insets: fits of the absorption to eq 1 for (a) 6.2 μM **5** and (b) 3.2 μM **6**……. 59

II.6 Proposed binding model for $[Rh_2(\mu\text{-}O_2CCH_3)_2(dap)(\eta^1\text{-}O_2CCH_3)(CH_3OH)]^+$……. 62

II.7 (a) Thermal denaturation of 100 μM calf-thymus DNA (1 mM phosphate, 2 mM NaCl, pH = 7.2) alone (o), and with 20 μM **5** (•) and **6** (Δ). (b) Relative viscosity changes of solutions containing 200 μM sonicated herring sperm DNA as the concentration of EtBr (o), **5** (•), Hoechst 33258 (□), and **6** (■) is increased (see text)…….. 65

II.8 Ethidium bromide stained agarose gels (2%) of 100 μM pUC18 plasmid in the presence of 20 μM metal complex in 5 mM Tris, 50 mM NaCl (pH = 7.5) irradiated with $\lambda_{irr} > 395$ nm. (a) Lane 1: plasmid only, dark; Lane 2: plasmid + *Sma*I; Lane 3: plasmid + **5**, dark; Lane 4: plasmid + **5**, irr. 15 min; Lane 5: plasmid + **6**, dark; Lane 6: plasmid + **6**, irr. 15 min. (b) Lane 1: plasmid only, dark; Lane 2: plasmid only, irr. 20 min; Lane 3: plasmid + **6**, dark; Lane 4: plasmid + **6**, irr. 20 min, air; Lane 5: plasmid + **6**, irr. 20 min, 50% $D_2O$; Lane 6: plasmid + **6**, irr. 20 min, under $N_2$; Lane 7: plasmid + **6**, irr. 20 min, freeze-pump-thaw…….. 68

II.9 Ethidium bromide stained agarose gel (2%) of 100 μM pUC18 plasmid, showing the photocleavage ($\lambda_{irr} > 395$ nm, 15 min) by 10 μM metal complex in 5 mM Tris, 50 mM NaCl, pH = 7.5. Lane 1: plasmid, dark; Lane 2: plasmid + SmaI; Lane 3: plasmid + **7**, dark; Lane 4: plasmid + **7**, irr., air; Lane 5: plasmid + **7**, irr, freeze-pump-thaw; Lane 6, plasmid + **5**, dark; Lane 7: plasmid + **5**, irr, air; Lane 8: plasmid + **6**, dark; Lane 9: plasmid + **6**, irr., air…….. 69

FIGURE Page

II.10 Plot of percent survival of human skin cells (Hs-27) as a function of concentration of (a) **5** and (b) **6** in the dark (•) and irradiated with 400–700 nm light for 30 min (o)……74

III.1 Schematic representation of adduct formed between $Rh_2(\mu\text{-}O_2CCH_3)_4$ and $C_6H_5CH_2SH$…… 80

III.2 Diagram of the proposed mechanistic pathway of the reactions between $[Rh_2(\mu\text{-}O_2CCH_3)_2(phen)_2]^{2+}$ and molecules containing sulfhydryl group…. 81

III.3 Changes observed in the UV-spectrum of compound **7** after the addition of glutathione…….87

III.4 EPR spectrum of compound **7** after the addition of glutathione……90

III.5 a) Dirhodium complex used in the study by Bear and co-workers b)EPR spectrum of complex shown in (a) after reduction…….91

III.6 Illustration of the 0.04 contour surface diagrams for the DFT calculated three lowest unoccupied MOs for the model complex $[Rh_2(\mu\text{-}O_2CH)_2(dppz)(bpy)(H_2O)_2]^{2+}$……..93

III.7 Illustration of the 0.04 contour surface diagrams for the DFT calculated four highest occupied MOs for the model complex $[Rh_2(\mu\text{-}O_2CH)_2(dppz)(bpy)(H_2O)_2]^{2+}$……..94

III.8 Ethidium bromide stained agarose gel (2%) of 100 μM pUC18 plasmid, showing the photocleavage ($\lambda_{irr}$ > 395 nm, 20 min) by 20 μM metal complex in 5 mM Tris, 50 mM NaCl, pH = 7.5. Lane 1: plasmid, dark; Lane 2: plasmid + **6** + 50 μM glutathione, irr.; Lane 3: plasmid + **6** + 50 μM glutathione, irr.; Lane 4: plasmid + **6** + 100 μM glutathione, irr.; Lane 5: plasmid + **6** + 200 μM glutathione, irr.; Lane 6, plasmid + **6** + 300 μM glutathione, irr.; Lane 7: plasmid + **6** + 400 μM glutathione, irr.; Lane 8: plasmid + **6** + 500 μM glutathione, irr……..98

FIGURE Page

III.9 Ethidium bromide stained agarose gel (2%) of 100 μM pUC18 plasmid, showing the photocleavage ($\lambda_{irr}$ > 395 nm, 20 min) by 20 μM metal complex in 5 mM Tris, 50 mM NaCl, pH = 7.5. Lane 1: plasmid, dark; Lane 2: plasmid + **7** + 50 μM glutathione, irr.; Lane 3: plasmid + **7** + 50 μM glutathione, irr.; Lane 4: plasmid + **7** + 100 μM glutathione, irr.; Lane 5: plasmid + **7** + 200 μM glutathione, irr.; Lane 6, plasmid + **7** + 300 μM glutathione, irr.; Lane 7: plasmid + **7** + 400 μM glutathione, irr.; Lane 8: plasmid + **7** + 500 μM glutathione, irr……99

III.10 Single cell electrophoresis of human skin cells exposed to 120 μM **7** for 30 min then (a) kept in the dark for 30 min and (b) irradiated with visible light for 30 min; the red color indicates stained DNA……... 101

IV.1 Thermal ellipsoid plot at the 50% probability level of the cation in **16**…… 120

IV.2 Schematic representations of compounds **1** - **4**, **6**, and **8**……...124

IV.3 Plot of the % product from the reaction of dirhodium tetraacetate with 9-EtGuaH, as a function of time (t) at 60 ºC ($k_{60}$ (ac) = 0.082 $h^{-1}$)……... 126

IV.4 Plot of the % product from the reaction of dirhodium trifluoroacetate with 9-EtGuaH, as a function of time (t) at 60 ºC ($k_{60}$ (trif) = 0.356 $h^{-1}$)….. 127

IV.5 Schematic representations of compounds **5**, **7**, and **10 – 12** (L = $CH_3OH$)... 131

IV.6 Schematic representations of compounds **13 – 17** (L = $CH_3CN$)…….. 132

V.1 Thermal ellipsoid plot at the 50% probability level of compound **19**…….... 148

V.2 Thermal ellipsoid plot at the 50% probability level of compound **22**…….... 152

V.3 Thermal ellipsoid plot at the 50% probability level of compound **8**……. 156

VI.1 Proposed mechanism for the photocatalytic generation of hydroxyl radical from dirhodium tetraacetate……... 162

VI.2 Proposed mechanism for the photocatalytic generation of hydroxyl radical from a dirhodium-dppz complex……..... 163

# LIST OF TABLES


| TABLE | | Page |
|---|---|---|
| I.1 | Cytotoxicity ($LD_{10}$) and hydrophobicity of dirhodium tetracarboxylate compounds…….. | 13 |
| II.1 | Crystal data and structural refinement parameters for compound **6a**…… | 49 |
| II.2 | Crystal data and structural refinement parameters for compound **6b**…… | 50 |
| II.3 | Selected bond distances (Å) for compound **6a**…….. | 51 |
| II.4 | Selected bond angles (°) for compound **6a**…….. | 51 |
| II.5 | Selected bond distances (Å) for compound **6b**…… | 52 |
| II.6 | Selected bond angles (°) for compound **6b**…….. | 52 |
| II.7 | Crystal data and structural refinement parameters for compound **7**……. | 56 |
| II.8 | Selected bond distances (Å) for compound **7**……... | 57 |
| II.9 | Selected bond angles (°) for compound **7**…… | 57 |
| II.10 | Cytotoxicity ($LC_{50}$) and photocytotoxicity ($LC_{50}^{*}$) values…… | 73 |
| III.1 | Inhibitory activity of $Rh_2(\mu\text{-}O_2CCH_3)_4$……. | 80 |
| III.2 | $t_{1/2}$ of product formed by the reaction of **6** and **7** with GSH……. | 86 |
| III.3 | Results of TD-DFT calculation on model complex $[Rh_2(\mu\text{-}O_2CCH_3)_2(dppz)(bpy)(H_2O)_2]^{2+}$……. | 96 |
| IV.1 | Crystal data and structural refinement parameters for compound **16**…… | 121 |
| IV.2 | Selected bond distances (Å) for compound **16**…….. | 122 |
| IV.3 | Selected bond angles (°) for compound **16**…… | 122 |
| IV.4 | Cytotoxicity ($LC_{50}$) values for complexes **1-4**, **6**, and **8**…… | 125 |

TABLE Page

IV.5 Cytotoxicity ($LC_{50}$) values for complexes **5**, **7**, **10**-**17**……...133

V.1 Crystal data and structural refinement parameters for compound **19**……150

V.2 Selected bond distances (Å) for compound **19**……151

V.3 Selected bond angles (°) for compound **19**……...151

V.4 Crystal data and structural refinement parameters for compound **22**……153

V.5 Selected bond distances (Å) for compound **22**……154

V.6 Selected bond angles (°) for compound **22**……...154

V.7 Crystal data and structural refinement parameters for compound **8**……...157

V.8 Selected bond distances (Å) for compound **8**……... 158

V.9 Selected bond angles (°) for compound **8**……158

# CHAPTER I

# INTRODUCTION

## *General Principles of Cancer Chemotherapy*

Cancer is the term that describes a group of genetic diseases that arise from an accumulation of mutations and causes uncontrolled proliferation of transformed cells.[1] There are approximately 200 documented types of cancer that correspond to different cellular systems in the body and differ from one other by their capacity to invade both neighboring or distant tissues and organs.[1,2] Cancer alterations originate in special genes called proto-oncogenes, which when transformed into oncogenes become responsible for the transformation of normal cells into malignant cells.[3] These transformed cells are then referred to as cancerous or tumoral in nature.[1-3]

The history of cancer chemotherapy harks back to the serendipitous discovery of the mustard family of agents in the first half of the twentieth century.[1,4-8] The important observation that sulphur mustard, used at that time as toxic agent in warfare, lowered the white-blood-cell count in people exposed to it, led scientists to test it in humans as a treatment for leukemia. Unfortunately, the compound proved to be far too toxic for therapeutical purposes. It was hypothesized that the high toxicity associated with the use of sulphur mustard was related to the electrophilicity of the compound, which makes it very reactive towards highly nucleophilic groups found in living cells. The development of less electrophilic compounds quickly followed those early experiments, and the first

---

This dissertation follows the style and format of the *Journal of the American Chemical Society*.

nitrogen mustards were introduced into clinic in 1946.[8,9]

A more reliable way of obtaining molecules with interesting anticancer properties originated after the progress achieved with the nitrogen mustards. Screening programs have been developed using a diverse numbers of cancer cell lines, and compounds are evaluated against all the cell lines.[10,11] The molecules tested in this way are either obtained from natural products, through synthetic methods, or a combination of both. An example of one of these programs is the National Cancer Institute's Developmental Therapeutics Program that has been in operation for nearly 50 years and tests approximately 60 human tumor cell lines.[10] Although the new approach did not entirely solve the problem of serendipity, it increased the chances of obtaining new anticancer-drug leads.[12,13]

A third, and more recent, method of new anticancer active drugs is the so called "rational" approach.[1] In this approach, thanks to the advances in molecular biology, the specific target is known;[1,2] more importantly, its three-dimensional structure is known,[1,2] and this allows for the rational design of molecules that can specifically interact with the target.[1,2,14,15] This method is currently combined with *in silico* screening resulting in a powerful method for obtaining possible lead molecules with high specificity.[1,2]

Anticancer drugs currently in use or in clinical trials target various important molecules involved in critical cellular processes.[1,2] For instance, they can inhibit the synthesis of purines,[16] or the conversion of ribonucleosides into deoxyribonucleotides.[17] They can also target DNA, as in the case of alkylating agents,[6] or they can alter microtubules polymerization, as for example taxol and its derivatives.[6]

Among the carcinostatic agents, those with alkylating properties should be highlighted. Alkylating drugs, such as the nitrogen mustards, were the first to be developed, and are the main contributors to the medical arsenal against cancer. They target nucleophilic sites on DNA, RNA, enzymes, and other proteins, causing damage that can be potentially detrimental to cells; however, evidence suggests that these nucleophilic reactions form products that are repairable with one likely exception, namely the adducts formed with DNA.[6] This DNA modification, along with the fact that rapidly proliferating tumors are more prone to suffer this deleterious effect, is one of the main reasons for the use of alkylating drugs, but there are numerous side-effects encountered in such cancer treatment.[5]

Compounds that are usually classified as being part of the family of alkylating drugs are those containing metal ions. Although these molecules do not alkylate their target *per se*, since no alkyl unit is transferred to either DNA or any other nucleophile, they are usually included in this family because they are capable of acting as an electrophile and bind to their targets in a fashion similar to an organic alkylator.

*Antitumor-Active Metallic Drugs*

The serendipitous discovery of the anticancer activity of *cis*-$[PtCl_2(NH_3)_2]$ (*cis*-diamminedichloroplatinum(II), commonly known as cisplatin (Figure I.1), in 1965 by Rosenberg and his colleagues at Michigan State University resulted in the re-birth of the field of medicinal bioinorganic chemistry.[18,19] In his famous experiment, Rosenberg and co-workers were studying the effect of an electric field on cell division. They observed that bacterial cell division was inhibited; however, the inhibition was not caused by the electric field generated, but by a compound that was being formed during the course of the experiment, namely *cis*-$[PtCl_2(NH_3)_2]$. Cisplatin was eventually approved by the FDA as an anticancer drug, and it has been used since then in combination with other drugs in the chemotherapeutic treatment of testicular, ovarian, cervical, head and neck, and non-small-cell lung cancer. During the past three decades two additional platinum-based compounds, diammine[1,1-cyclobutanedicarboxylato(2-)]-*O*,*O'*-platinum(II) (carboplatin) and (trans-L-diaminocyclohexane)oxalatoplatinum(II) (oxaliplatin), have been approved as anticancer drugs (Figure I.1).[20,21] In spite of the considerable success

of these drugs, there is still a pressing need for developing new anticancer agents with fewer deleterious side effects, as well as improved efficacy against cancer cell lines that are resistant towards cisplatin and its derivatives.[22]

Despite the fact that the three platinum drugs approved for treatment have a *cis* geometry, and that the first quantitative structure-activity relationship (QSAR) studies on platinum compounds suggested that this geometry was vital for the anticancer activity of the complexes, several *trans* derivatives have been shown to exhibit promising antitumor properties. These non-classical platinum complexes typically contain planar amine ligands, bulky aliphatic amines, and cyclic amines, and are particularly effective in cisplatin-resistant cell lines.[23,24] In addition, Farrell and coworkers have shown that multinuclear platinum compounds are also highly cytotoxic and exhibit outstanding anticancer properties. One member of this family of compounds, BBR3464 ([(*trans*-$PtCl(NH_3)_2$-$\mu$-(*trans*-$Pt(NH_3)_2$-$(NH_2(CH_2)_6NH_2)_2$)]$(NO_3)_4$), is currently in Phase II clinical trials (Figure I.1).[25,26]


*cis*-diamminedichloroplatinum(II) (cisplatin)

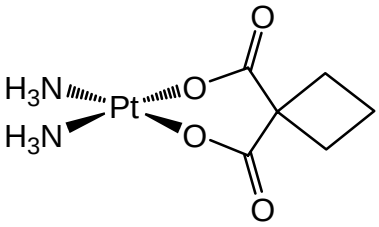


diammine[1,1-cyclobutanedicarboxylato(2-)]-*O*,*O*'-platinum(II) (carboplatin)

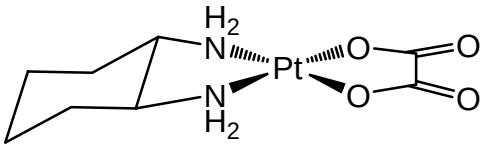


(*trans*-L-diaminocyclohexane)oxalatoplatinum(II) (oxaliplatin)

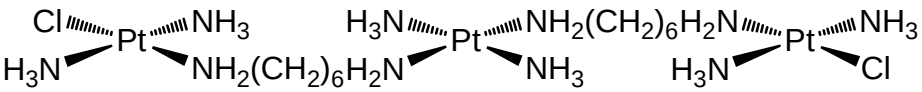


[(*trans*-$PtCl(NH_3)_2$-$\mu$-(*trans*-$Pt(NH_3)_2$-$(NH_2(CH_2)_6NH_2)_2$)]$(NO_3)_4$ (BBR3464)

**Figure I.1.** Schematic representations of Pt compounds that are anticancer active.

Platinum is not the only metal that can be used in the design of anticancer agents. Complexes containing metals such as ruthenium and titanium have been extensively investigated for antitumor properties.[25-29] Early work by Clarke and coworkers showed that Ru(III) complexes containing two chloride substitutents in a *cis* disposition are cytotoxic to cancer cells. Later, independent work by Alessio and Keppler resulted in two octahedral Ru(III) complexes *trans*-[Him]-[$RuCl_4$(DMSO)(Im)] (Im = imidazole; NAMI-A), and *trans*-[HInd]-[$RuCl_4$(DMSO)(Ind)] (Ind = indazole) entering clinical trials (Figure I.2).[27-29] The former complex is particularly interesting because it exhibits anti-metastatic activity, while being nontoxic to primary cancer cells. Titanium complexes have also shown promising activity as anticancer agents, and [$Cp_2TiCl_2$] is currently in Phase II clinical trials (Figure I.2). A second generation of titanium complexes containing aryl and heteroaryl substitutents has been tested successfully and some of them are candidates for further studies.

Understanding the mechanisms by which cells process metal-based drugs provides important insight for improving the design of these metallo-pharmaceuticals. In the case of platinum-based anticancer agents, the mechanism of action is believed to be formation of metal-DNA adducts that ultimately lead to cell death. In cisplatin, the platinum atom binds to the N7 positions of purine bases to form primarily 1,2- or 1,3-intrastrand crosslinks (Figures I.3 and I.4).[30,31] These modifications onto the DNA distort the structure of the DNA duplex and activate numerous cellular processes that mediate the cytotoxicity of these compounds.[31] Ruthenium complexes such as NAMI also bind to the N7 position of guanine bases and form 1,2-intrastrand crosslinks, but, recent

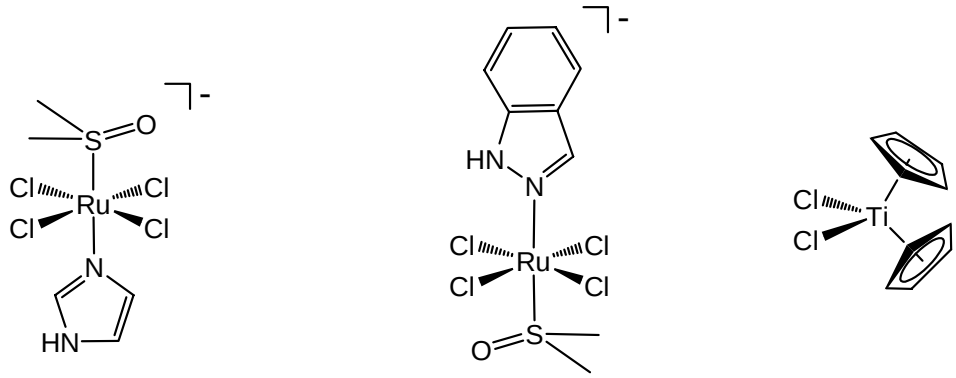


*trans*-[$RuCl_4$(DMSO)(Im)]$^-$ (NAMI-A) *trans*-[$RuCl_4$(DMSO)(Ind)]$^-$ $Cp_2TiCl_2$

**Figure I.2.** Schematic representations of Ru and Ti anticancer active compounds.

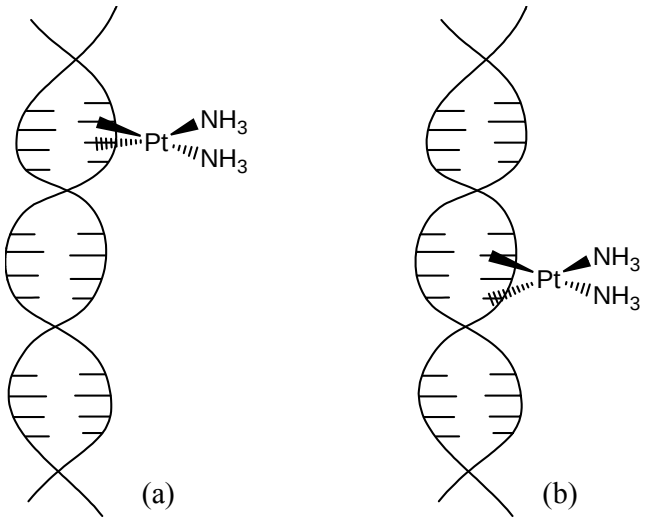


**Figure I.3.** Intrastrand crosslinks formed by cisplatin: (a) 1,2-intrastrand, and (b) 1,3-intrastrand.

studies support the view that, despite the ability of NAMI-A to bind DNA, its activity is based mainly on its ability to interfere with type IV collagenolytic activity reducing the metastatic potential of tumors.[27,28]

The antitumor activity of titanium complexes is mainly related to its ability to bind proteins. Unlike the platinum- and ruthenium-based antitumor agents, budotitane and titanocene dichloride do not bind to the N7 purine site in DNA, but prefer the ribose hydroxyl groups (Figure I.4).[32,33] Overall, they exhibit a strong preference for binding to proteins, in particular transferrin, and it is thought that budotitane and titanocene dichloride use this protein as a carrier to enter cells.[32-34] In addition, it has been suggested that the anti-cancer activity of these complexes is related to their ability to inhibit topoisomerase II activity.[32-34]

Metal-based drugs are among the most potent of anticancer compounds. They can effectively target DNA as well as proteins encountered in cells. Clearly, the use of metal centers other than those in the aforementioned text may also result in the discovery of potent chemotherapeutics with enhanced efficacy. One class of metal complexes that deserves particular attention is the family of compounds that contain a $Rh_2$(II,II) unit. A detailed discussion of previous anticancer activity studies and attempts to understand the mechanism of action of dirhodium complexes is presented in the following section.

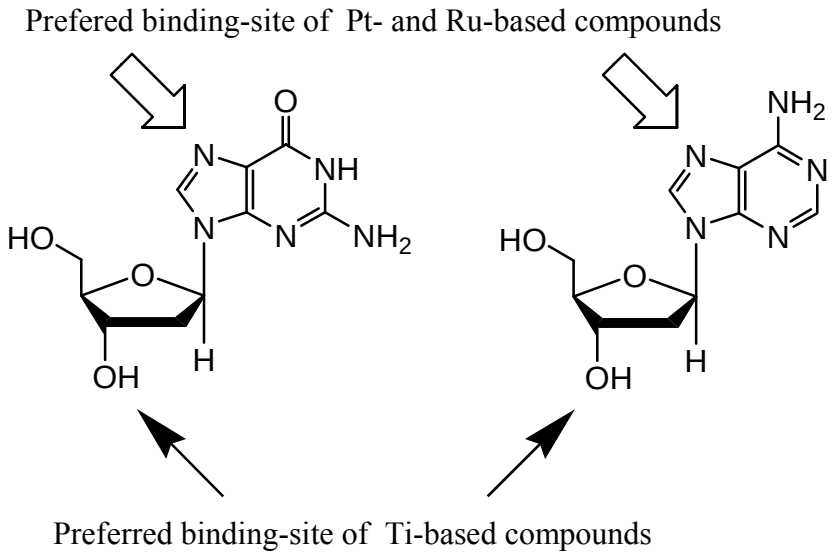


**Figure I.4.** Schematic depictions of metal-based compound binding sites.

*Dirhodium Complexes*

**Dirhodium complexes as anticancer agents**

Dinuclear metal-metal bonded compounds of rhodium have attracted attention since the 1970's for their cytostatic properties and are among the most promising non-platinum anticancer complexes.[35] It was first shown by Bear and his collaborators that dirhodium tetraacetate exhibits appreciable cytostatic activity against a variety of cell lines including sarcoma 180, Ehrlich ascites tumor, and P388 lymphocytic leukemia.[36,37] Since this time, the antitumor activities of other dirhodium complexes have also been reported. Following Bear's studies, Piraino and co-workers reported that $Rh_2(\mu\text{-}O_2CCH_3)_2(DTolF)_2L_2$ (DTolF = *N,N'*-ditolylformamidinate and L = solvent molecules) exhibits antitumor activity against sarcoma cells.[38] Some years later, Pruchnik *et al*. showed that cationic diimine complexes of dirhodium(II,II), namely $Rh_2(\mu\text{-}O_2CCH_3)_2(diimine)_2^{2+}$ (diimine = 2,2'-bipyridine (bpy), and 1,10-phenanthroline (phen)), also exhibit antitumor activity, in some cases higher than that of cisplatin.[39] More recently, Esposito and collaborators demonstrated that another member of the dirhodium family, namely $Rh_2(\mu\text{-}ONHCCF_3)_4$, is active against U937 and K562 human leukemia cells as well as Ehrlich ascites tumor cells both *in vitro* and *in vivo*.[40,41] Schematic representations of some the dirhodium compounds mentioned above are illustrated in Figure I.5.

Systematic studies of structure-activity relationships among dirhodium complexes have shed some light on their antineoplastic activity. A study performed on the dirhodium tetracarboxylate complexes, $Rh_2(\mu\text{-}O_2CR)_4$ (R = $CH_3$, $C_2H_5$, $C_3H_7$), which

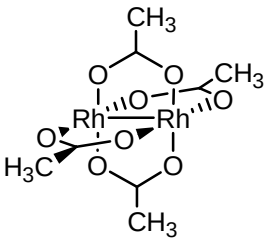

$Rh_2(\mu\text{-}O_2CCH_3)_4$

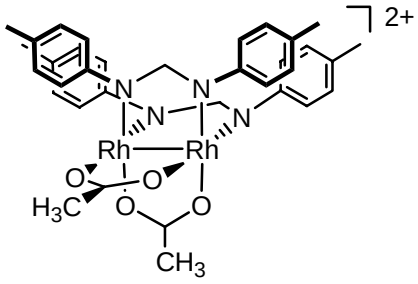

$Rh_2(\mu\text{-}O_2CCH_3)_2(DTolF)_2$

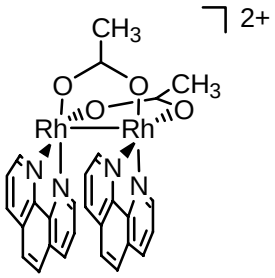

$[Rh_2(\mu\text{-}O_2CCH_3)_2(phen)_2]^{2+}$

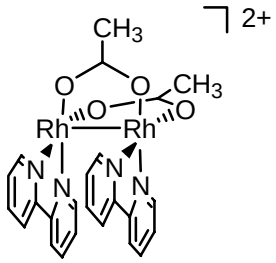

$[Rh_2(\mu\text{-}O_2CCH_3)_2(bpy)_2]^{2+}$

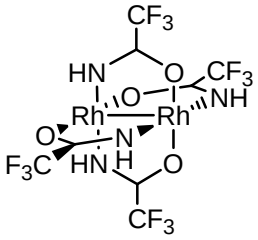

$Rh_2(\mu\text{-}HNOCCF_3)_4$

**Figure I.5.** Dirhodium complexes with antitumor activity.

exhibit cytostatic activity against Ehrlich ascites tumor, Leukemia L1210, and Sarcoma 180 cells, revealed that the activity in the series $Rh_2(\mu\text{-}O_2CR)_4$ (R = $CH_3$, $C_2H_5$, $C_3H_7$) increases with the hydrophobicity of the R group, but that a further lengthening of the carboxylate group beyond the pentanoate group reduces the therapeutic efficacy (Table I.1).[42] A plausible explanation for the increased activity of the compounds is that they become more lipid-soluble, therefore, a larger amount of compound can be more readily transported into the interior of the cell.[42] This reasoning is confirmed by the observation that the partition coefficient correlates with the amount of rhodium absorbed by cells.[42] In the case of the pentanoate and hexanoate derivatives, the activity could not be measured because of the extremely low solubility in water of the compounds.[42] In another study, involving the dirhodium(II,II) formamidinato class, an additional fact was revealed. The tetra-substituted compound $Rh_2(\mu\text{-DTolF})_4$ exhibits no appreciable cytotoxicity,[38]

**Table I.1.** Cytotoxicity ($LD_{10}$) and hydrophobicity of dirhodium tetracarboxylate compounds (modified from ref. 42).

| Complex | $LD_{10}$ (mol/kg) | Partition Coefficient (1-octanol) |
|---|---|---|
| $Rh_2(\mu\text{-}O_2CCH_3)_4$ | $2.6 \times 10^{-4}$ | $6.54 \times 10^{-2}$ |
| $Rh_2(\mu\text{-}O_2CCH_2CH_3)_4$ | $1.9 \times 10^{-5}$ | 8.17 |
| $Rh_2(\mu\text{-}O_2C(CH_2)_2CH_3)_4$ | $6.0 \times 10^{-6}$ | 898 |
| $Rh_2(\mu\text{-}O_2C(CH_2)_3CH_3)_4$ | Insoluble | > 3000 |
| $Rh_2(\mu\text{-}O_2C(CH_2)_4CH_3)_4$ | Insoluble | > 3000 |

however, the heteroleptic $Rh_2(\mu\text{-DTolF})_2(\mu\text{-}O_2CCF_3)_2$, with two labile trifluoroacetato bridging groups, shows comparable antitumor activity to cisplatin.[38] The authors suggested that this behavior was due to the higher reactivity of the latter compound with two labile trifluoroacetate ligands as compared to the former complex.

The antitumor activity of dirhodium complexes is thought to be analogous to that of cisplatin, i.e. binding of DNA nucleobases, although activity due to direct binding to enzymes is also a possibility.[42] Early, it was postulated that the activity of dirhodium tetraacetate was due to the binding of this complex to DNA through its axial positions, but, since it was known that this binding mode is weak, due to the strong trans-effect of the dirhodium unit, it was obvious that the activity of this complex could not originate solely from this DNA binding mode. The use of bidentate nitrogen chelating ligands helped to prove that dirhodium complexes can bind to two adjacent nucleobases in a manner akin to cisplatin, and that the binding mode of dirhodium complexes to DNA may involve not only the axial positions, but also the equatorial sites (Scheme I.1).[43-45] It is also important to point out that reactions of $Rh_2(\mu\text{-}O_2CCH_3)_4$ with bpy and phen reveal that two adjacent nucleobases are capable of displacing two of the bridging acetate ligands, a fact that is counterintuitive to the original assumption that the only reasonable binding mode was at the axial positions.[43-45]

**Scheme I.1.** Possible mechanism for the reaction of adjacent nucleobases and dirhodium tetraacetate (modified from ref. 43).

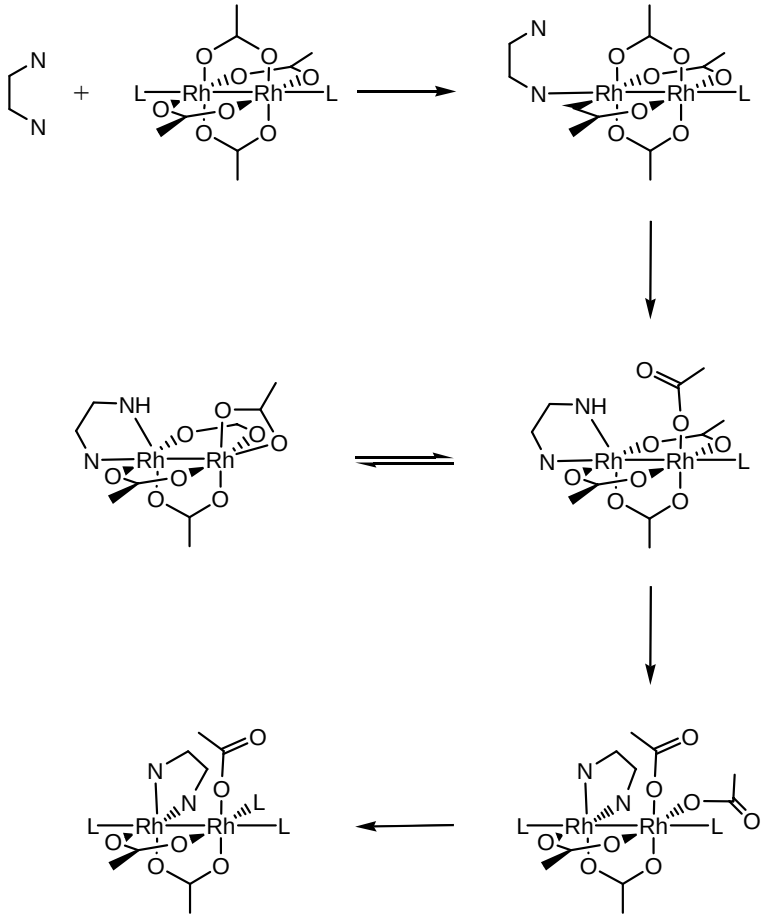

**Interaction of dirhodium complexes and nucleobases**

Several model systems of nucleic acid binding to the $Rh_2(\mu\text{-}O_2CCH_3)_4$ core have been structurally characterized;[46-50] these constitute excellent illustrations of the diverse nucleobase chemistry of dirhodium(II,II) complexes. Adenine and guanine binding to dirhodium(II,II) carboxylate complexes has been found to occur either through the axial position or in a bridging fashion through the equatorial sites.[46-50] Adenine is known to strongly bind to $Rh_2(\mu\text{-}O_2CCH_3)_4$ through the axial position due to the hydrogen-bonding interactions between the exocyclic amine group and an oxygen atom from the carboxylato bridge as observed in a crystallographic study of the bis(1-methyladenosine) adduct of $Rh_2(\mu\text{-}O_2CCH_3)_4$ (Figure I.6).[46] In the case of guanine, there is no direct evidence of binding to $Rh_2(\mu\text{-}O_2CCH_3)_4$ through the axial position. It has been proposed that the oxygen atom at position 6 of the purine is involved in a repulsive interaction with the carboxylate oxygen atoms. Guanine, however, axially binds to $Rh_2(\mu\text{-}O_2CCH_3)_2(\mu\text{-}HNOCCF_3)_2$, forming a hydrogen bond between the O6 and the NH group of the trifluoroacetamide bridge (Figure I.7).[46]

Early reports concerning the antitumor activity of dirhodium tetraacetate erroneously established that this compound did not react with guanine, since no color change was observed upon addition of either guanine or guanosine to a solution of the metal complex.[47] It was later discovered, however, that $Rh_2(\mu\text{-}O_2CCH_3)_4$ reacts with 9-ethylguanine, a model compound for guanine and guanosine, in $H_2O$ forming a dimetal complex that contains either *protonated* or *deprotonated* 9-ethylguanine that bridge the two rhodium atoms via N7/O6 in a cis disposition with head-to-head (H-H) or head-to-tail

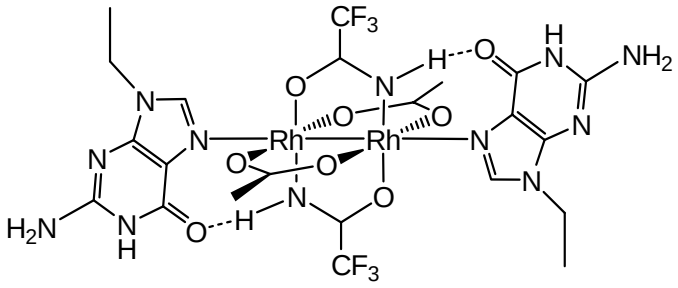

**Figure I.6.** Schematic representation of the adduct formed between $Rh_2(\mu\text{-}O_2CCH_3)_4$ and 1-methyladenosine.

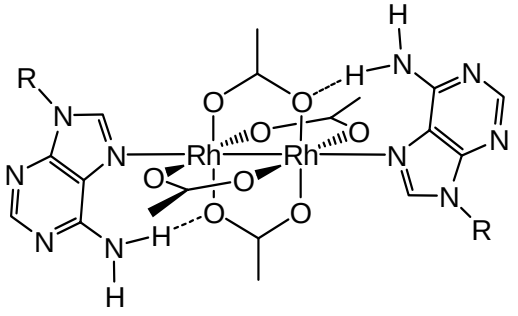

**Figure I.7.** Schematic representation of the adduct formed between $Rh_2(\mu\text{-}O_2CCH_3)_2(\mu\text{-}HNOCCF_3)_2$ and 9-ethylguanine (R = Et).

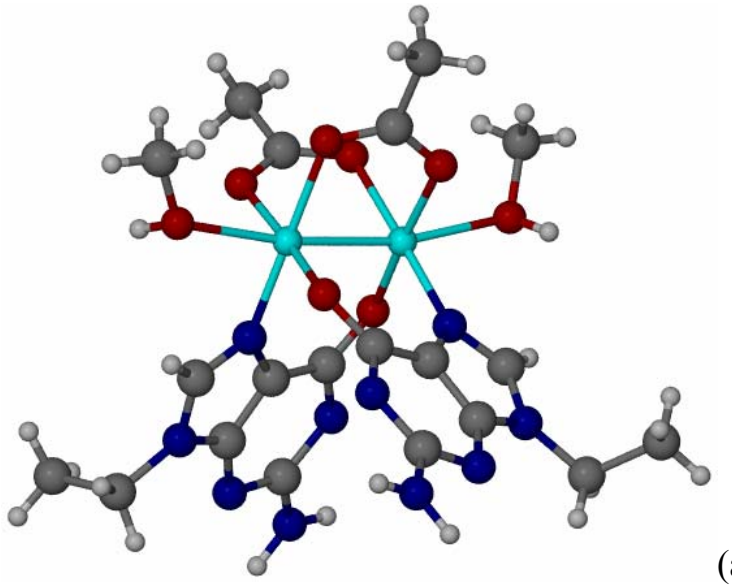

(a)

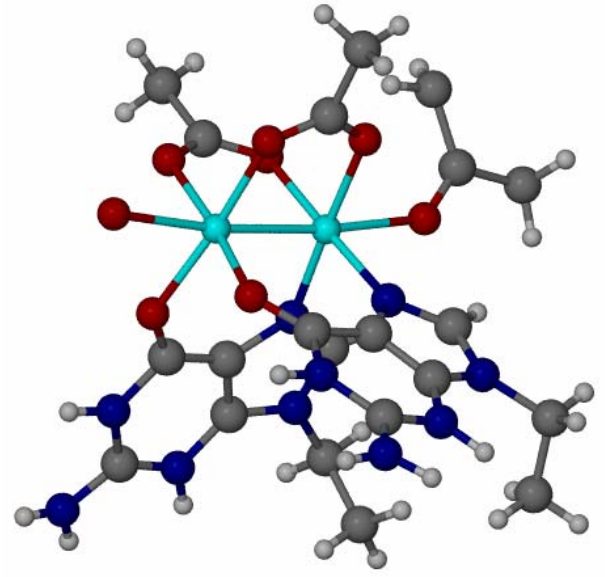

(b)

**Figure I.8.** Molecular structure of (a) H-T *cis*-[ $Rh_2(\mu\text{-}O_2CCH_3)_2(9\text{-EtGua})_2(CH_3OH)_2$] and (b) H-H *cis*-[ $Rh_2(\mu\text{-}O_2CCH_3)_2(9\text{-EtGua})_2((CH_3)_2CO)(H_2O)]^{2+}$.

(H- T) orientations (Figure I.8).[48] Likewise, $Rh_2(\mu\text{-}O_2CCF_3)_4$ reacts with two equivalents of 9-ethylguanine to form a dirhodium complex that contains two bridging *protonated* 9-ethylguanine molecules in only the H-T arrangement. In these reactions, the N1 position is either protonated or deprotonated, depending on the p$K_b$ of the leaving group. In the acetato-bridged compound, the purine is deprotonated at N1, whereas in the trifluoroacetate analogue, the N1 site is protonated, in accord with the lower basicity of $CF_3CO_2^-$ (p$K_b \approx 13.5$) compared to $CH_3CO_2^-$ (p$K_b \approx 9.2$).[48]

In a similar fashion, adenine can also bind equatorially to the dirhodium unit, however, reactions of $[Rh_2(DTolF)_2(CH_3CN)_6](BF_4)_2$ with 9-EtAdeH afford only the H-T isomer of *cis*-$[Rh_2(DTolF)_2(9\text{-}EtAdeH)_2(CH_3CN)](BF_4)_2$ with two 9-EtAdeH molecules bridging at *eq* sites via N7/N6 (Figure I.9).[49,50] Additionally, binding of adenine in a

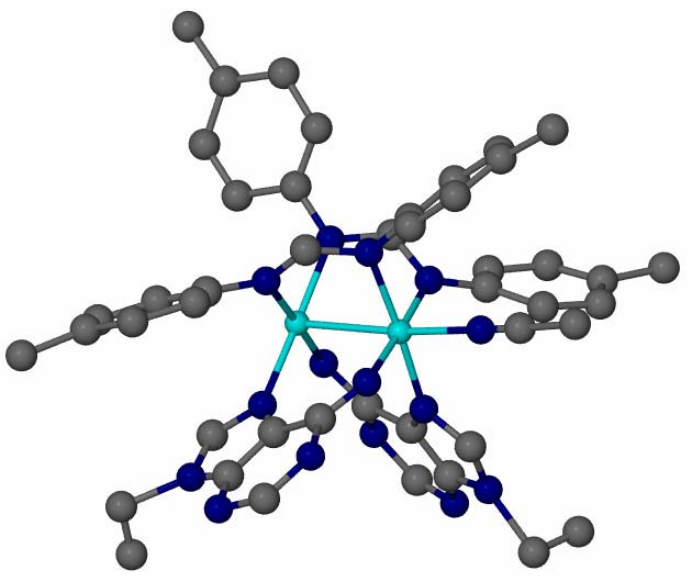

**Figure I.9.** Molecular structure of H-T *cis*-$[Rh_2(DTolF)_2(9\text{-}EtAdeH)_2(CH_3CN)]^{2+}$.

bridging fashion to a dinuclear center has also been observed in the complex *cis*-[$Mo_2$($\mu$-$O_2CCF_3$)$_2$(9-EtAdeH)$_2$]($BF_4$)$_2$, which was isolated as the H-T isomer. Variable temperature $^1$H NMR studies indicate that in the case of *cis*-[$Rh_2$(DTolF)$_2$(9-EtAdeH)$_2$($CH_3CN$)]($BF_4$)$_2$, 9-EtAdeH is present in its rare imino form. The stabilization of the imino form, as a result of the presence of the dirhodium complex, will alter the hydrogen bonding scheme of the nucleobase, a fact that might be related to the deleterious effect of this family of dimetal complexes on cells since it can ultimately result in nucleobase mispairing and cell mutations (Scheme I.2).

**Scheme I.2**

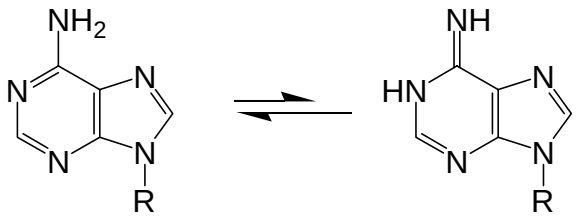


Amino form Imino form

**Dirhodium complexes and their interactions with dinucleotides**

$^1$H-NMR studies of the reactions of $Rh_2$($\mu$-$O_2CCH_3$)$_4$ and [$Rh_2$(DTolF)$_2$($CH_3CN$)$_6$]($BF_4$)$_2$ with the dinucleotides d(GpG) and d(pGpG) reveal that the bidentate N7/O6 binding observed previously for 9-ethylguanine is also possible when the two guanine bases are joined by a phosphodiester bond.[51-53] In the case of $Rh_2$($\mu$-$O_2CCH_3$)$_4$, these studies indicate that, for both dinucleotide adducts, the guanine bases are arranged in a H-H arrangement and, as in the case of 9-EtGuaH, there is an increase in the

acidity of the purine sites N1-H (p*K*a ≈ 5.7) (Figure I.10). As in the case of the cisplatin adduct of d(pGpG), *cis*-[$Pt(NH_3)_2$(pGpG)], the $Rh_2(\mu\text{-}O_2CCH_3)_2$(pGpG) adduct is observed to exist as a left-handed conformer HH1L, whereas the $Rh_2(\mu\text{-}O_2CCH_3)_2$(GpG) adduct exhibits two major *right* handed conformers HH1R (~75%) and HH2R (~25%), which differ in the relative canting of the two bases.[51,52] In the case of $[Rh_2(DTolF)_2(CH_3CN)_6](BF_4)_2$, the formation of the H-H isomer of $Rh_2(DTolF)_2$(GpG) was observed, but unlike the $Rh_2(\mu\text{-}O_2CCH_3)_2$(GpG) product, only the right-handed HH1R conformer was observed in solution (Figure I.11).[53] This difference is attributed to the presence of the bulkier and more electron donating formamidinato bridging group which induces conformational changes to the dirhodium d(GpG) adduct. The acidity of the N1-H purine site is also affected, and as, in the previous case, it increases (p*K*a ≈ 7.5), although to a lesser degree. This difference may also originate in the higher Lewis basicity of the formamidinato ligand as compared to the acetate ion. It is clear from these collective results that the DNA adducts formed by the dirhodium core are intimately related to the nature of the bridging groups that are not substituted in these reactions.[53]

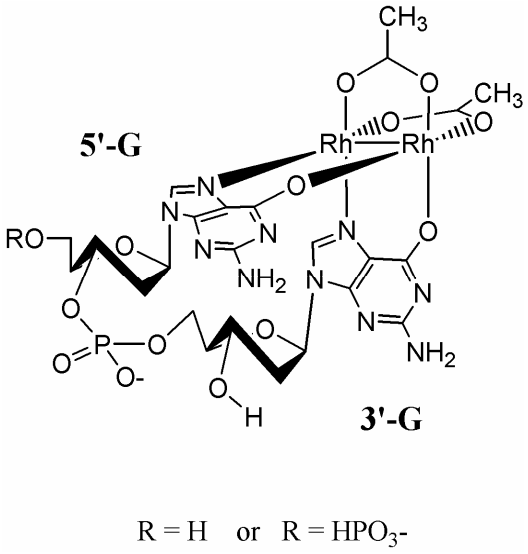


**Figure I.10.** Structures of $Rh_2(\mu\text{-}O_2CCH_3)_2$(GpG) and $Rh_2(\mu\text{-}O_2CCH_3)_2$(pGpG) (ref. 51, 52).

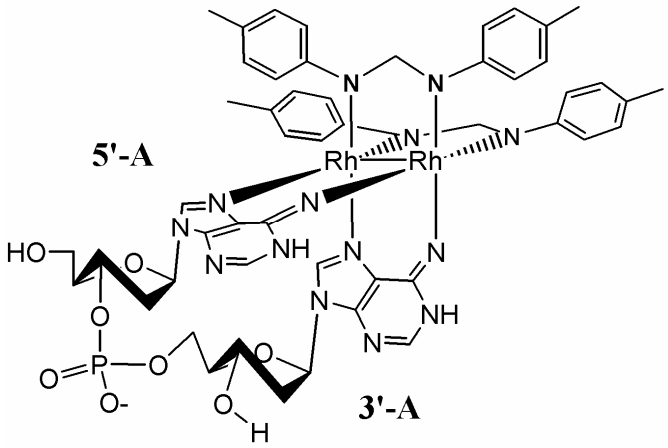


**Figure I.11.** Structure of $Rh_2(DTolF)_2$(GpG) (ref. 53).

**Dirhodium complexes and their interactions with double-stranded DNA**

Reactions of $Rh_2(\mu\text{-}O_2CCH_3)_4$, $[Rh_2(\mu\text{-}O_2CCH_3)_2(CH_3CN)_6]^{2+}$, and $Rh_2(\mu\text{-}O_2CCF_3)_4$ with single-stranded oligonucleotide tetramers, octamers, and dodecamers were studied by matrix-assisted laser desorption ionization (MALDI) and nanoelectrospray (nanoESI) coupled to time-of-flight mass spectrometry (TOF MS).[54] In order to obtain important information regarding the binding preference of these complexes with key dinucleotide sequences, the oligomers that were investigated were designed to contain AA, GG, GA, and AG dipurine sites. The study revealed that the dimetal unit remains intact and that the dirhodium bis-acetate oligonucleotide adducts are the main products of the reactions.[54] In addition, adducts containing less than two bridging acetates were also observed for longer oligonucleotides. From the MALDI experiments, it was also possible to establish a relative order of reactivity of the dirhodium complexes studied as well as cisplatin and *cis*-$[Pt(NH_3)_2(OH_2)_2]^{2+}$ (activated cisplatin): *cis*-$[Pt(NH_3)_2(OH_2)_2]^{2+}$ ~ $Rh_2(\mu\text{-}O_2CCF_3)_4$ > *cis*-$[Pt(NH_3)_2Cl_2]$ (cisplatin) >> $[Rh_2(\mu\text{-}O_2CCH_3)_2(CH_3CN)_6]^{2+}$ > $Rh_2(\mu\text{-}O_2CCH_3)_4$.[55] This order of reactivity is in accord with the known relative lability of the leaving group(s) for each complex. The enhanced reactivity of $Rh_2(\mu\text{-}O_2CCF_3)_4$ as compared to that of $Rh_2(\mu\text{-}O_2CCH_3)_4$ correlates with the increased basicity of $CH_3CO_2^-$ ($pK_b$ 9.2) compared to that of $CF_3CO_2^-$ ($pK_b$ 13.5), which makes $CF_3CO_2^-$ a better leaving group. The higher reactivity of $[Rh_2(\mu\text{-}O_2CCH_3)_2(CH_3CN)_6]^{2+}$ as compared to that of $Rh_2(\mu\text{-}O_2CCH_3)_4$ can be explained on the basis of the presence of the more labile monodentate equatorial acetonitrile groups in the former compound. Finally, the study

also established that both GG, as well as AA sites are the targeted residues in these oligomers.[55]

Despite earlier claims that $Rh_2(\mu\text{-}O_2CCH_3)_4$ was not able to react with double-stranded DNA (dsDNA), work in our laboratories established that dirhodium tetraacetate, and its derivatives do indeed bind to dsDNA. A study aimed at investigating the interactions of dsDNA and dirhodium carboxylate compounds revealed that $Rh_2(\mu\text{-}O_2CCH_3)_4$, $Rh_2(\mu\text{-}O_2CCF_3)_4$, and $[Rh_2(\mu\text{-}O_2CCH_3)_2(CH_3CN)_6]^{2+}$ are capable of forming DNA interstrand crosslinks (Figure I.12).[56] Additionally, it was observed that other adducts, namely monofunctional and intrastrand adducts, are also formed during the reaction. The adducts formed between DNA and the dirhodium core most likely involve all the variety of coordination modes observed in model complexes including *ax*/*ax*, *ax*/*eq*, and *eq*/*eq*.[56]

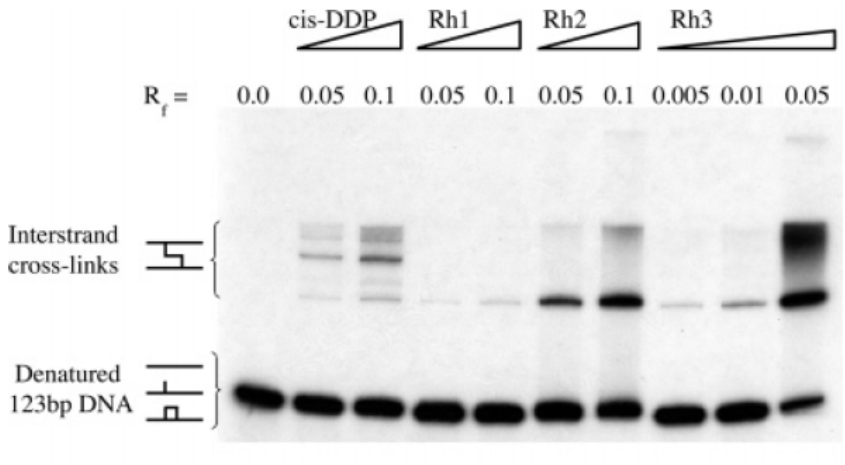


**Figure I.12.** Denaturating PAGE (5%) of reactions between cisplatin (cis-DDP), $Rh_2(\mu\text{-}O_2CCH_3)_4$ (Rh1), $[Rh_2(\mu\text{-}O_2CCH_3)_2(CH_3CN)_6]^{2+}$ (Rh2), and $Rh_2(\mu\text{-}O_2CCF_3)_4$ (Rh3) (taken from ref. 56).

**Inhibition of transcription by dirhodium complexes**

It has also been reported that several dirhodium compounds inhibit transcription, a process by which cells copy DNA into RNA.[57-58] Interestingly, it was found that $Rh_2(\mu\text{-}O_2CCH_3)_4$ and *cis*-$[Rh_2(\mu\text{-}O_2CCH_3)_2(phen)_2]^{2+}$ (phen = 1,10-phenanthroline) were more active than *cis*-$[Pt(NH_3)_2(H_2O)_2]^{2+}$, commonly referred to as "activated cisplatin". The relative concentrations, [complex]/[DNA], of $Rh_2(\mu\text{-}O_2CCH_3)_4$ and *cis*-$[Rh_2(\mu\text{-}O_2CCH_3)_2(phen)_2]^{2+}$at which 50% of the transcription is inhibited ($R_{inh}^{50}$), are 0.0031 and 0.0011, respectively; while the $R_{inh}^{50}$ value found for activated cisplatin is 0.0085 (Figure I.13). It was also observed that, unlike cisplatin, the mechanism of the inhibition of transcription by $Rh_2(\mu\text{-}O_2CCH_3)_4$ and *cis*-$[Rh_2(\mu\text{-}O_2CCH_3)_2(phen)_2]^{2+}$ is the binding of the complexes to the enzyme T7-RNA polymerase (T7-RNAP).[57] More recently, the ability to inhibit transcription of four other dirhodium complexes, namely $Rh_2(\mu\text{-}O_2CCF_3)_4$, $Rh_2(\mu\text{-}HNOCCH_3)_4$, $Rh_2(\mu\text{-}HNOCCF_3)_4$, and *cis*-$[Rh_2(\mu\text{-}O_2CCH_3)_2(CH_3CN)_6]^{2+}$ was also reported.[58] In these studies, it was shown that the nature of the bridging ligand affects the ability and the mechanism of the complexes to inhibit transcription. As for $Rh_2(\mu\text{-}O_2CCF_3)_4$, $Rh_2(\mu\text{-}HNOCCF_3)_4$, and *cis*-$[Rh_2(\mu\text{-}O_2CCH_3)_2(CH_3CN)_6]^{2+}$ the mechanism of inhibition was found to be the same as the one reported for $Rh_2(\mu\text{-}O_2CCH_3)_4$ and *cis*-$[Rh_2(\mu\text{-}O_2CCH_3)_2(phen)_2]^{2+}$ , namely binding to T7-RNAP; conversely $Rh_2(\mu\text{-}HNOCCH_3)_4$ does not appear to bind T7-RNAP.[58] The differences in the reactivity and the mechanism of transcription inhibition among dirhodium complexes with different bridging ligands is explained by the changes in the Lewis basicity of the axial site due to the presence of different atoms, nitrogen and/or oxygen, binding the metal center.[58]

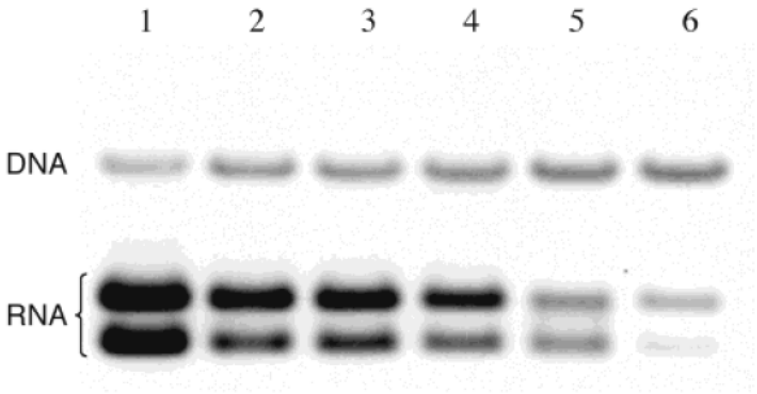


**Figure I.13.** Agarose gel of transcribed mRNA in the presence of *cis*-$[Rh_2(\mu\text{-}O_2CCH_3)_2(phen)_2]^{2+}$at various complex/[template DNA base] ratios, *R*. Lanes 1-6, *R* = 0.0000, 0.0005, 0.0010, 0.0015, 0.0020, 0.0025 (taken from ref. 57).

**Excited state properties of $Rh_2(\mu\text{-}O_2CCH_3)_4$**

Turro and coworkers have recently reported the observation of a transient species formed upon excitation of $Rh_2(\mu\text{-}O_2CCH_3)_4(L)_2$ (L = $CH_3OH$, tetrahydrofuran, $PPh_3$, pyridine) with a short laser pulse.[59] The transient species are long-lived, and depending on the axial ligands have a lifetime that ranges from 3.5 $\mu$s (L = THF) to 5.0 $\mu$s (L = $PPh_3$). Although many of the transient species formed from metal complexes are due to the loss of a ligand, this is not case for $Rh_2(\mu\text{-}O_2CCH_3)_4$, in which case no lost of ligands was observed. Additionally, no emission from any of the transient complexes was observed, however, energy transfer from the excited state to the $^3\pi\pi^*$ excited state of perylene was observed. The authors also demonstrated that the excited-state energy, $E_{00}$, of the transient species formed from $Rh_2(\mu\text{-}O_2CCH_3)_4(PPh_3)_2$ was between 1.34 and 1.77 eV.[59]

Investigation of the reactivity with DNA of the species formed upon excitation was later reported by the same group.[60] Excitation of $Rh_2(\mu\text{-}O_2CCH_3)_4(H_2O)_2$ with visible light in the presence of either 3-cyano-1-methylpyridinium tetrafluoroborate or 1,8-anthraquinone disulfonate results in the formation of the one-electron-oxidized complex, $[Rh_2(\mu\text{-}O_2CCH_3)_4(H_2O)_2]^+$, which efficiently cleaves dsDNA.[60] The photo-induced DNA cleavage of $Rh_2(\mu\text{-}O_2CCH_3)_4(H_2O)_2$ is more effective under $N_2$ atmosphere than in air, consistent with the quenching of the excited state of the rhodium complex by $O_2$ resulting in a decreased production of the active species, $[Rh_2(\mu\text{-}O_2CCH_3)_4(H_2O)_2]^+$. The presence of $PPh_3$ or pyridine in the axial positions inhibits the photocleavage ability of the complex, underlining the importance of the aquo-adduct,

$Rh_2(\mu\text{-}O_2CCH_3)_4(H_2O)_2$.[60] DFT calculations have shown that the one-electron-oxidized complex, $[Rh_2(\mu\text{-}O_2CCH_3)_4(H_2O)_2]^+$, can generate hydroxyl radicals, species that might be involved in the DNA-cleavage mechanism.[61]

It is obvious from the research conducted to date, that dirhodium(II,II) complexes are a diverse and promising class of cytotoxic compounds. My research project involved the syntheses of a series of $Rh_2$(II,II) complexes with the electron acceptor dipyrido[3,2-a:2′,3′-c]phenazine (dppz) ligand in order to study the ability of these complexes to increase their cytotoxicity upon irradiation. In addition, studies on the molecular characteristics that affect the *in vitro* activity of these compounds were performed. Finally, dirhodium complexes containing naturally occurring polyamines were also synthesized and investigated. All of these topics will be covered in the following chapters. The last chapter will discuss the conclusions of the studies presented and continuing studies for future work.

# CHAPTER II

# SYNTHESIS, DNA BINDING AND PHOTOCLEAVAGE OF DIRHODIUM(II,II) DPPZ COMPLEXES*

## *Introduction*

The success of the platinum-based compounds as antitumor agents and the emerging practical uses of photodynamic therapy have led to the exploration of various new transition metal complexes for potential use in photochemotherapy.[62-65] Crucial challenges involving the use of cisplatin and its analogues include their effectiveness towards some cancers and not others and the resistance developed by tumor cells to the drugs.[62,66] The severe toxic side-effects of these drugs as well as other antitumor drugs is also a major concern.[62,67] An alternative approach to localize the action of compounds to the target cells, and in this way eliminate or hamper the side-effects, is the activation of otherwise nontoxic drugs through irradiation of tumors with visible or near-IR light, a field generally known as photodynamic therapy (PDT).[68-71] Many compounds are currently being investigated for potential use in PDT; these are typically based on derivatives of porphyrins and phthalocyanins.[72-75] The photoactive drug Photofrin®

---

* Reprinted in part from "Direct DNA Photocleavage by a New Intercalating Dirhodium(II,II) Complex: Comparison to $Rh_2(\mu\text{-}O_2CCH_3)_4$" Bradley, P. M.; Angeles-Boza, A. M., Dunbar, K. R., Turro, C. *Inorg. Chem.* **2004**, *43*(8), 2450-2452; "DNA Binding and Photocleavage in vitro by New Dppz Dirhodium(II,II) Complexes: Correlation to Cytotoxicity and Photocytotoxicity" Angeles-Boza, A. M.; Bradley, P. M.; Fu, P. K.-L.; Wicke, S. E.; Bacsa, J.; Dunbar, K. R., Turro, C. *Inorg. Chem.* **2004**, *43*(26), 8510-8519; and "Photocytotoxicity of a New $Rh_2$(II,II) Complex: Increase in Cytotoxicity upon Irradiation Similar to Hematoporphyrin" Angeles-Boza, A. M.; Bradley, P. M.; Fu, P. K.-L.; Shatruk, M.; Hilfiger, M.G.; Dunbar, K. R.; Turro, C. *Inorg. Chem*. **2005**, *44*(21), 7262-7264. Copyright 2004, 2005, with permission from the American Chemical Society.

which is in use for the photodynamic treatment of lung and esophageal cancers is composed of a mixture of hematoporphyrin and its derivatives.[76] Typically, $^1O_2$ produced through energy transfer from the drug's long-lived $^3\pi\pi^*$ excited state is the reactive species that results in damage to biomolecules. Drawbacks of current PDT agents are their prolonged cutaneous sensitivity and the requirement of $O_2$ for their function, since once consumed, $O_2$ must diffuse to the proximity of the agent.[69,71,77,78] In addition, some of the most malignant and drug resistant cancer cells are hypoxic (they lack oxygen).[71,78] New classes of transition metal PDT agents may prove to be useful in circumventing the problems associated with the current drugs.

Metal complexes containing the dipyrido[3,2-a:2′,3′-c]phenazine (dppz) ligand, for example $[Ru(L)_2(dppz)]^{2+}$ (L = bpy (2,2′-bipyridine), phen (1,10-phenanthroline)), have been explored extensively as reporters of structure,[79-85] sequence,[81] crosslinking,[86] drug binding,[87] electron transfer,[88-90] and nucleic acid solvation environment and dynamics in DNA duplexes.[91-94] The DNA photocleavage by $[Ru(bpy)_3]^{2+}$ and related Ru(II) complexes, including intercalated $[Ru(bpy)_2(dppz)]^{2+}$, is observed only in the presence of $O_2$, and it likely proceeds via the formation of $^1O_2$ through energy transfer from the excited state of the complex.[95] Since the first reports of the "light switch" effect, numerous mononuclear and bimetallic dppz complexes containing a wide variety of metal centers were reported and typically exhibit strong binding to DNA owing to the intercalation of the dppz ligand ($K_b$ values range from ~$10^4$ to ~$10^8$ $M^{-1}$).[96-99] It was shown that bimetallic complexes of dppz also bind strongly to DNA, but the two metal

centers in the systems reported to date are not in close proximity, and their photoreactivity towards nucleic acids has not been explored.[100,101]

Bimetallic complexes that exhibit strong metal-metal interactions often afford reactive excited states that are not available in mononuclear complexes. For example, hydrogen abstraction from the DNA backbone upon photoexcitation of $[Pt_2(pop)_4]^{4-}$ ($pop^{2-}$ = $HO_2POPO_2H^{2-}$) was reported, which results in DNA cleavage.[102,103] The cleavage of duplex DNA by the triplet excited state of $[Pt_2(pop)_4]^{4-}$ is not enhanced by piperidine treatment, consistent with hydrogen abstraction rather than with a mechanism involving guanine oxidation.[104] In model systems, it was shown that $[Pt_2(pop)_4]^{4-}$ reacts with nucleic acids and nucleotides through 4′- and 5′-hydrogen abstraction from the deoxyribose backbone.[102,103] The overall negative charge of the complex, however, precludes it from binding to the double helix, thereby slowing the bimolecular rate of photocleavage which renders the process inefficient. In order to circumvent electrostatic repulsion between anionic complexes and DNA, neutral and cationic dirhodium complexes were explored as agents for DNA photocleavage.[60] Complexes of the type $Rh_2(\mu\text{-}O_2CCH_3)_4(L)_2$ (L = alcohols, $PPh_3$, py, THF, $H_2O$) possess long-lived excited states ($\tau$ = 3.5 to 5.0 ms) that can be accessed with visible light (500 to 700 nm).[59] The compound $Rh_2(\mu\text{-}O_2CCH_3)_4(OH_2)_2$ exhibits weak DNA binding ($K_b = 4.6 \times 10^2\ M^{-1}$), and has been shown to photocleave DNA, but only in the presence of electron acceptors.[60]

In order to increase the DNA binding of dirhodium complexes and achieve direct DNA photocleavage, the photoreactive dirhodium(II,II) core was combined with

intercalating dppz ligands. This chapter describes the synthesis and characterization of dirhodium(II,II) complexes containing the dppz ligand. The DNA binding and photocleavage properties of some of the complexes were measured *in vitro*, and the results were correlated to the differences in the cytotoxicity and photo-cytotoxicity of these complexes towards human skin cells.

## *Experimental Section*

### Materials

Sodium chloride, sodium phosphate, gel loading buffer (0.05% (w/v) bromophenol blue, 40% (w/v) sucrose, 0.1 M EDTA (pH = 8.0), 0.5% (w/v) sodium lauryl sulfate), Tris base, Tris/HCl, and ethidium bromide were purchased from Sigma and used as received. Calf thymus DNA was purchased from Sigma and was dialyzed against 5 mM Tris, 50 mM NaCl (pH = 7.5) buffer three times during a 48 hour period prior to use. The pUC18 plasmid was purchased from Bayou Biolabs and purified using the Concert Miniprep System from Life Technology. *Sma*I was purchased from Invitrogen and used as received. Acetonitrile and dichloromethane were dried over 3 and 4 Å molecular sieves, respectively, and distilled under a nitrogen atmosphere prior to use. All reactions were carried out under nitrogen using standard Schlenk-line techniques. The reagents $RhCl_3$, sodium acetate, $NaBF_4$, and polystyrene sulfonate (PSS) were purchased from Aldrich and used without further purification. The compounds $Rh_2(\mu\text{-}O_2CCH_3)_4$ (**1**),[105] $Rh_2(\mu\text{-}O_2CCF_3)_4$ (**2**),[105] $[Rh_2(\mu\text{-}O_2CCH_3)_2(phen)_2](O_2CCH_3)_2$ (**3**),[44] $[Rh_2(\mu\text{-}O_2CCF_3)_2(phen)_2](O_2CCF_3)_2$ (**4**),[44] and dppz

were synthesized by previously reported methods.[106] The compound *cis*-[$Rh_2$(μ-$O_2CCF_3$)$_2$(dppz)$_2$]($O_2CCF_3$)$_2$ (**8**) was synthesized as reported in Chapter IV.

*cis-[$Rh_2$(μ-$O_2CCH_3$)$_2$(dppz)(η$^1$-$O_2CCH_3$)($CH_3OH$)]($O_2CCH_3$)* ***(5)***

A suspension of dppz (53.8 mg, 0.19 mmol) in $CH_2Cl_2$ was added to a slurry of **1** (100 mg, 0.19 mmol) in $CH_2Cl_2$. The mixture was stirred for 36 h under refluxing conditions and the resulting green precipitate was filtered and washed with $CH_2Cl_2$. The product was suspended into methanol and stirred for 24 h at room temperature. The solution was concentrated and diethyl ether was added to precipitate a green solid which was collected by filtration (91% yield). ESI-MS ([$Rh_2$(μ-$O_2CCH_3$)$_2$(dppz)(η$^1$-$O_2CCH_3$)]$^+$): calc. m/z = 664.941, obsd. m/z = 664.88. $^1$H NMR (300 MHz) in $CD_3OD$, δ / ppm (mult., int., assignment): 1.11 (s, 3H, $CH_3CO_2$), 1.88 (s, 3H, $CH_3CO_2$), 2.35 (s, 3H, $CH_3CO_2$), 2.41 (s, 3H, $CH_3CO_2$), 8.15 (m, 4H, dppz), 8.51 (m, 2H, dppz), 8.88 (dd, 2H, dppz), 9.79 (dd, 2H, dppz). UV-vis in $H_2O$, λ / nm (ε / $M^{-1}cm^{-1}$): 278 (57,870), 360 (11,730), 428 (3,177), 590 (354).

*cis-[$Rh_2$(μ-$O_2CCH_3$)$_2$(dppz)$_2$]($O_2CCH_3$)$_2$* ***(6)***

A solution of **1** (100 mg, 0.19 mmol) in acetonitrile was treated with solid dppz (107.7 mg, 0.38 mmol) and the suspension was heated to reflux for 24 h. After this time period, the red mixture was cooled to room temperature, filtered and washed with acetonitrile to afford a red solid (93% yield). Subsequent crystallization from a methanol/benzene/diethyl ether solution in an excess of $NaBF_4$ produced crystals suitable for X-ray characterization. ESI-MS ([$Rh_2$(μ-$O_2CCH_3$)$_2$(dppz)$_2$]$^{2+}$): calcd. m/z = 444.513, obsd. m/z = 443.98. $^1$H NMR of the diacetate salt (300 MHz) in

$CDCl_3/CD_3OD$ (1:1 v:v), δ / ppm (mult., int., assignment): 1.75 (s, 6H, $CH_3CO_2$), 2.67 (s, 6H, $CH_3CO_2$), 7.73 (m, 4H, dppz), 7.81 (m, 4H, dppz), 7.90 (m, 4H, dppz), 8.64 (d, 4H, dppz), 9.05 (d, 4H, dppz). UV-vis in $H_2O$, λ / nm (ε / $M^{-1}cm^{-1}$): 203 (69,390), 276 (86,430), 363 (15,170), 434 (5,459).

*cis-[$Rh_2$(μ-$O_2CCH_3$)$_2$(bpy)(dppz)]($O_2CCH_3$)$_2$* ***(7)***

A solution of *cis*-[$Rh_2$(μ-$O_2CCH_3$)$_2$(bpy)(η$^1$-$O_2CCH_3$)($CH_3OH$)]($O_2CCH_3$) (**5**; 403.3 mg, 0.64 mmol) in $CH_3CN$ (30 mL) was treated with dppz (183.5 mg, 0.65 mmol) in $CH_3CN$ (30 mL) and refluxed for 24 h under $N_2$. After this time period, the red-brown product was collected by vacuum filtration and washed with diethyl ether (2 × 15 mL) and recrystallized from $CH_3OH/CH_2Cl_2$ (63% yield). ESI-MS ([$Rh_2$(μ-$O_2CCH_3$)$_2$(bpy)(dppz)]($O_2CCH_3$)]$^+$): calcd. m/z = 821.426, obsd. m/z = 821.00. $^1$H NMR: ($CDCl_3$) δ (ppm) 1.88 (s, 6H, $CH_3CO_2$-axial), 2.59 (s, 6H, $CH_3CO_2$-bridge), 7.32 (d, 2H, bpy), 7.45 (t, 2H, bpy), 7.61 (t, 2H, bpy), 7.92 (m, 2H, dppz), 8.16 (m, 2H, dppz), 8.47 (d, 2H, bpy), 8.50 (m, 2H, dppz), 8.78 (d, 2H, dppz), 9.51 (d, 2H, dppz). UV-Vis (MeOH): λ, nm (ε, $M^{-1}cm^{-1}$): 530 (sh,350), 432 (3100), 366 (12000), 282 (61000).

## Methods

*X-ray Crystallographic Studies*

***X-ray Structural Study of cis-[$Rh_2(\mu$-$O_2CCH_3)_2(dppz)_2](O_2CCH_3)_2$ (6).*** For the X-ray crystallographic analysis, two red prismatic crystals of **6**, **6a** (approximate dimensions: 0.17 x 0.08 x 0.22 $mm^3$) and **6b** (approximate dimensions: 0.37 x 0.25 x 0.19 $mm^3$) were selected. The crystals were grown under different conditions. Compound **6a** was grown from a solution of **6** in $CH_3CN/CH_3CH_2OH$ in the presence of two equivalents of $NaBF_4$, whereas **6b** was grown form a solution of $CH_3OH$/benzene layered with diethyl ether in the presence of excess $NaBF_4$. The crystals were coated with Paratone oil, transferred to a nylon loop, and placed in a cold $N_2$ stream at 110(2) K. An indexing of the preliminary diffraction patterns indicated that both crystals were monoclinic. For **6a**, a total of 17,935 reflections were collected in the range $2.40 \leq \theta \leq 27.49°$, and in the case of **6b**, 11,775 total reflections were collected in the range $1.73 \leq \theta \leq 27.21°$. The data collection covered approximately a hemisphere of reciprocal space, by a combination of three or four sets of exposures; each set had a different $\phi$ angle for the crystal and each exposure covered 0.3° in $\Omega$. Crystal decay, which was monitored by analyzing duplicate reflections, was found to be less than 1%, therefore, no decay corrections were applied. During the final cycles of refinement, all atoms with the exception of hydrogen atoms were refined anisotropically. Hydrogen atoms belonging to hydroxo groups were placed in suitable positions with idealized tetrahedral X-O-H geometries. Hydrogen atoms belonging to methyl groups were placed in regions of maximum electron density around the methyl C atoms, and the torsional angles were

refined with idealized C-H distances and tetrahedral angles. The structure of **6a** was solved and refined in the chiral space group $P2_1$, whereas **6b** was solved in the $P2_1/n$ space group.

***X-ray Structural Study of cis-[Rh$_2$($\mu$-O$_2$CCH$_3$)$_2$(bpy)(dppz)](O$_2$CCH$_3$)$_2$ (7).*** For the X-ray crystallographic analysis, a red prismatic crystal of **8** (approximate dimensions: 0.24 x 0.16 x 0.18 mm$^3$) was selected. The crystal was coated with Paratone oil, transferred to a nylon loop, and placed in a cold $N_2$ stream at 110(2) K. An indexing of the preliminary diffraction patterns indicated that the crystal was monoclinic. A total of 46,469 reflections were collected in the range $1.58 \leq \theta \leq 27.48^{o}$. Hydrogen atoms belonging to methyl groups were placed in regions of maximum electron density around the methyl C atoms. The structure was solved and refined in the space group $P2_1/n$. The final refinement cycle was based on 9,275 unique reflections (6,225 with $F_\sigma^2 > 2\sigma(F_\sigma^2)$), 583 parameters, and 33 restraints ($R1$ = 0.0871, $wR2$ = 0.2534). The maximum and minimum peaks in the final difference Fourier map corresponded to 1.90 and –1.083 e/Å$^3$, respectively, with a goodness-of-fit value of 1.087.

*Melting Point Experiments*

Solutions containing 100 μM calf-thymus DNA and 20 μM of either **5** or **6** (1 mM phosphate buffer, 2 mM NaCl, pH = 7.2) were used to determine the melting temperatures.

*DNA Photocleavage Experiments*

The DNA photocleavage experiments were carried out using 20 μL of total sample volume in 0.5 mL transparent eppendorf tubes containing 100 μM pUC18 plasmid and various concentrations of each metal complex. Irradiation of the solutions was performed either in air, under a positive pressure of argon or nitrogen following bubbling for ~15 minutes, or after 5 freeze-pump-thaw cycles in quartz tubes equipped with a Kontes stopcock (using ~3-fold greater solution volume). Following irradiation, 4 μL of the DNA gel loading buffer was added to each 20 μL sample. The electrophoresis was carried out using either 1% or 2% agarose gel stained with 0.5 mg/L eithidium bromide in 1X TAE buffer (40 mM tris-acetate, 1 mM EDTA, pH ~ 8.2); other conditions are specified as needed.

*DNA Binding Constants Determination*

The binding constants of the metal complexes to calf-thymus DNA determined by optical titrations at room temperature were measured with 5 μM metal complex and the calf thymus DNA concentration was varied from 0 to 100 μM (5 mM Tris/HCl, pH 7.5). The dilution of metal complex concentration at the end of each titration was negligible. The DNA binding constant, $K_b$, was obtained from fits of the titration data to eq 1,[107,108]

$$\frac{\varepsilon_a - \varepsilon_f}{\varepsilon_b - \varepsilon_f} = \frac{b - (b^2 - 2K_b{}^2 C_t [DNA]_t / s)^{1/2}}{2K_b C_t} \qquad (1)$$

where $b = 1 + K_b C_t + K_b [DNA]_t / 2s$, $C_t$ and $[DNA]_t$ represent the total complex and DNA concentrations, respectively, *s* is base pair binding site size, and $\varepsilon_a$, $\varepsilon_f$, and $\varepsilon_b$ represent the apparent, free complex, and bound complex molar extinction coefficients, respectively. The value of $\varepsilon_b$ was determined from the plateau of the DNA titration, where addition of DNA did not result in further changes to the absorption spectrum.

*Cytotoxicity and Photocytotoxicity*

Human skin fibroblasts (Hs-27) were obtained from the American Type Culture Collection, cell line CRL-1634 (Manassas). Cells were cultured in Dulbecco's modified Eagle medium, containing 10% fetal bovine serum (Life Technologies), 50 μg/mL gentamicin, 4.5 mg/ml glucose, and 4 mM L-glutamine (Invitrogen Life Technology). Cell cultures were incubated in a humidified atmosphere containing 5% $CO_2$ at 37 $^oC$. For assessing the cytotoxicity and photocytotoxicity of different compounds, subconfluent (50% - 80% confluent) monolayers of Hs-27 in 60 mm culture dishes were used. The monolayers were washed twice with phosphate-buffered saline (PBS) to ensure that the culture dishes were free of any culture medium, and then fresh medium containing different concentrations of each compound was added to cover the fibroblasts. The cells were irradiated through the PBS buffer, which does not absorb light in the visible region. After irradiation, the cells were removed from the dishes by trypsinization, seeded into 24-well culture dishes, and incubated for 2 to 4 days or until the untreated control group reached confluence. N-lauroyl sarcosine (200 μL, 40 mM) was then added to each well and the cells were allowed to lyse for at least 15 min.

Quantitative determination of the protein content in each well was undertaken using Peterson's Modification of the Micro-Lowry Method (Sigma reagent kit),[109] where the lysate was treated with 200 μL Lowry reagent for 20 min and then with 100 μL Folin-Ciocalteau phenol reagent for 30 min or until color developed. A portion of the contents (200 μL) of each well was transferred to a 96-well plate for absorbance determination using a multiwell plate reader (Dynatech Laboratory). The absorbance at 630 nm was monitored, which is proportional to the total protein content and the number of cells in each well.[109]

**Instrumentation**

The $^{1}$H NMR spectra of **5**, **6**, and **7** were recorded on a Unity-300 NMR spectrometer. Absorption measurements were performed either on a Shimadzu UVPC-3001 spectrophotometer or on a Hewlett-Packard diode array spectrometer (HP 8453) with HP8453 Win System software equipped with a Peltier temperature controlled sample cell and driver (HP89090A) for thermal denaturation studies. The relative changes in viscosity were measured on a Cannon-Manning Semi-Micro viscometer for transparent liquids. The viscometer was immersed in a constant temperature water bath (24 $^{o}$C) controlled by a Neslab (Model RGE-100) circulator. The ethidium bromide stained agarose gels were imaged using a GelDoc 2000 transilluminator (BioRad) equipped with Quality One (v. 4.0.3) software.

X-ray diffraction data were collected either on a Bruker APEX CCD or a Bruker SMART CCD diffractometer with graphite monochromated Mo-$K_\alpha$ radiation ($\lambda$ = 0.71073 Å). The frames were integrated with the Bruker SAINT software,[110] and a semi-empirical absorption correction using multiple-measured reflections was applied using SADABS.[111] The structures were solved and refined using X-SEED,[112] a graphical interface to SHELX97.[113]

The DNA photocleavage experiments were conducted using a 150 W Xe arc lamp in a PTI housing (Milliarc Compact Lamp Housing) as the light source powered by an LPS-220 power supply (PTI) with an LPS-221 igniter (PTI). The wavelength of the light reaching the samples was controlled by placing high-pass colored glass filters (Melles Griot) and a 10 cm water cell in the light path. Irradiation of cell cultures was accomplished through the use of two 40 W GE watt-miser bulbs (General Electric) with an Acrylite OP-3 high-pass filter, keeping the total irradiation below 5 J/cm$^2$ and providing a broadband source of irradiation (400 – 700 nm). It should be noted that cell irradiation intensities greater than 5 J/cm$^2$ have been shown to result in concomitant cell death in the absence of any external agents, and should therefore be avoided when testing compounds with potential applications to live tissue.[114]

*Results and Discussion*

**Synthesis and structural characterization**

*Synthesis and Structural Characterization of cis-[$Rh_2(\mu\text{-}O_2CCH_3)_2(dppz)(\eta^1\text{-}O_2CCH_3)(CH_3OH)](O_2CCH_3)$* ***(5)***

The synthesis of **5** was performed in a similar fashion to the preparation of other mono-diimine complexes of dirhodium. A slurry of $Rh_2(\mu\text{-}O_2CCH_3)_4$ (**1**) in $CH_2Cl_2$ reacts with one equivalent of dppz (dppz = dipyrido[3,2-a:2′,3′-c]phenazine) to yield an intermediate that is converted to *cis*-$[Rh_2(\mu\text{-}O_2CCH_3)_2(dppz)(\eta^1\text{-}O_2CCH_3)(CH_3OH)]^+$ (**5**) (Scheme II.1) by stirring the product of the reaction in $CH_3OH$ until a green solution is obtained. Characterization of **5** was achieved by $^1H$ NMR spectroscopy in $CD_3OD$ and ESI mass spectrometry. Four separate acetate resonances were observed in the structure of *C1* symmetry, corresponding to two in bridging positions (2.35, and 2.41 ppm), one coordinated to a single rhodium atom in a terminal fashion (1.11 ppm), and the third as an unbound counterion (1.88 ppm). The aromatic dppz resonances of **5** appear at 8.15, 8.51, 8.88, 8.64 and 9.79 ppm, and are typical for a coordinated dppz ligand (Figure II.1).[115,116] The ESI-MS shows a parent peak at m/z = 664.88 corresponding to the species $[Rh_2(\mu\text{-}O_2CCH_3)_2(dppz)(\eta^1\text{-}O_2CCH_3)]^+$.

*Synthesis and Structural Characterization of $[Rh_2(\mu\text{-}O_2CCH_3)_2(dppz)_2](O_2CCH_3)_2$* ***(6)***

The complex $Rh_2(\mu\text{-}O_2CCH_3)_4$ (**1**) in $CH_3CN$ reacts with two equivalents of dppz (dppz = dipyrido[3,2-a:2′,3′-c]phenazine) to yield *cis*-$[Rh_2(\mu\text{-}O_2CCH_3)_2(dppz)_2](O_2CCH_3)_2$ (**6**) after heating to reflux for 24 hours (Scheme II.1). The molecular structure of **6**, was determined by X-ray crystallographic methods.

**Scheme II.1.** Synthetic scheme depicting the synthesis of compounds **5**, **6**, and **7**.

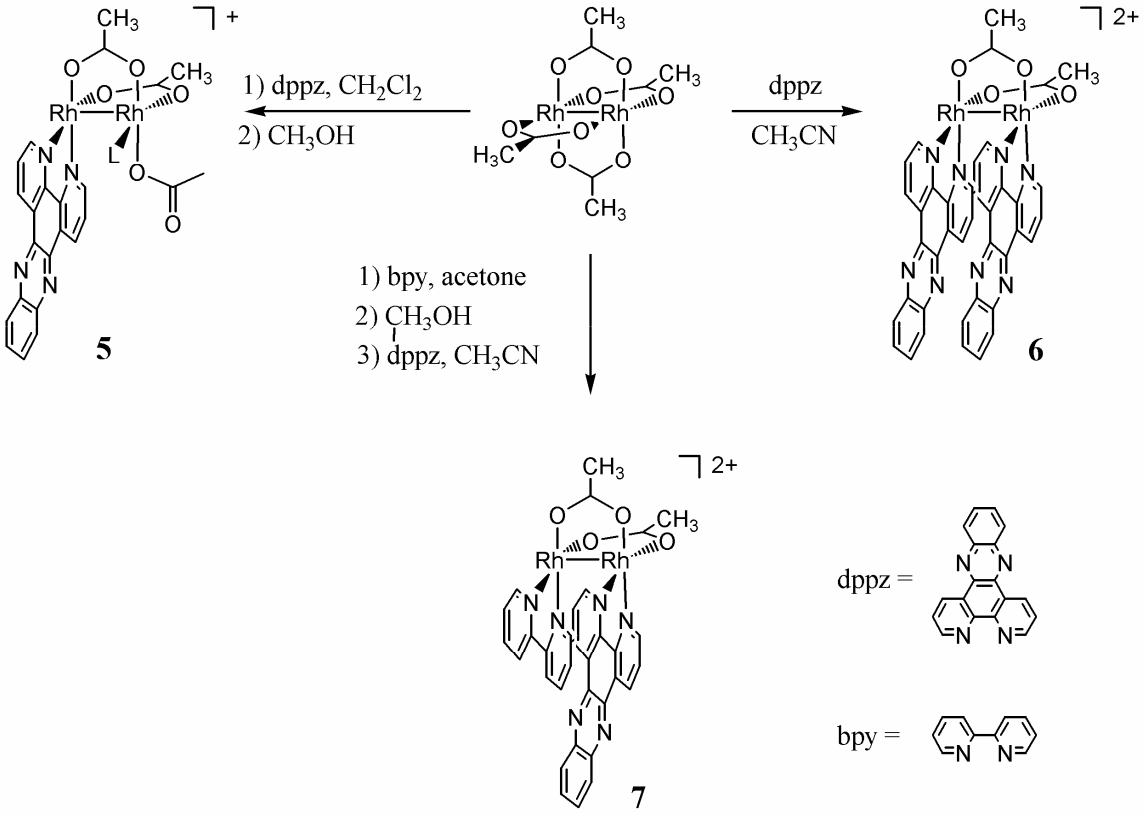

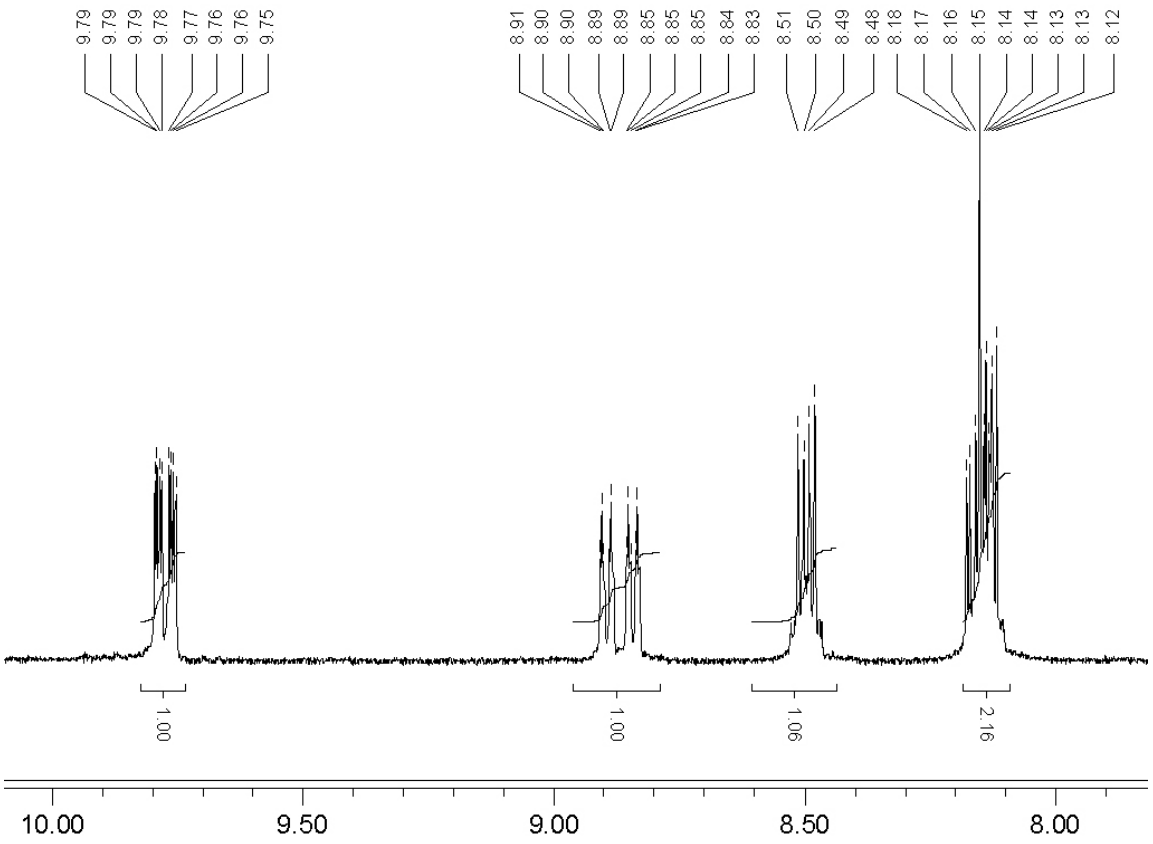


**Figure II.1.** $^{1}$H-NMR spectrum of the aromatic region of *cis*-[$Rh_2$($\mu$-$O_2CCH_3$)$_2$(dppz)($\eta^1$-$O_2CCH_3$)($CH_3OH$)]($O_2CCH_3$) (**5**).

The molecular structures of **6a** and **6b** consist of a dinuclear $Rh_2$(II,II) core with a pair of chelating dppz ligands coordinated to each Rh atom in a *syn* disposition, and two bridging acetates occupying the remaining equatorial sites. An acetate ion and a $CH_3CH_2OH$ group coordinated at the axial positions complete an irregular octahedral coordination sphere about each Rh atom in **6a**, whereas **6b** contains a methanol molecule coordinated to each axial position. The structure of the dinuclear cation in **6a** and **6b** are depicted in Figures II.2 and II.3 and are similar to those reported for related dirhodium complexes.[45,117] The Rh-Rh internuclear distances in **6a** and **6b**, 2.5519(6) and 2.533(1) Å, respectively, are similar to those reported for $[Rh_2(\mu\text{-}O_2CCH_3)_4(L)_2]^{2+}$ (L = bpy, phen, 4,7-dimethyl-phen, 3,4,7,8-tetramethyl-phen), 2.548(4), 2.5557(4), 2.565(1), and 2.564(1) Å, respectively.[45,117] Similarly, in *cis*-$[Rh_2(\mu\text{-}O_2CCF_3)_4(bpy)_2]^{2+}$ a Rh-Rh distance of 2.570(6) Å was reported.[45] The lengths of the Rh-N bonds in **6**, which range from 2.005(4) to 2.016(4) Å, are also comparable to those observed in the analogous bpy, phen, and substituted phen complexes.[45]

A striking feature of **6a** and **6b** is the close proximity of the two dppz ligands, with a nearly eclipsed conformation across the metal-metal bond dictated by the rigid bridging acetate groups. In the absence of bridging ligands, a staggered conformation about a Rh-Rh single bond is expected, since no electronic barrier to rotation is present. The internal twist angle away from the eclipsed geometry of ~ 13° in **6a** and **6b** is significantly greater than that observed for the bis-bpy analogue (6.2°), but similar to those in the corresponding phen and substituted phen complexes (16-20°).[45,117] The

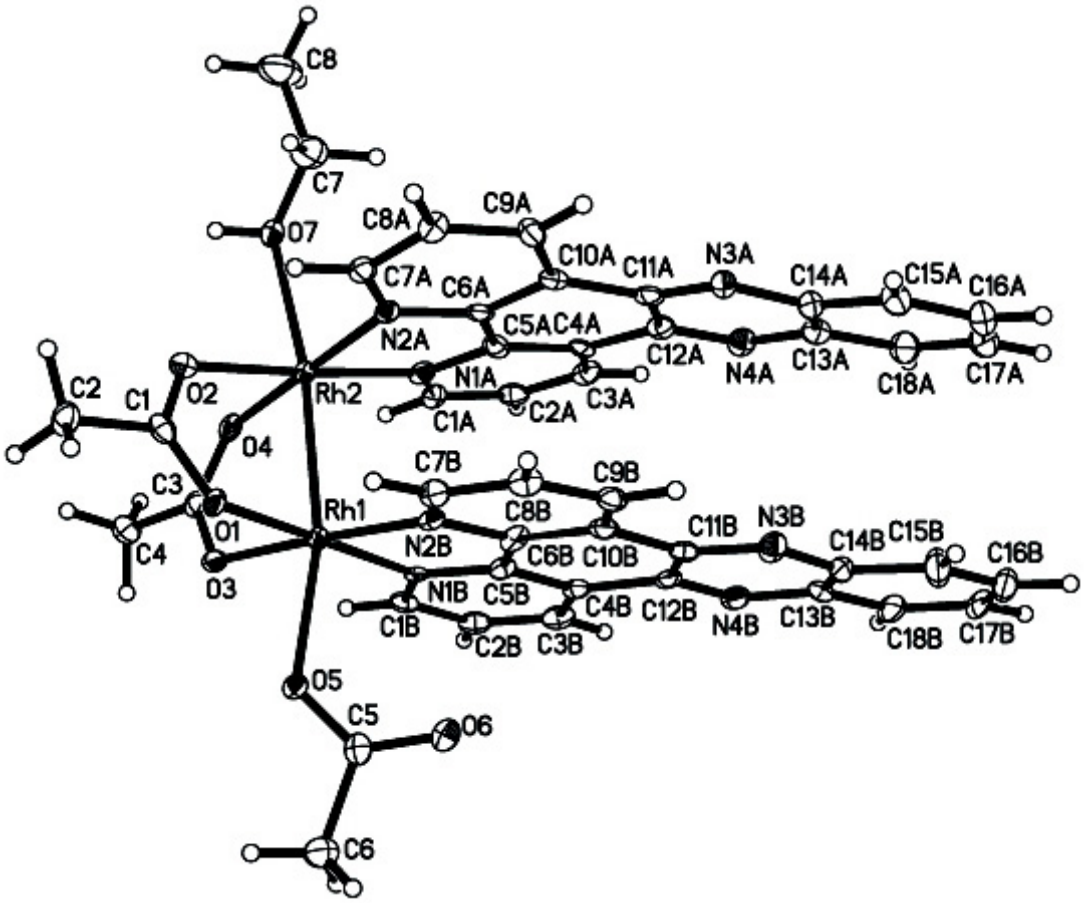


**Figure II.2.** Thermal ellipsoid plot at the 50% probability level of the cation in **6a**.

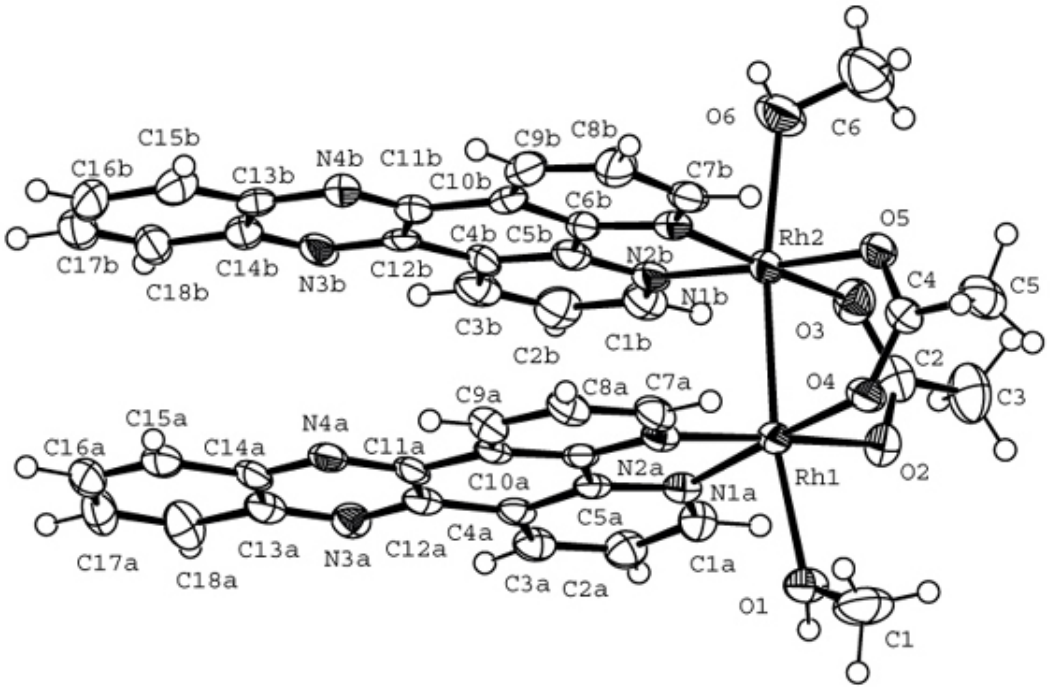


**Figure II.3.** Thermal ellipsoid plot at the 50% probability level of the cation in **6b**.

dihedral torsional angle defined by the two planes normal to the three aromatic rings of both dppz ligands closest to the metal is 15.1(2)° and 13.7(3)° for **6a** and **6b**, respectively. Similar values were observed in $[Rh_2(\mu\text{-}O_2CCH_3)_2(bpy)_2]^{2+}$ (15.8°) and $[Rh_2(\mu\text{-}O_2CCH_3)_4(L)_2]^{2+}$ (L = bpy, phen, 4,7-dimethyl-phen, 3,4,7,8-tetramethyl-phen), with deviations that range from 9.0° to 10.4°.[45]

The splaying of the dppz ligands from a parallel orientation and the twisting from an eclipsed geometry serve to reduce steric interactions between the ligands, since the short Rh-Rh bond distance would otherwise bring them closer than is favorable for π-π stacking interactions.[118] Since the dppz ligands are distorted, and their best least squares planes are not exactly parallel to each other, a unique interplanar distance cannot be defined for these ligands. The shortest non-bonded atomic contacts, however, provide an indication of the separation of the two dppz ligands in these molecules, with 3.494(7) Å and 3.503(6) Å being the shortest distance between the outermost rings for **6a** and **6b**, respectively. The shortest atomic contacts between dppz ligands occurs closest to the metal-metal bond, for example, in **6a** the atomic distances for N1a···N1b, C7a···C7b, N2a···N2b, and C1a···C1b are 3.050(5) Å, 3.289(5) Å, 3.058(5) Å, and 3.242(5) Å, respectively. Selected crystal parameters for compounds **6a** and **6b** are listed in Tables II.1 and II.2. Selected bond lengths and angles for compounds **6a** and **6b** are listed in Tables II.3, II.4, II.5 and II.6, respectively.

**Table II.1.** Crystal data and structural refinement parameters for compound **6a**.

| | |
|---|---|
| Empirical formula | $C_{46}H_{41}BF_4N_8O_8Rh_2$ |
| Formula weight | 1126.50 |
| Temperature | 100(2) K |
| Wavelength | 0.71073 Å |
| Crystal system | Monoclinic |
| Space group | P21 |
| a | 9.5905(19) Å |
| b | 23.870(5) Å |
| c | 10.132(2) Å |
| α | 90° |
| β | 108.44(3)° |
| γ | 90° |
| Volume | 2200.3(8) $Å^3$ |
| Z | 2 |
| Density (calculated) | 1.700 $Mg/m^3$ |
| Crystal size | 0.22 x 0.17 x 0.08 $mm^3$ |
| Theta range for data collection | 2.40 to 27.49°. |
| Reflections collected | 17935 |
| Independent reflections | 6822 [R(int) = 0.0500] |
| Data / restraints / parameters | 6822 / 85 / 627 |
| Goodness-of-fit on $F^2$ | 1.022 |
| Final R indices [I>2sigma(I)] | R1 = 0.0389, wR2 = 0.0668 |
| R indices (all data) | R1 = 0.0456, wR2 = 0.0688 |

$R_1 = \Sigma||F_o| - |F_c||/\Sigma|F_o|$; $wR_2 = [\Sigma[w(F_0^2-F_c^2)^2]/\Sigma[w(F_0^2)^2]]^{1/2}$

**Table II.2.** Crystal data and structural refinement parameters for compound **6b**.

| | |
|---|---|
| Empirical formula | $C_{55}H_{51}B_2F_8N_8O_7Rh_2$ |
| Formula weight | 1315.48 |
| Temperature | 100(2) K |
| Wavelength | 0.71073 Å |
| Crystal system | Monoclinic |
| Space group | P21/n |
| a | 13.698(3) Å |
| b | 23.472(5) Å |
| c | 17.318(4) Å |
| $\alpha$ | 90° |
| $\beta$ | 102.47(3)° |
| $\gamma$ | 90° |
| Volume | 5436.7(19) $Å^3$ |
| Z | 4 |
| Density (calculated) | 1.607 $Mg/m^3$ |
| Crystal size | 0.37 x 0.25 x 0.19 $mm^3$ |
| Reflections collected | 43341 |
| Independent reflections | 11775 [R(int) = 0.0785] |
| Data / restraints / parameters | 11775 /100 / 681 |
| Goodness-of-fit on $F^2$ | 1.110 |
| Final R indices [I>2sigma(I)] | R1 = 0.0968, wR2 = 0.2020 |
| R indices (all data) | R1 = 0.1570, wR2 = 0.2332 |

$R_1 = \Sigma||F_o| - |F_c||/\Sigma|F_o|$; $wR_2 = [\Sigma[w(F_0^2-F_c^2)^2]/\Sigma[w(F_0^2)^2]]^{1/2}$

**Table II.3.** Selected bond distances (Å) for compound **6a**.

| | Bond Distances (Å) |
|---|---|
| Rh(1)-N(1B) | 2.005(4) |
| Rh(1)-N(2B) | 2.007(4) |
| Rh(1)-O(3) | 2.040(3) |
| Rh(1)-O(1) | 2.044(3) |
| Rh(1)-O(5) | 2.187(3) |
| Rh(1)-Rh(2) | 2.5519(6) |
| Rh(2)-N(2A) | 2.009(4) |
| Rh(2)-N(1A) | 2.016(4) |
| Rh(2)-O(4) | 2.048(3) |
| Rh(2)-O(2) | 2.051(3) |
| Rh(2)-O(7) | 2.334(3) |

**Table II.4.** Selected bond angles (°) for compound **6a**.

| | Bond Angles (°) |
|---|---|
| O(7)-Rh(2)-Rh(1) | 171.10(9) |
| O(5)-Rh(1)-Rh(2) | 167.10(8) |
| N(2B)-Rh(1)-O(5) | 94.34(14) |
| O(3)-Rh(1)-O(5) | 84.77(13) |
| O(1)-Rh(1)-O(5) | 87.18(13) |
| O(4)-Rh(2)-O(7) | 86.97(13) |
| O(2)-Rh(2)-O(7) | 90.75(13) |
| N(1B)-Rh(1)-Rh(2) | 96.61(11) |
| N(1B)-Rh(1)-O(5) | 91.38(14) |

**Table II.5.** Selected bond distances (Å) for compound **6b**.

| | Bond Distances (Å) |
|---|---|
| Rh(1)-N(1A) | 2.009(7) |
| Rh(1)-N(2A) | 2.018(7) |
| Rh(1)-O(4) | 2.033(6) |
| Rh(1)-O(2) | 2.046(6) |
| Rh(1)-O(1) | 2.284(5) |
| Rh(1)-Rh(2) | 2.533 (1) |
| Rh(2)-N(1B) | 1.995(7) |
| Rh(2)-N(2B) | 2.004(7) |
| Rh(2)-O(3) | 2.024(6) |
| Rh(2)-O(5) | 2.039(6) |
| Rh(2)-O(6) | 2.300(6) |

**Table II.6.** Selected bond angles (°) for compound **6b**.

| | Bond Angles (°) |
|---|---|
| O(1)-Rh(1)-Rh(2) | 171.4(2) |
| O(6)-Rh(2)-Rh(1) | 172.5 (2) |
| N(1A)-Rh(1)-O(1) | 89.1(2) |
| N(2A)-Rh(1)-O(1) | 90.3(2) |
| N(1B)-Rh(2)-O(6) | 89.0(2) |
| N(2B)-Rh(2)-O(6) | 87.8(3) |
| O(4)-Rh(1)-O(2) | 88.7(2) |
| O(3)-Rh(2)-O(5) | 88.9(3) |

The $^1$H NMR spectrum in $CDCl_3/CD_3OD$ (1:1, v:v) is consistent with retention of the solid-state structure of **6** dissolved in this mixture. Two acetate resonances are observed at 1.75 and 2.67 ppm corresponding to two free and two bridging acetates, respectively. The aromatic dppz protons appear at 7.73, 7.81, 7.90, 8.64 and 9.05 ppm, and are shifted upfield as compared to those of **5**. This shift is attributed to additional shielding of the dppz protons due to the close proximity of the second dppz ligand. Similar shifts of the aromatic protons were observed for *cis*-$[Rh_2(\mu\text{-}O_2CCH_3)_4(L)_2]^{2+}$ (L = bpy, phen), whose structures are similar to that of **6**.[45] The $^1$H NMR spectrum of **6** in solution is consistent with an eclipsed $C_{2v}$ symmetry of the ligands, indicating that a dynamic process is ocurring involving rotational oscillation about the Rh-Rh bond.[45]

*Synthesis and Structural Characterization of cis-*$[Rh_2(\mu\text{-}O_2CCH_3)_2(bpy)(dppz)](O_2CCH_3)_2$ ***(7)***

The complex *cis*-$[Rh_2(\mu\text{-}O_2CCH_3)_2(bpy)(dppz)](O_2CCH_3)_2$ (**7**) was prepared by refluxing *cis*-$[Rh_2(\mu\text{-}O_2CCH_3)_2(bpy)(\eta^1\text{-}O_2CCH_3)(CH_3OH)](O_2CCH_3)$ (**5**; 0.64 mmol) and dppz (0.65 mmol) in $CH_3CN$ (30 mL) for 24 h under $N_2$ (Scheme II.1). Crystals suitable for X-ray crystallography were grown from a solution of **7** in $CH_3OH$ in the presence of $NaBF_4$ and NaCl. The molecular structure of the complex cation consists of a dinuclear $Rh_2$(II,II) core with two acetato bridging ligands in *cis* disposition and chelating bpy and dppz ligands coordinated to each Rh atom. The axial positions are occupied by a chloride anion and a methanol molecule (Figure II.4). The Rh-Rh distance in **7**, 2.5529(5) Å, is similar to those found for **6** and **7**, 2.5519(6) and 2.567(1) Å,

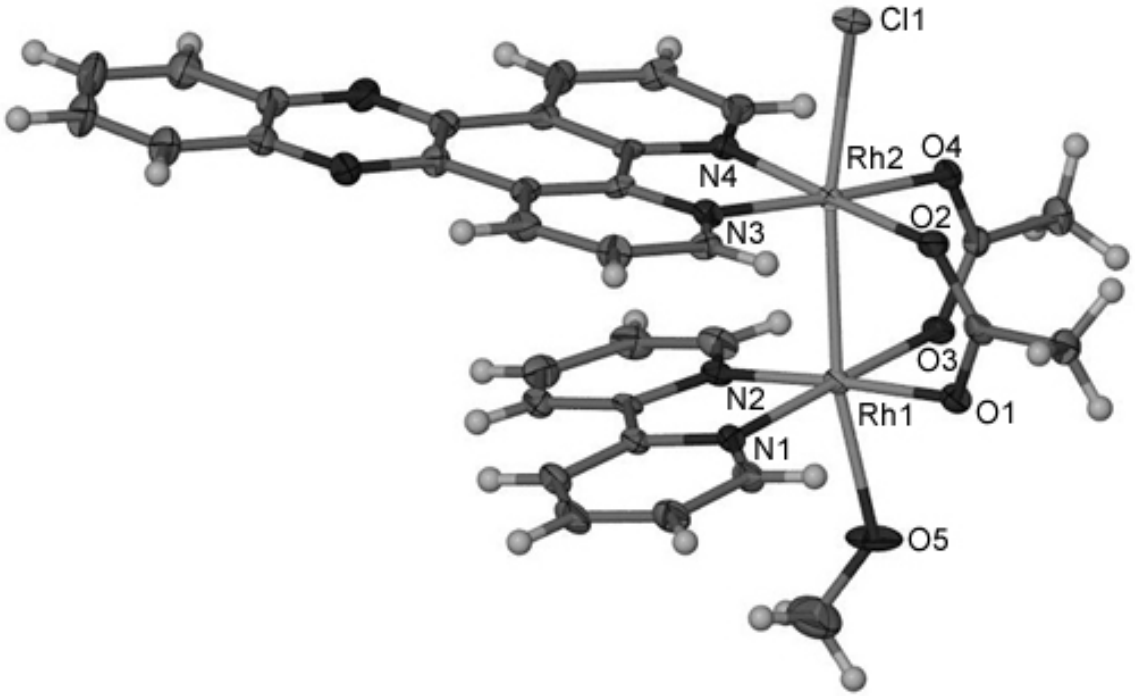


**Figure II.4.** Thermal ellipsoid plot at the 50% probability level of the cation in **7**.

respectively. The internal twist angle across the metal-metal bond of 9.0(5)° in **7** is smaller than the one observed for the bis-dppz analogue (13°) but larger than that of the corresponding bis-bpy complex (6.2°). The Rh-$O_{eq}$ bond lengths in **7**, which range from 2.041(6) to 2.055(6) Å, are longer than those in the analogous bis-dppz complex (2.009(2)-2.056(2) Å). The Rh-$N_{dppz}$ bonds, 2.006(3) to 2.011(3) Å, are similar to those found for **6a**, (2.005(4) to 2.016(4) Å), and **6b**, (1.995(7) to 2.018(7) Å). The Rh-$N_{bpy}$ bonds, 1.987(3) to 2.007(3) Å, are similar to those found for *cis*-[$Rh_2$($\mu$-$O_2CCH_3)_2$(bpy)$_2$($CH_3CN)_2$]($PF_6)_2$ (1.984(11) to 2.003(10) Å). Selected crystal crystal data parameters for compounds **7** are listed in Table II.7. A summary of selected bond distances and angles for compound **7** is listed in Tables II.8 and II.9, respectively.

The $^1$H NMR spectrum of complex **7** in $CDCl_3/CD_3OD$ (1:1, v:v) is similar to those observed for **6** and *cis*-[$Rh_2$($\mu$-$O_2CCH_3)_2$(bpy)$_2$]($O_2CCH_3)_2$. The heteroleptic compound **7** exhibits peaks at 7.32 (d, 2H, bpy), 7.45 (t, 2H, bpy), 7.61 (t, 2H, bpy) 7.92 (m, 2H, dppz), 8.16 (m, 2H, dppz), 8.47 (d, 2H, bpy), 8.50 (m, 2H, dppz), 8.78 (d, 2H, dppz), and 9.51 (d, 2H, dppz) ppm. A greater shielding of the aromatic protons engaged in $\pi$-stacking interactions typically results in upfield shifts of the $^1$H NMR resonances. Such shifts are observed in the bpy ligand of **7**, which exhibits larger upfield shifts than those reported for the bis-bpy complex, as a consequence of increased shielding of the bpy ligand in **7**.

**Table II.7.** Crystal data and structural refinement parameters for compound **7**.

| | |
|---|---|
| Empirical formula | $C_{36}H_{39}BF_4ClN_6O_8Rh_2$ |
| Formula weight | 1011.81 |
| Temperature | 110(2) K |
| Wavelength | 0.71073 Å |
| Crystal system | Monoclinic |
| Space group | P21/n |
| a | 11.855(2) Å |
| b | 20.514(4) Å |
| c | 16.602(2) Å |
| $\alpha$ | 90° |
| $\beta$ | 90.368(11)° |
| $\gamma$ | 90° |
| Volume | 4037.5(12) $Å^3$ |
| Z | 4 |
| Density (calculated) | 1.665 $g/cm^3$ |
| Crystal size | 0.33 x 0.09 x 0.02 $mm^3$ |
| Reflections collected | 46469 |
| Independent reflections | 9275 [R(int) = 0.0795] |
| Data / restraints / parameters | 9275 / 33 / 583 |
| Goodness-of-fit on $F^2$ | 1.087 |
| Final R indices [I>2sigma(I)] | R1 = 0.0473, wR2 = 0.0974 |
| R indices (all data) | R1 = 0.0975, wR2 = 0.1270 |

$R_1 = \Sigma||F_o| - |F_c||/\Sigma|F_o|$; $wR_2 = [\Sigma[w(F_0^2-F_c^2)^2]/\Sigma[w(F_0^2)^2]]^{1/2}$

**Table II.8.** Selected bond distances (Å) for compound **7**.

| | Bond Distances (Å) |
|---|---|
| Rh(1)-Rh(2) | 2.5529(5) |
| Rh(1)-N(1) | 1.987(3) |
| Rh(1)-N(2) | 2.007(3) |
| Rh(1)-O(1) | 2.041(2) |
| Rh(1)-O(3) | 2.055(2) |
| Rh(1)-O(5) | 2.273(3) |
| Rh(2)-N(4) | 2.006(3) |
| Rh(2)-N(3) | 2.011(3) |
| Rh(2)-O(4) | 2.051(2) |
| Rh(2)-O(2) | 2.056(2) |
| Rh(2)-Cl(1) | 2.4983(9) |

**Table II.9.** Selected bond angles (°) for compound **7**.

| | Bond Angles (°) |
|---|---|
| O5 Rh1 Rh2 | 169.21(7) |
| Cl1 Rh2 Rh1 | 171.19(2) |
| N1 Rh1 N2 | 80.7(1) |
| N4 Rh2 N3 | 81.6(1) |
| O1 Rh1 O3 | 88.13(9) |
| O4 Rh2 O2 | 88.98(9) |
| N1 Rh1 O5 | 90.4(1) |
| N2 Rh1 O5 | 91.5(1) |
| N4 Rh2 O4 | 95.4(1) |
| N3 Rh2 O4 | 176.1(1) |

**Electronic absorption and DNA binding**

The electronic absorption spectra of **5** and **6** in 5 mM Tris, 50 mM NaCl (pH = 7.0) are shown in Figure II.5, which are similar to those recorded in water, and in $CH_3OH$. The absorption at 360 nm ($\varepsilon$ = 11,700 $M^{-1}cm^{-1}$), 363 nm ($\varepsilon$ = 15,200 $M^{-1}cm^{-1}$), 363 ($\varepsilon$ = 15,170 $M^{-1}cm^{-1}$), and 360 ($\varepsilon$ = 16,400 $M^{-1}cm^{-1}$) observed in **5**, **6**, and **7**, respectively, can be assigned as arising from a dppz $\pi\pi^*$ ligand-centered (LC) transition. This LC transition at ~360 nm has also been observed in various dppz transition metal complexes.[107,119] In all complexes the absorption tails off into the visible region, with a maximum at 428 nm ($\varepsilon$ = 3,180 $M^{-1}cm^{-1}$) in **5**, at 434 nm ($\varepsilon$ = 5,460 $M^{-1}cm^{-1}$) in **6**, and at 378 nm ($\varepsilon$ = 2,710 $M^{-1}cm^{-1}$) in **7**. Similar transitions are also observed in the corresponding complexes of bpy at 424 nm ($\varepsilon$ = 2,010 $M^{-1}cm^{-1}$) in *cis*-$[Rh_2(\mu\text{-}O_2CCH_3)_2(bpy)(\eta^1\text{-}O_2CCH_3)(CH_3OH)]^+$ and 432 nm ($\varepsilon$ = 2,080 $M^{-1}cm^{-1}$) in *cis*-$[Rh_2(\mu\text{-}O_2CCH_3)_2(bpy)_2]^{2+}$,[45,117] as well as in $[Rh_2(\mu\text{-}O_2CCH_3)_2(L)_2]^{2+}$ (L = substituted 2,2′-bipyrine, 1,10-phenanthroline).[45] A weaker transition is observed for $Rh_2(O_2CCH_3)_4$ at 443 nm ($\varepsilon$ = 112 $M^{-1}cm^{-1}$) in water, which was previously assigned to Rh–Rh($\pi^*$) $\rightarrow$Rh–O($\sigma^*$). Since the intensity of the absorption at similar energies for **5**, **6**, and **7** are ~30 and ~50-fold more intense than that for $Rh_2(\mu\text{-}O_2CCH_3)_4$, it is likely that these transitions in the $Rh_2$-dppz family of complexes are charge transfer in nature and involve the dppz ligands. The weak absorption at $\lambda$ > 500 nm in each complex is believed to arise from metal-centered (MC) transitions associated with the bimetallic core, since they are also observed in $Rh_2(\mu\text{-}O_2CCH_3)_4$ and *cis*-$[Rh_2(\mu\text{-}O_2CCH_3)_2(L)_2]^{2+}$

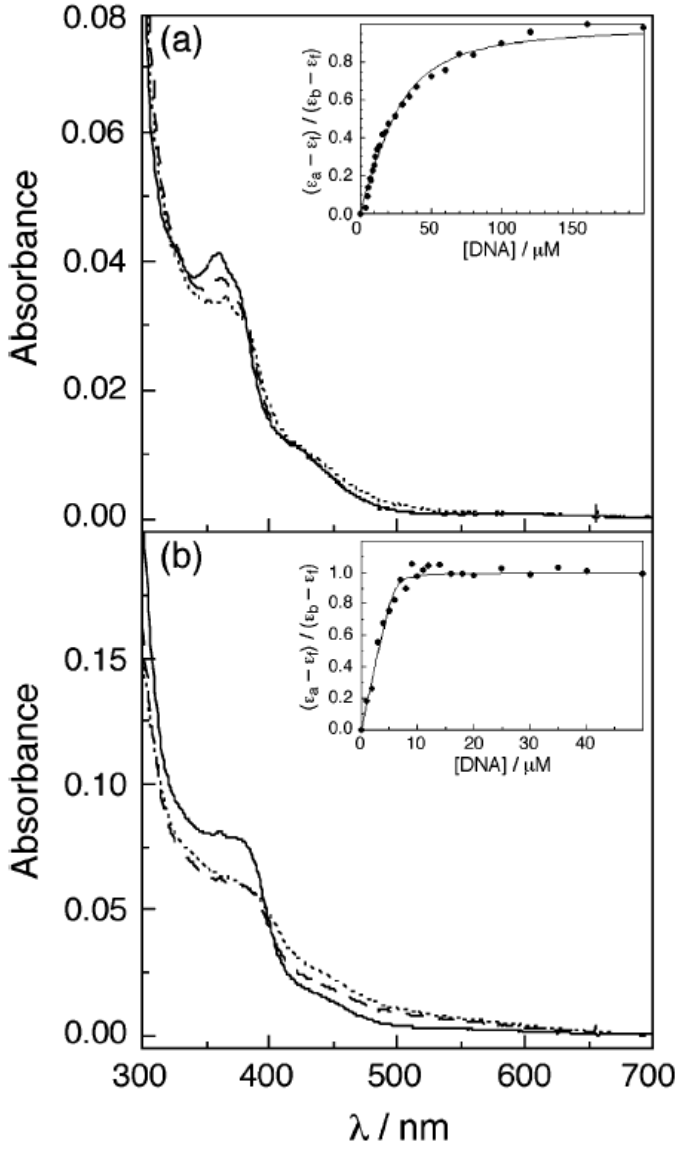


**Figure II.5.** Electronic absorption spectra of 5 μM (a) **5** and (b) **6** in 5 mM Tris (pH = 7.5) in water (——) and in the presence of 100 mM calf-thymus DNA (- - - ) and 100 mM PSS (— — ). Insets: fits of the absorption to eq 1 for (a) 6.2 μM **5** and (b) 3.2 μM **6** (see text).

(L = bpy, phen).[45,120,121] In $Rh_2(\mu\text{-}O_2CCH_3)_4$, the transition at 585 nm ($\varepsilon$ = 235 $M^{-1}cm^{-1}$) has been assigned to Rh–Rh($\pi^*$) $\rightarrow$Rh–Rh($\sigma^*$).

Negative deviations from Beer's law are observed for **5** and **6** in water at concentrations greater than 20 μM (360 nm) and 5 μM (363 nm), respectively. These deviations are likely due to hydrophobic interactions or intermolecular π-stacking of the dppz ligands, which are commonly observed for organic aromatic compounds and metal complexes with hydrophobic ligands in water.[122,123] The aggregation appears to be more pronounced for the bis-dppz complex, **6**, than for **5**, consistent with the more hydrophobic nature of the former arising from the presence of a second dppz ligand in the coordination sphere.

The spectral changes of 5 μM solutions (5 mM tris, 50 mM NaCl, pH = 7) of **5** and **6** upon addition of 100 μM DNA are shown in Figure II.5. Complexes **5**, **6**, and **7** exhibit pronounced hypochromism of the dppz ππ* transition, but only **5** and **6** exhibit a bathochromic shift. Binding of a 5 μM concentration of the complex to DNA results in 18% hypochromicity in **5** at 360 nm, 22% in **6** at 363 nm, and 27% in **7** at 366. Similar hypochromicity was reported for $[Ru(NH_3)_4(dppz)]^{2+}$ and $[Ru(phen)_2(dppz)]^{2+}$, which are believed to bind to DNA through intercalation of the dppz ligand with binding constants, $K_b$, of $1.24\times10^5$ $M^{-1}$ (*s* = 0.02) and $5.1\times10^6$ $M^{-1}$ (*s* = 0.6), respectively.[119] Fits of eq 1 using the decrease in the dppz ππ* absorption as a function of increasing DNA concentration for various concentrations of **5** and **6** in 5 mM Tris (pH = 7.0) results in $K_b$ = $4.4(7)\times10^5$ $M^{-1}$, *s* = 2.1(3) and $K_b$ = $7.0(9)\times10^6$ $M^{-1}$, *s* = 0.9(1), respectively. Typical

fits are shown in the insets of Figure II.5 for 6.2 μM **5** and 3.2 μM **6** in 5 mM Tris (pH = 7.0). Addition of 50 mM NaCl (5 mM Tris, pH = 7.0) leads to a small decrease in the apparent binding constant of **5**, with $K_b = 2.4(9)\times10^5$ $M^{-1}$, $s = 1.4(3)$, and a greater decrease in that of **6**, $K_b = 1.3(6)\times10^6$ $M^{-1}$, $s = 1.0(3)$.

Hypochromic and bathochromic shifts of LC transitions in aromatic ligands typically arise from π-stacking interactions in polar solvents, which, in this case, may result from intercalation between the DNA bases or from the formation of aggregates of the hydrophobic molecules in water.[120-123] It had been shown previously that polyanions facilitate the aggregation of cationic hydrophobic molecules on their surface in aqueous media,[65,124-126] including those which use DNA as a template.[127] The structure of **5** (Scheme II.1), with a single dppz ligand protruding from the dirhodium core, suggests that the complex should be able to intercalate between the DNA bases without significant steric constraints. A similar complex, $[Rh_2(\mu\text{-}O_2CCH_3)_2(dap)(\eta^1\text{-}O_2CCH_3)(CH_3OH)]^+$ (dap = 1,2-diazaperylene), has been shown by 2D NMR spectroscopy studies to bind through a intercalative as well as an coordinative mode to DNA.[128] As observed in Figure II.6, the proposed model contains the perylene unit intercalated between the DNA bases, whereas one of the rhodium atoms is bound to N7 of one of the adenine bases. In contrast, from the distance between the outermost rings of the two dppz ligands in the crystal structures of **6a** and **6b** (3.494(7) Å and 3.503(6) Å, respectively), one would not expect that the complex could intercalate between the DNA bases, which are ~3.4 Å apart in B-DNA. In the case of compound **7**, partial intercalation could be possible since a section of the

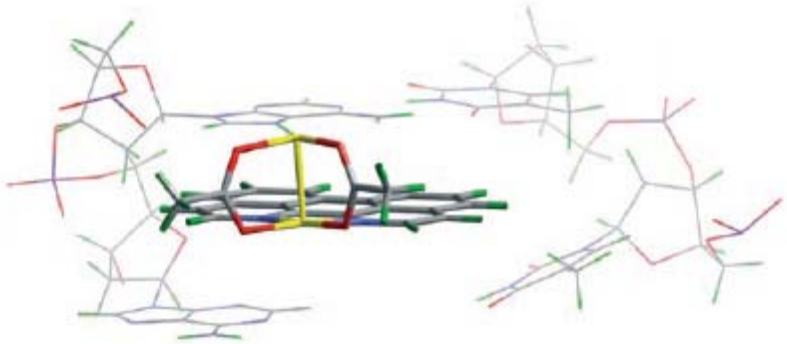

**Figure II.6.** Proposed binding model for $[Rh_2(\mu\text{-}O_2CCH_3)_2(dap)(\eta^1\text{-}O_2CCH_3)(CH_3OH)]^+$ (taken from ref. 128).

dppz ligand extends beyond the volume occupied by the bpy ligand. In spite of these logical predictions, the apparent DNA binding constant obtained from the hypochromicity of the dppz-centered transition (eq 1) of **6** is 16 times higher than that of **5**. The greater ionic strength effect on the binding constant of **6** compared to **5** may be due to greater aggregation of the former on the anionic DNA backbone. Such templated aggregation may be explained by electrostatic binding of the cationic complexes to the phosphate backbone of the host DNA polyanion, coupled to cooperative intermolecular hydrophobic interactions between the dppz ligands. The fitted value of *s*, the number of DNA bases associated with the complex, also provides information on surface aggregation. The values of *s* obtained from the fits range from 1.4 to 2.0 for complex **5**, but values of $s \leq 1$ are obtained for **6**. Aggregation of hydrophobic molecules on the DNA surface result in low values of the binding site size, with $s < 1$.[119] Therefore, both the ionic strength dependence and value of *s* are consistent with greater surface aggregation (π-stacking) of **6** relative to **5** aided by the anionic DNA backbone.

Additional experiments aimed at the elucidation of the possible intercalation and surface aggregation of **5** and **6** were performed. These include optical titrations with PSS (PSS = polystyrene sulfonate), a polyanion that does not support intercalation, shifts in the DNA melting temperature, and changes in viscosity of the DNA solutions in the presence of **5** and **6**.

The spectral changes to solutions of **6** that result from titrations with PSS are nearly superimposable with those observed in the presence of similar concentrations of DNA (Figure II.5). Figure II.5b shows the absorption changes to a 5 μM solution of **6** (5

mM Tris, pH = 7.0) upon addition of 100 μM PSS and 100 μM DNA, where similar hypochromicity is observed in the presence of both polyanions. Although some spectral changes are evident when a comparable experiment is performed with **5** (Figure II.5a), the addition of 100 μM DNA results in greater hypochromicity (18%) than PSS (11%). The changes in absorption for both complexes in the presence of PSS can be attributed to enhanced aggregation of **5** and **6** induced by the polyanion; the hypochromicity observed in **6** in the presence of DNA is solely due to surface aggregation driven by electrostatic and hydrophobic interactions, whereas **5** exhibits both surface aggregation and intercalation. This type of aggregation has been shown to take place in aqueous media for cationic hydrophobic molecules and metal complexes with a variety of polyanions, including dendrimers, PSS, and DNA.[120-124]

As shown in Figure II.7a, the melting temperature ($T_m$) of 100 μM calf-thymus DNA in 5 mM phosphate buffer, 2 mM NaCl (pH = 7.2) was measured to be 57 ± 2 °C. A small shift in $T_m$ to 63 ± 2 °C was observed in the presence of 20 μM **6** (Figure II.7a). A similar $\Delta T_m$ was also observed upon addition of 20 μM $MgCl_2$ ($\Delta T_m$ = 5 °C), an indication that the modest shift is due to the presence of a divalent cation and not intercalation. In contrast, Figure II.7a shows that the addition of 20 μM **5** to the DNA solution results in a large shift in the melting temperature to 78 ± 2 °C. The large increase in the DNA melting temperature observed for **5**, $\Delta T_m$ = 21 °C, is consistent with intercalation of the complex and is similar to that previously measured for the known intercalator $[Rh(phi)_2(phen)]^{3+}$ (phi = 9,10-phenanthrenequinone diimine).[129]

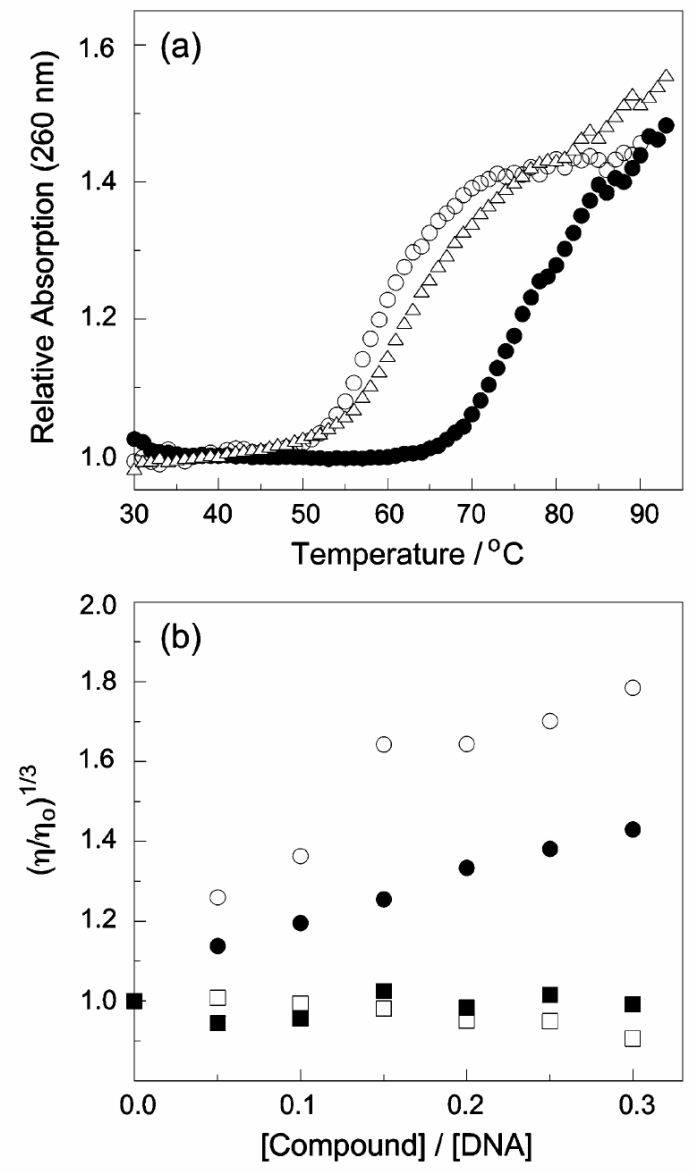


**Figure II.7.** (a) Thermal denaturation of 100 μM calf-thymus DNA (1 mM phosphate, 2 mM NaCl, pH = 7.2) alone (o), and with 20 μM **5** (•) and **6** (Δ). (b) Relative viscosity changes of solutions containing 200 μM sonicated herring sperm DNA as the concentration of EtBr (o), **5** (•), Hoechst 33258 (□), and **6** (■) is increased (see text).

Intercalation of molecules between DNA bases is known to increase the viscosity of the solution owing to unwinding and elongation of the double helix.[130] It is evident from Figure II.7b that the addition of **5** to DNA results in an increase in the relative viscosity of the solution, although to a lesser extent than the changes observed for the same concentration of ethidium bromide (EtBr) which is known to intercalate between the DNA bases with $K_b = 1.7 \times 10^5$ $M^{-1}$.[131,132] In contrast, similar concentrations of **6**, and **7**, much like the minor groove binder Hoechst 33258, do not result in changes in the relative viscosity (Figure II.7b). Since the DNA binding constants measured by using dialysis were $1 \times 10^4$ $M^{-1}$, $4 \times 10^3$ $M^{-1}$ and $2.8 \times 10^3$ $M^{-1}$ for **5**, **6**, and **7** respectively, the greater increase in viscosity observed for EtBr as compared to **5** at each [probe]/[DNA] is likely due to the lower binding constant of the latter to DNA.

The large $\Delta T_m$ and increase in viscosity induced by **5** are consistent with its intercalation between the DNA bases, whereas the modest value of $\Delta T_m$ and the lack of increase in viscosity support a non-intercalative binding mode for both **6** and **7**. It should be noted that the DNA binding constants measured using dialysis for **5** and **6** are ~2-3 orders of magnitude lower than those determined from the optical titrations, which can be explained by the aggregation of **5** and **6** aided by the DNA polyanion. These results clearly demonstrate the importance of using several techniques to ascertain whether intercalation is occurring and underscore the fact that optical titrations alone may result in erroneous assignments of DNA binding modes and binding constants.

**DNA photocleavage**

As shown in Figures II.8a and II.9, **5**, **6**, and **7** are able to photocleave plasmid DNA upon absorption of photons in the visible region ($\lambda_{irr} \geq 395$ nm, 15 min). The control lane in Figure II.8a (Lane 1), which contains 100 μM pUC18 plasmid alone in the dark, shows the position of the undamaged supercoiled pUC18 plasmid (Form I) with a small amount of nicked, circular DNA (Form II). The migration of cut, linear plasmid (Form III) is depicted in Lane 2 (Figure II.8a) for pUC18 plasmid treated with *Sma*I restriction enzyme. It is evident from Lanes 3 and 5 (Figure II.8a) that exposure of 100 μM pUC18 plasmid to 20 μM **5** and **6** in the dark, respectively, does not result in DNA cleavage. Irradiation of 100 μM pUC18 in the presence of 20 μM **5** and **6** ($\lambda_{irr} \geq$ 395 nm, 15 min) results in the formation of nicked DNA (Form II), as shown in Lanes 4 and 6, respectively (Figure II.8a). Although complex **6** exhibits ~30% greater molar absorptivity than **5** at ~430 nm, greater photocleavage is observed for **5** (Lane 4) as compared to **6** (Lane 6). The difference in the DNA photocleavage may be due to the ability of **5** to intercalate, thus resulting in greater reactivity. The photocleavage of 100 μM pUC18 plasmid (form I) by 10 μM **7** ($\lambda_{irr} \geq 395$ nm, 15 min) is shown in Figure II.9. Lane 1 shows the position of 100 μM pUC18 plasmid alone in the dark, and it is similar to Lane 3 (plasmid + **7** in the dark), which reveals that **7** does not cleave the plasmid without irradiation. Nicked, circular plasmid (form II) is formed upon irradiation of **7** with visible light in air (lane 4) and in deoxygenated solution (lane 5).

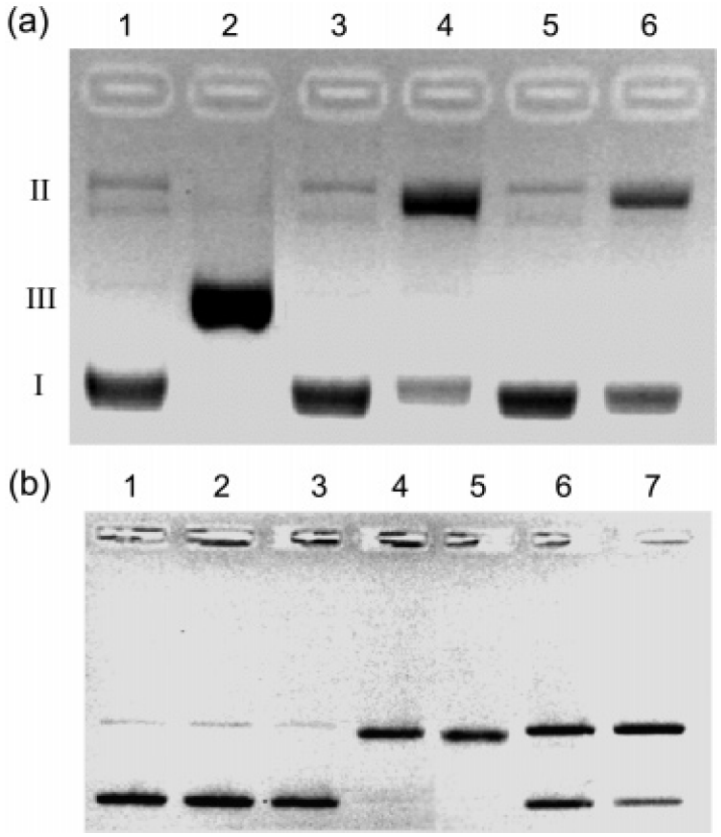


**Figure II.8.** Ethidium bromide stained agarose gels (2%) of 100 μM pUC18 plasmid in the presence of 20 μM metal complex in 5 mM Tris, 50 mM NaCl (pH = 7.5) irradiated with $\lambda_{irr} > 395$ nm. (a) Lane 1: plasmid only, dark; Lane 2: plasmid + *Sma*I; Lane 3: plasmid + **5**, dark; Lane 4: plasmid + **5**, irr. 15 min; Lane 5: plasmid + **6**, dark; Lane 6: plasmid + **6**, irr. 15 min. (b) Lane 1: plasmid only, dark; Lane 2: plasmid only, irr. 20 min; Lane 3: plasmid + **6**, dark; Lane 4: plasmid + **6**, irr. 20 min, air; Lane 5: plasmid + **6**, irr. 20 min, 50% $D_2O$; Lane 6: plasmid + **6**, irr. 20 min, under $N_2$; Lane 7: plasmid + **6**, irr. 20 min, freeze-pump-thaw.

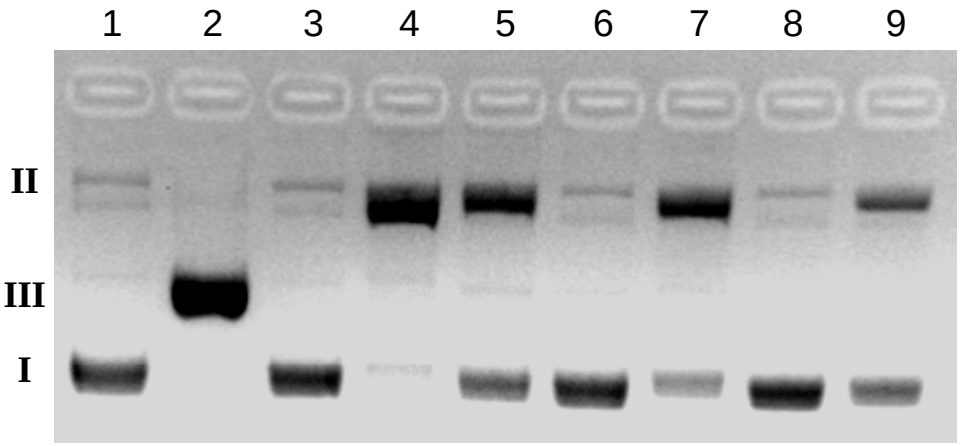


**Figure II.9.** Ethidium bromide stained agarose gel (2%) of 100 μM pUC18 plasmid, showing the photocleavage ($\lambda_{irr}$ > 395 nm, 15 min) by 10 μM metal complex in 5 mM Tris, 50 mM NaCl, pH = 7.5. Lane 1: plasmid, dark; Lane 2: plasmid + SmaI; Lane 3: plasmid + **7**, dark; Lane 4: plasmid + **7**, irr., air; Lane 5: plasmid + **7**, irr, freeze-pump-thaw; Lane 6, plasmid + **5**, dark; Lane 7: plasmid + **5**, irr, air; Lane 8: plasmid + **6**, dark; Lane 9: plasmid + **6**, irr., air.

Although some of the photocleavage by these complexes observed with $\lambda_{irr} \geq$ 395 nm appears to depend on the presence of oxygen, cleavage is still observed in deoxygenated solutions. Figure II.8b shows that irradiation ($\lambda_{irr} \geq$ 395 nm, 20 min) of 100 μM plasmid alone (5 mM Tris, pH = 7.5, 50 mM NaCl) does not result in photocleavage (Lanes 1 and 2). The amount of photocleavage by 20 μM **6** (5 mM Tris, pH = 7.5, 50 mM NaCl) is similar when conducted in 50% $D_2O$ (Lane 5) as compared to that in $H_2O$ (Lane 4) under similar conditions. Samples containing 100 μM plasmid and 20 μM **6** (5 mM Tris, pH = 7.5, 50 mM NaCl) bubbled with $N_2$ (Lane 6) or subjected to five freeze-pump-thaw cycles (Lane 7) resulted in slightly less photocleavage than those performed in air (Lane 4), but a significant degree of photocleavage is apparent under deoxygenated conditions. Figure II.9 shows that **7** is also able to photocleave DNA in the absence of oxygen (Lane 5); although, similar to **5** and **6**, to a lesser degree. These results indicate that oxygen plays a role in the observed DNA photocleavage of **5**, **6** and **7**, but that an oxygen-independent pathway that results in cleavage is also operative. The DNA photocleavage by Rh(III) complexes possessing 9,10-phenanthrenequinone diimine (phi) ligands had been previously shown to follow both oxygen-dependent and independent mechanisms.[133]

It should be noted that $Rh_2(\mu\text{-}O_2CCH_3)_4$ (**1**), and $[Rh_2(\mu\text{-}O_2CCH_3)_2(phen)_2](O_2CCH_3)_2$ (**3**) do not photocleave DNA directly, but require an electron acceptor in solution for reactivity.[60] It is believed that the photogenerated mixed-valent $Rh_2$(II/III) complex is the reactive species that effects DNA cleavage.[60] As

shown in Figures II.8 and II.9, **5**, **6**, and **7** are able to photocleave DNA directly, without an electron acceptor in solution. Recent calculations and experimental results concerning metal-to-ligand charge transfer (MLCT) excited states of Ru(II) and Re(I) dppz complexes may explain the difference in photoreactivity observed for the dirhodium-dppz family of complexes as compared to $Rh_2(\mu\text{-}O_2CCH_3)_4$ (**1**) and $[Rh_2(\mu\text{-}O_2CCH_3)_2(phen)_2](O_2CCH_3)_2$ (**3**). Experiments and calculations support the conclusion that the lowest-lying excited states in $[Ru(bpy)_2(dppz)]^{2+}$ and fac-$[Re(CO)_3(dppz)(py)]^{+}$ are Md$\rightarrow\pi^*$(phz) MLCT in nature, and that the transferred electron is localized in the phenazine (phz) part of the dppz ligand.[134,135] In both complexes this $^3$MLCT state is non-emissive, and emission is observed from a slightly higher energy triplet state in equilibrium with the Md$\rightarrow\pi^*$(phz) $^3$MLCT. A different ordering of states was later calculated for $[Ru(bpy)_2(dppz)]^{2+}$, but it was still predicted that the lowest-lying $^3$MLCT state remained localized on the phenazine part of the dppz ligand.[136] In **5**, **6** and **7**, a similar low-lying Md$\rightarrow\pi^*$(phz) $^3$MLCT state is present as shown by DFT and TD-DFT calculations (Chapter III). The spatial separation of the charge would be expected to render this excited state long-lived, which would then result in DNA cleavage by the oxidized dirhodium core.

**Cytotoxicity and photocytotoxicity**

The toxicity of all the complexes towards human skin cell (Hs-27) cultures was determined by measuring the percent survival in the presence of various amounts of complex relative to a control, that was not exposed to cytotoxic agents. Interpolation of

the data points was used to determine the concentration of complex required to achieve 50% cell death, $LC_{50}$ (LC = lethal concentration). The photocytotoxicity was determined from measurements of $LC_{50}$ values for Hs-27 cell cultures exposed to 400-700 nm light for 30 min (5 J/cm$^2$). Table II.10 shows the cytotoxicity and photocytotoxicity of the compounds studied. As an example, plots of percent Hs-27 survival as a function of increasing concentrations of two of the compounds, **5** and **6**, in the dark and irradiated with visible light are shown in Figure II.10. The $LC_{50}$ values determined for compounds **1** – **4**, which do not contain the dppz ligand, in the dark are similar to those obtained upon irradiation (30 min exposure). In contrast, the metal complexes containing the electron acceptor dppz ligand show differences in the $LC_{50}$ values obtained under the same conditions. In the case of the mono-substituted compound, **5**, the $LC_{50}$ value determined in the dark is slightly higher than the one determined upon irradiation, 27 ± 2 μM and 21 ± 3 μM, respectively. Higher $LC_{50}$ values were measured for the bis-dppz compound **6** (135 ± 8 μM) and the mixed-ligand compound **7** (208 ± 10 μM) in the dark indicative of significantly lower cytotoxicity. Upon irradiation with visible light, the cytotoxicity of **6** and **7** increase significantly, resulting in $LC_{50}$ = 39 ± 1 μM and 44 ± 2 μM, respectively. There is also an increase in the cytotoxicity of the trifluoroacetato-bridged compound **8** ($LC_{50}$ = 58 ± 3) upon irradiation ($LC_{50}$ = 27 ± 1), although, it is not as high as those encountered for those with bridging acetate ligands **6** and **8**. It should be noted that the $LC_{50}$ value measured for **6** and **7** in the dark are either similar or higher to that of cisplatin (131 ± 10 μM) for Hs-27

**Table II.10.** Cytotoxicity ($LC_{50}$) and photocytotoxicity ($LC_{50}^{*}$) values.

| Complex | | $LC_{50}$ (μM)[a] | $LC_{50}^{*}$ (μM)[b] |
|---|---|---|---|
| Hematoporphyrin | | 21 ± 1 | 3.8 ± 0.2 |
| Cisplatin | | 131 ± 10 | 110 ± 8 |
| $Rh_2(\mu\text{-}O_2CCH_3)_4$ | **1** | 15 ± 2 | 13 ± 2 |
| $Rh_2(\mu\text{-}O_2CCF_3)_4$ | **2** | 7.7 ± 0.5 | 8.0 ± 0.5 |
| $[Rh_2(\mu\text{-}O_2CCH_3)_2(phen)_2]^{2+}$ | **3** | 290 ± 15 | 294 ± 15 |
| $[Rh_2(\mu\text{-}O_2CCF_3)_2(phen)_2]^{2+}$ | **4** | 152 ± 7 | 151 ± 8 |
| $[Rh_2(\mu\text{-}O_2CCH_3)_2(\eta^1\text{-}O_2CCH_3)(dppz)(MeOH)]^{+}$ | **5** | 27 ± 2 | 21 ± 3 |
| $[Rh_2(\mu\text{-}O_2CCH_3)_2(dppz)_2]^{2+}$ | **6** | 135 ± 8 | 39 ± 1 |
| $[Rh_2(\mu\text{-}O_2CCH_3)_2(dppz)(bpy)]^{2+}$ | **7** | 208 ± 10 | 44 ± 2 |
| $[Rh_2(\mu\text{-}O_2CCF_3)_2(dppz)_2]^{2+}$ | **8** | 58 ± 3 | 27 ± 1 |

[a] Hs-27 human skin cells exposed to each compound for 30 min in the dark.

[b] Hs-27 human skin cells exposed to each compound for 30 min under irradiation.

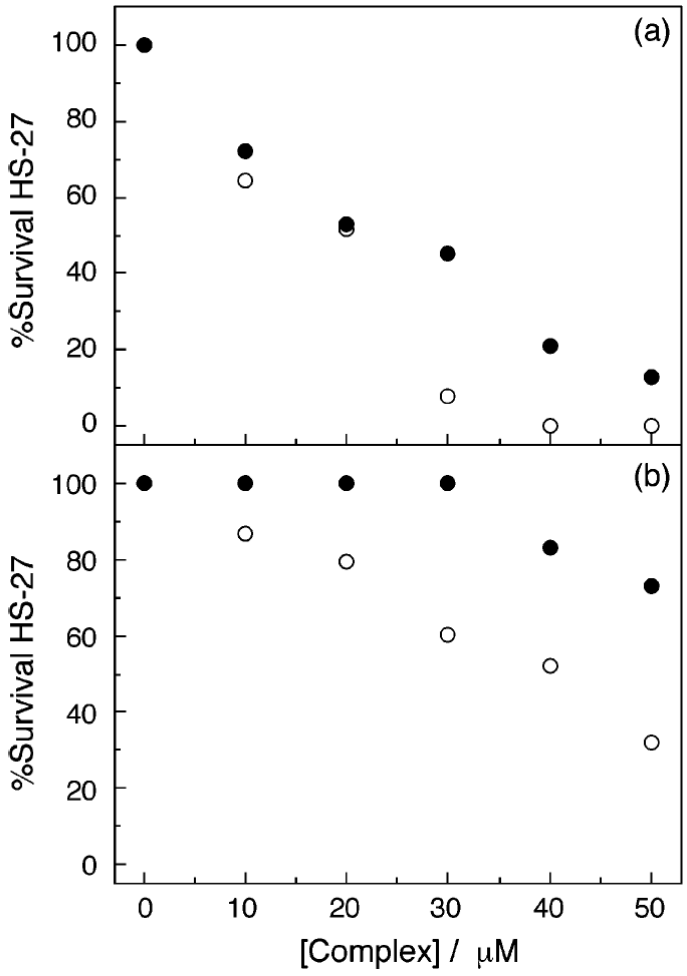


**Figure II.10.** Plot of percent survival of human skin cells (Hs-27) as a function of concentration of (a) **5** and (b) **6** in the dark (•) and irradiated with 400–700 nm light for 30 min (o).

cells under similar experimental conditions in the dark. As expected, irradiation with visible light has little effect on the cytotoxicity of cisplatin, $LC_{50}$ = 110 ± 10 μM. It should be noted that the $LC_{50}$ value measured here for cisplatin is generally greater than those previously reported, however, the difference can be explained by the short exposure time required for the direct comparison to the photolyzed samples in the present study and different toxicity of the complex as a function of cell line. For comparison the $LC_{50}$ values reported for 24 hr exposure to cisplatin of human epidermal cells, human uterus cancer cells (HeLa), and human leukemia cells (U-937) were <4 μM, 8 μM, and 50 μM, respectively.[137,138] In a different study, 24 hr exposure of cisplatin to HeLa cells resulted in $LC_{50}$ = 0.50 ± 0.05 μM,[139] and human colon cancer cells in contact with cisplatin for 2 hr led to $LC_{50}$ = 26 μM.[140] In addition, the $LC_{50}$ values recently reported for a variety of cells lines for cisplatin range from 7 μM to 164 μM (24 hr).[141]

The cytotoxic effect of **5** in the dark is not unexpected given its ability to intercalate DNA and shift its melting temperature by 21 $^{o}$C. These features may disrupt crucial cellular functions, such as transcription and DNA replication. Irradiation of Hs-27 cultures exposed to **5** with visible light does not appear to result in significant additional cell death, although the DNA photocleavage by **5** is greater than what is observed for **6** (Figure II.9a). In contrast, the $LC_{50}$ values of **6** and **7** decrease upon photolysis. Figure II.10 shows 100% survival of Hs-27 cells exposed to 30 μM **6** in the dark, but the same concentration of **6** results in ~40% cell death when the culture is irradiated with visible light. Also, the cytotoxicity of **7** is increased in a 79 ± 10% upon

irradiation, which is similar to that determined for the main component of Photofrin®, hematoporphyrin, which exhibits a 82 ± 10% increase under these irradiation conditions. Compound **7**, however, has the advantage of being less cytotoxic than hematoporphyrin in the dark. The inability of **6** and **7** to intercalate the DNA base π-stack may account for their low $LC_{50}$ value in the dark relative to that measured for **5**. Additional factors besides intercalation, however, are likely to play a role in the cytotoxicity of dirhodium complexes, since the $LC_{50}$ values for the non-intercalating complex $Rh_2(\mu\text{-}O_2CCH_3)_4$ ($K_b = 4.6 \times 10^2\ M^{-1}$) are 15 ± 2 μM and 13 ± 2 μM in the dark and irradiated, respectively. Also, compound **8** has a moderately high cytotoxicity ($LC_{50}$ = 58 ± 3) despite the fact that is unable to intercalate due to the presence of the two dppz ligands as in compound **6**. Nevertheless, the low toxicity of **6** and **7** in the dark and their increase upon irradiation are desirables features for a potential photochemotherapy agent, where an otherwise nontoxic compound becomes lethal upon exposure to low energy visible light.

*Concluding Remarks*

New dirhodium complexes possessing the ligand dipyrido[3,2-a:2′,3′-c]phenazine (dppz), *cis*-$[Rh_2(\mu\text{-}O_2CCH_3)_2(\eta^1\text{-}O_2CCH_3)(dppz)(MeOH)]^+$ (**5**), $[Rh_2(\mu\text{-}O_2CCH_3)_2(dppz)_2]^{2+}$ (**6**), $[Rh_2(\mu\text{-}O_2CCH_3)_2(dppz)(bpy)]^{2+}$ (**7**), and $[Rh_2(\mu\text{-}O_2CCF_3)_2(dppz)_2]^{2+}$ (**8**) were synthesized and characterized. These complexes photocleave pUC18 plasmid in vitro under irradiation with visible light ($\lambda_{irr} \geq 400$ nm, 15-20 min), resulting in the nicked, circular form. The toxicity of these complexes toward human skin cells increases when the cell cultures are irradiated with visible light. In particular, compound **7** shows an increase in its cytotoxicity upon irradiation similar to that of hematoporphyrin. Although the mechanism that results in cell death by photolysis of **7** remains unknown, this compound is a promising candidate for further PDT studies.

# CHAPTER III

# EFFECT OF GLUTATHIONE ON THE ACTIVITY OF DIRHODIUM(II,II) DPPZ COMPLEXES

## *Introduction*

The main goals of medicinal chemistry are to find new lead compounds as well as to continually improve the properties of old ones. It is clear that, to succeed in the latter objective, it is necessary to understand the chemical properties and the reactivity of the compound of interest. Recent advances in understanding the mechanism of action of dirhodium compounds have been discussed in some detail in Chapter I. It is well known that most of these agents have DNA as their main target,[35] but they can also readily react with proteins and peptides, particularly those containing nitrogen and sulfur atoms.[142-146] Glutathione (γ-glutamylcysteinyl, GSH), a non-protein tripeptide is the most prevalent intracellular thiol with concentrations up to 10 mM.[147,148] The presence of glutathione can be either detrimental or favorable to the activity of the metal complexes.[147-149] For example, a study performed on human small cell lung carcinoma showed that, in cisplatin-resistant cells, the amount of GSH is higher than in the parent sensitive cells.[148] Nevertheless, in the case of platinum(IV) complexes, which undergo ligand substitution reactions more slowly than their platinum(II) analogues, the presence of thiol-containing molecules is required to activate by reduction the more reactive +2 state.[149]

Studies of the interaction of $Rh_2(\mu\text{-}O_2CCH_3)_4$ and its analogues with S-based compounds have determined the importance of these reactions in the activity of these complexes.[35] Early reports by Bear and coworkers revealed that $Rh_2(\mu\text{-}O_2CCH_3)_4$ can

inhibit enzymes containing sulfhydryl groups in or near their active site, while enzymes lacking this group were not affected. Table III.1 lists enzymes with and without the sulfhydryl groups along with the inhibitory activity by $Rh_2(\mu\text{-}O_2CCH_3)_4$.[143]

Subsequent research has been devoted to the understanding of the reactivity of dirhodium(II,II) complexes with sulfur-containing molecules; information gathered to this point, however, does not allow for a complete picture of the reaction mechanism to be revealed. For instance, the formation of an axial adduct of $Rh_2(\mu\text{-}O_2CCH_3)_4$ and $C_6H_5CH_2SH$ was reported in 1980 (Figure III.1).[150] It has also been observed by using $^1$H-NMR spectroscopic titration that L-cysteine displaces acetate ligands from $Rh_2(\mu\text{-}O_2CCH_3)_4$ without disrupting the $Rh_2$ core.[151] A report from our group focused on the reactions of $[Rh_2(O_2CCH_3)_2(\text{diimine})_2(CH_3CN)_2]^{2+}$ (diimine = bpy, phen) with benzene thiolate and 2-aminothiophenol, which acted as mimics of L-cysteine and glutathione, respectively.[145-146] It was shown that, when the dirhodium complex reacts with a 10-fold excess of thiolate, the two acetate molecules are displaced and the product formed, $Rh_2(\eta^1\text{-}C_6H_5S)_2(\mu\text{-}C_6H_5S)_2(\text{diimine})_2$, contains a $Rh_2$(II,II) unit bridged by thiolate molecules. If this complex is exposed to a flow of $O_{2(g)}$ for 15 minutes, the $Rh_2$ unit is disrupted and only Rh(III) complexes are recovered as products.[145-146] From this last study a reaction scheme (Figure III.2) was proposed by us which shows that the $Rh_2$ unit is stable to the presence of the thiolate ligands until $O_{2(g)}$ is introduced in the reaction.[146]

**Table III.1** Inhibitory activity of $Rh_2(\mu\text{-}O_2CCH_3)_4$ (modified from ref. 143)

| Enzyme | Inhibition by $Rh_2(\mu\text{-}O_2CCH_3)_4$ |
|---|---|
| Glucose oxidase* | No |
| Peroxidase* | No |
| Pyruvate kinase | Yes |
| Glycerolphosphate dehydrogenase | Yes |
| Glucose-6-phosphate dehydrogenase | Yes |

* Enzymes without essential sulfhydryl groups.

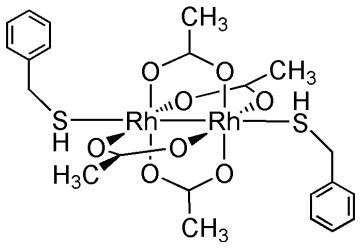


**Figure III.1.** Schematic representation of adduct formed between $Rh_2(\mu\text{-}O_2CCH_3)_4$ and $C_6H_5CH_2SH$.

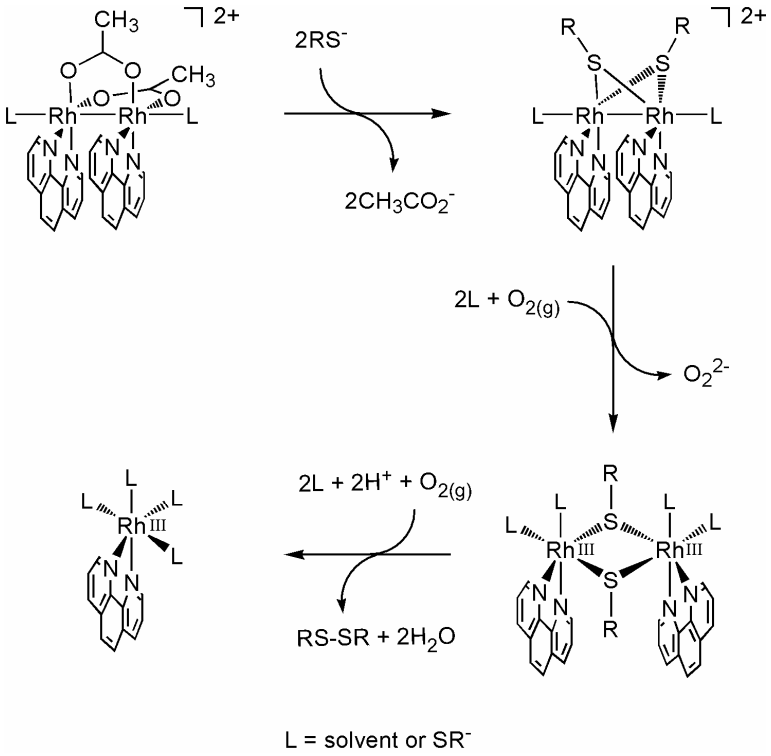


**Figure III.2.** Diagram of the proposed mechanistic pathway of the reactions between $[Rh_2(\mu\text{-}O_2CCH_3)_2(phen)_2]^{2+}$ and molecules containing sulfhydryl group.

The research described in this chapter involves the reactivity of compounds of the $[Rh_2(\mu\text{-}O_2CCH_3)_2(dppz)(N\text{-}N)]^{2+}$ type, where N-N = dppz (dipyrido[3,2-*a:2',3'-c*]phenazine), and bpy (2,2'-bipyridine), with glutathione, as well as the effect of glutathione in the DNA-photocleavage ability of dirhodium(II,II) dppz complexes. In addition, DFT and TD-DFT calculations on the model complex $[Rh_2(\mu\text{-}O_2CCH_3)_2(dppz)(bpy)(H_2O)_2]^{2+}$ are presented in order to explain the behavior of the dirhodium-dppz family of complexes in the presence of glutathione.

## *Experimental Section*

### Materials

Sodium chloride, sodium phosphate, gel loading buffer (0.05% (w/v) bromophenol blue, 40% (w/v) sucrose, 0.1 M EDTA (pH = 8.0), 0.5% (w/v) sodium lauryl sulfate), Tris base, Tris/HCl, and ethidium bromide were purchased from Sigma and used as received. The pUC18 plasmid was purchased from Bayou Biolabs and purified using the Concert Miniprep System from Life Technology. *Sma*I was purchased from Invitrogen and used as received. Acetonitrile, and dichloromethane were dried over 3 Å and 4 Å molecular sieves, respectively, and distilled under a nitrogen atmosphere prior to use. $RhCl_3$ was purchased from Pressure Chemicals Inc. The reagents sodium acetate, 2,2'-bipyridine, 1,10-phenanthroline were purchased from Acros and used without further purification. The ligands L-cysteine and glutathione were purchased from Sigma and used without further purification. HPLC-grade water and glacial acetic acid were obtained from EM. The compounds $Rh_2(\mu\text{-}O_2CCH_3)_4$ and dppz

(dppz = dipyrido[3,2-*a:2′,3′-c*]phenazine) were synthesized by previously reported methods.[105,106]

**Methods**

*DNA Photocleavage*

The DNA photocleavage experiments were carried out using 20 μL of total sample volume in 0.5 mL transparent eppendorf tubes containing 100 μM pUC18 plasmid and 20 μM of each metal complex. Irradiation of the solutions was performed either in air for ~20 minutes. Following irradiation, 4 μL of the DNA gel loading buffer was added to each 20 μL sample. The electrophoresis was carried out using either 1% or 2% agarose gel stained with 0.5 mg/L eithidium bromide in 1X TAE buffer (40 mM tris-acetate, 1 mM EDTA, pH ~ 8.2); other conditions are specified as needed.

*Computational Details*

Density functional theory (DFT) calculations were performed with the hybrid Becke-3 parameter exchange functional and the Lee-Yang-Parr non-local correlation functional (B3LYP) implemented in the Gaussian 98 program suite.[152-154] Geometry optimizations were carried out using the SDD basis set-relativistic effective core potential (RECP), which combines the Huzinaga–Dunning double-ζ basis set on the main group elements with the Stuttgart–Dresden basis set-RECP combination on the rhodium metals, while for all other atoms, the 6-311G(d) basis set was employed.[155] To model the $Rh_2$ complexes in aqueous solution, the molecules were embedded in a dielectric medium as an approximation to include solvent polarization effects. The inclusion of the dielectric medium was considered using the Tomasi's Polarized

Continuum Model (PCM) reaction field model for the optimization of molecular geometry and the calculation of excitation energies.[156-157] Time-dependent calculations were performed using the Gaussian program suite. All calculations were done on an Altix 3700 128-processor SGI computer located at the Texas A&M supercomputing facility.

*Reactions between $[Rh_2(\mu\text{-}O_2CCH_3)_2(dppz)_2](O_2CCH_3)_2$ **(6)** and Glutathione (GSH)*

To separate aqueous solutions (5 mL) of **6** (0.1 mM) was slowly added 1, 2, 3, 4, and 5 mL of an aqueous solution (pH = 7) of GSH (1.0 mM). In all cases, the red-orange solutions rapidly turned blue as the GSH was added. The reaction was followed using UV-spectroscopy. The blue color remains for ca. 8 for the solution containing 1 mL of 1.0 mM of GSH, and up to ~24 hours for the solution treated with 5 mL of 1.0 mM of GSH. After which time the reaction mixture slowly turns to an orange color.

*Reactions between $[Rh_2(\mu\text{-}O_2CCH_3)_2(dppz)(bpy)](O_2CCH_3)_2$ **(7)** and Glutathione (GSH)*

To separate aqueous solutions (5 mL) of **7** (0.1 mM) was slowly added 1, 2, 3, 4, and 5 mL of an aqueous solution (pH = 7) of GSH (1.0 mM). In all cases, the red-orange solutions instantaneously turned blue as the GSH was added. The reaction was followed using UV-spectroscopy. The blue color persisted for ca. 12 for the solution containing 1 mL of 1.0 mM of GSH, and up to ~28 hours for the solution treated with 5 mL of 1.0 mM of GSH. After which time the reaction mixture slowly turns to an orange color.

*Reactions between $[Rh_2(\mu\text{-}O_2CCH_3)_2(bpy)_2](O_2CCH_3)_2$ **(9)** and Glutathione (GSH)*

An aqueous solution (5 mL) of **9** (0.1 mM) was slowly treated with 1, 2, 3, 4, and 5 mL of an aqueous solution (pH = 7) of GSH (1.0 mM). In all cases, the red-orange

solutions quickly turned blue as the GSH was added, and after a period of c.a. 1.0 - 1.5 hours they became dark yellow in color.

*Reduction of $[Rh_2(\mu\text{-}O_2CCH_3)_2(dppz)_2](O_2CCH_3)_2$ **(6)** in Ethanol*

A solution of $Rh_2(\mu\text{-}O_2CCH_3)_2(dppz)_2](O_2CCH_3)_2$ (**6**) in ethanol (10 mL) was refluxed under $N_2$(g) for 15 minutes. During the course of the reaction an intense blue color developed, which disappeared upon exposure of the solution to air.

*Reduction of $[Rh_2(\mu\text{-}O_2CCH_3)_2(dppz)(bpy)](O_2CCH_3)_2$ **(7)** in Ethanol*

A solution of $Rh_2(\mu\text{-}O_2CCH_3)_2(dppz)(bpy)](O_2CCH_3)_2$ (**7**) in ethanol (10 mL) was refluxed under $N_2$(g) for 15 minutes. During the course of the reaction an intense blue color developed, which disappeared upon exposure of the solution to air.

*Single-cell Electrophoresis*

Human skin cells (~500,000 cells), Hs-27, were incubated with 120 μM **7** for 30 min in PBS (PBS with $Ca^{2+}$ and $Mg^{2+}$). Irradiation was conducted with visible light (400-700 nm) for 30 min, after which the cells were embedded in 1% low melting agarose in PBS without $Ca^{2+}$ or $Mg^{2+}$. The cells were immediately lysed in cold lysis solution (2.5 M NaCl, 100 mM EDTA, 1% N-laurylsarcocine, 10 mM Tris-base, pH = 10, with 10% DMSO and 1% Triton X-100) for one hour at 4 °C. The DNA was allowed to unwind for 20 min in electrophoresis buffer (300 mM NaOH, 1 mM EDTA, pH = 13.2) at 4°C and the gel was washed in neutralizing buffer (400 mM Tris-HCl, pH = 7.5) three times for 5 min. The gel was run at 20 V, 300 mA for 20 min. The gel was stained with propidium iodide and was imaged under a fluorescence microscope in the orange range of the spectrum at 562-588 nm ($\lambda_{exc}$ = 488 nm).[155]

*Results and Discussion*

**Reactions between $[Rh_2(\mu\text{-}O_2CCH_3)_2(dppz)_2](O_2CCH_3)_2$ (6) and $[Rh_2(\mu\text{-}O_2CCH_3)_2(dppz)(bpy)](O_2CCH_3)_2$ (7) with glutathione (GSH)**

The reactions of $[Rh_2(\mu\text{-}O_2CCH_3)_2(dppz)_2](O_2CCH_3)_2$ (**6**) and $[Rh_2(\mu\text{-}O_2CCH_3)_2(dppz)(bpy)](O_2CCH_3)_2$ (**7**) with different amounts of glutathione (GSH), ranging from 2 to 10 equivalents undergo the same color change and produce a deep blue colored solution. An intense new absorption band ($\varepsilon = 1.1 \times 10^2$ $M^{-1}cm^{-1}$) at ~810 nm appears in the visible spectrum. The color remains for hours until it slowly disappears to give an orange solution. The final UV spectra do not show the original band at 810 nm, and they resemble the spectra of the initial compounds. The changes observed in compound **7** when reacted with 2 equivalents of reduced glutathione are shown in Figure III.3. The lifetime of the blue product was measured and is shown in Table III.2.

**Table III.2** $t_{1/2}$ of product formed by the reaction of **6** and **7** with GSH

| Compound | Equivalents of GSH | $t_{1/2}$ (hours)[a] |
|---|---|---|
| **6** | 2 | 08.0 ± 0.2 |
| | 4 | 10.1 ± 0.2 |
| | 6 | 14.2 ± 0.3 |
| | 8 | 18.5 ± 0.3 |
| | 10 | 23.8 ± 0.5 |
| **7** | 2 | 12.5 ± 0.2 |
| | 4 | 16.2 ± 0.3 |
| | 6 | 20.5 ± 0.3 |
| | 8 | 24.3 ± 0.5 |
| | 10 | 28.2 ± 0.7 |

[a] $t_{1/2}$ was obtained from the average of two individual measurements

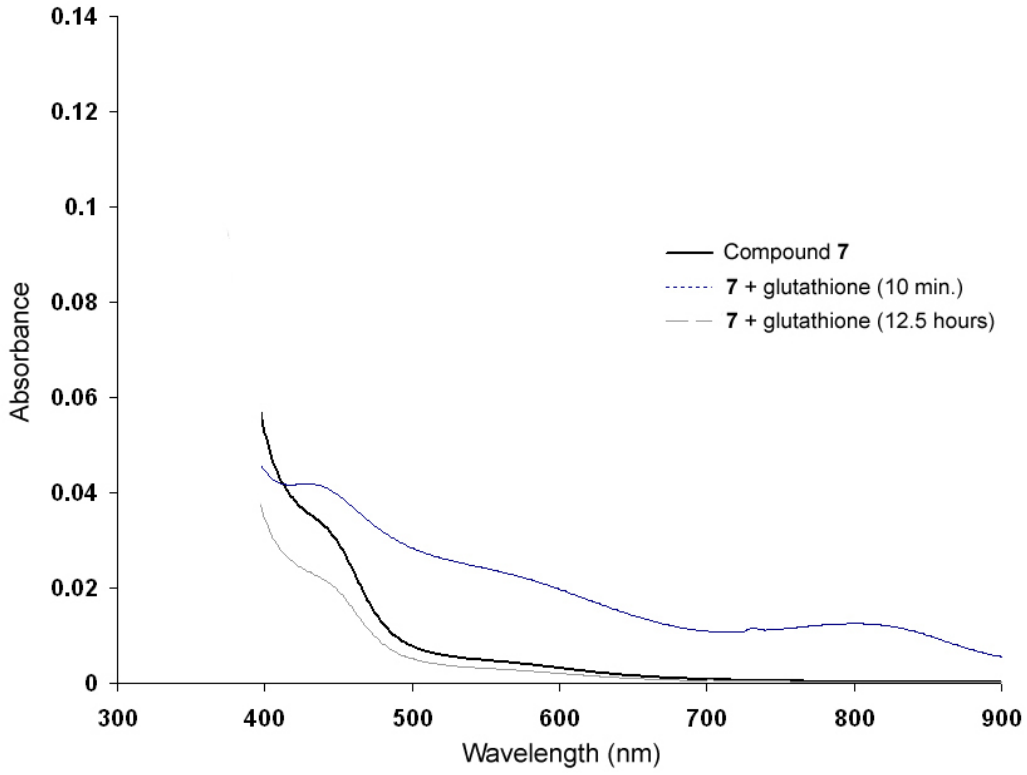


**Figure III.3.** Changes observed in the UV-spectrum of compound **7** after the addition of glutathione.

As observed in Figure III.3, after the blue compound disappears the initial compound **7** is partially regenerated (~65%). The same result is observed for compound **6** (~69%). Results from the ESI-MS experiments also provide additional evidence that the parent compounds are regenerated. Aliquots of each of the reactions were analyzed by this technique and in all cases the main peaks belong to oxidized glutathione and compounds **6** or **7**, respectively. Minor peaks also appeared, which are most likely due to partial decomposition of the compounds, although no assignment was possible.

In the case of compound $[Rh_2(\mu\text{-}O_2CCH_3)_2(bpy)_2](O_2CCH_3)_2$ (**9**), which does not contain the dppz ligand, no initial compound was recovered after the reaction, as observed by UV-spectroscopy. This result was confirmed by ESI-MS, which did not reveal any peaks corresponding to the dirhodium species. The yellow-brown precipitate recovered is insoluble in water and methanol. Products of the same color and similar solubility properties are also obtained from the reactions of **6** and **7** with glutathione, and this is the source of the loss of ~30 - 35 % of the complexes observed in the UV spectra.

It is known that dirhodium complexes of the general structure $[Rh_2(\mu\text{-}O_2CCH_3)_2(diimine)_2]^{2+}$ (diimine = bpy, phen) are reduced in the presence of an alcohol such as ethanol or isopropanol.[159-161] Pruchnik *et al*. reported several examples in which the diimine complexes were reduced by one electron after refluxing a solution of the compound in either ethanol or isopropanol/water under $N_{2(g)}$.[159-161] During the reaction, the solution turns blue, and the reduced complex is isolated. In order to test if compounds containing the dppz ligand are reduced in the same manner, solutions of compounds **6** and **7** in ethanol were refluxed under $N_{2(g)}$ for 15 minutes. The solution

changes color from yellow-orange to blue, which indicates the formation of the reduced species. This process is reversible and the original complex can be recovered by exposing the solution to air. The blue color obtained in these reactions resembles the color observed in the reactions of **6** and **7** with reduced glutathione.

To obtain more information about the reactions of the $Rh_2$-dppz complexes with glutathione, EPR studies of the blue compound were undertaken. A sample of the reaction of **7** with two equivalents of GSH was examined by EPR spectroscopy. Figure III.4 shows the frozen-glass (77 K) EPR spectra of the blue product of the reaction of **7**. The spectrum is isotropic with $g \approx 2.0$, and the signal is broad (≈ 50 G), suggesting a delocalized organic radical. There is no hyperfine splitting due to $^{103}$Rh (I = ½) centers, which suggests that the radical is mainly delocalized on the ligand(s). Isotropic signals with similar characteristics have been observed previously by Bear and co-workers, who reported that upon reduction of members of the family of $[Rh_2(\mu\text{-}O_2CCH_3)_3(L)]^+$ complexes, L = multidentate ligand containing a 1,8-naphthyridine fragment (Figure III.5), isotropic signals with $g = 1.99$ with no hyperfine splitting due to $^{103}$Rh were obtained.[162] The authors concluded that the electron was added to a ligand-based orbital and that extensive delocalization of the electron was the cause of the broad signal.[162] In addition, our group reported an EPR spectroscopic measurement of the product of the one-electron reduction of $[Rh_2(\mu\text{-}O_2CCH_3)_2(bpy)_2][O_2CCH_3]_2$ in an acetonitrile frozen glass solution as a broad featureless isotropic signal at $g \approx 2.00$.[44] Therefore, it is plausible to assume that GSH reduces the $Rh_2$-dppz complexes to form a radical species

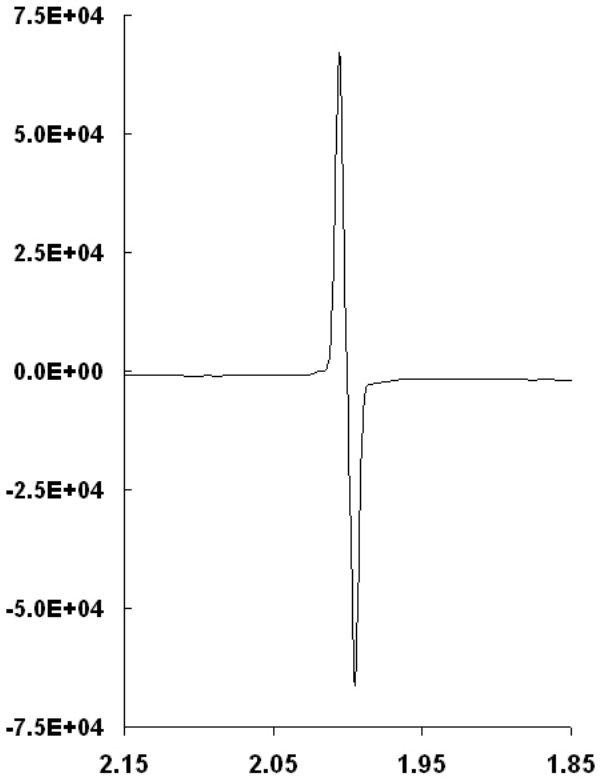


**Figure III.4.** EPR spectrum of compound **7** after the addition of glutathione.

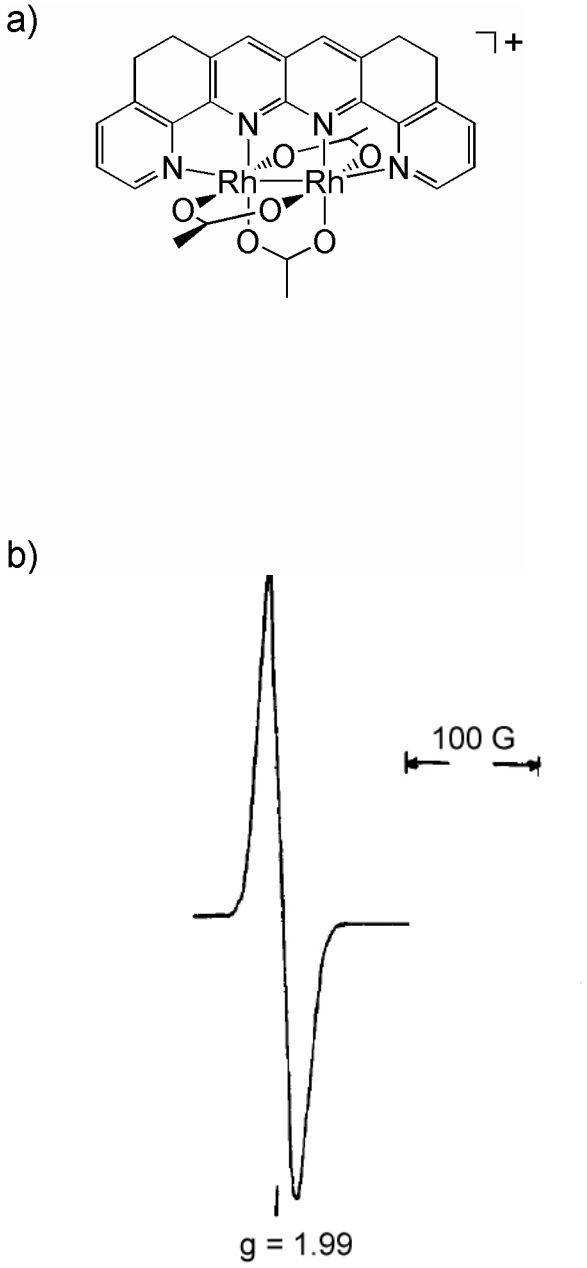


**Figure III.5.** a) Dirhodium complex used in the study by Bear and co-workers (see text) b) EPR spectrum of complex shown in (a) after reduction (taken from ref. 162).

with the electron delocalized on the ligand(s). Exposure to air regenerates the initial $Rh_2^{II/II}$ compound.

The afore-mentioned results would only be possible if the LUMO of the dirhodium-dppz complexes is a mainly ligand-based orbital. It is well known that dirhodium complexes possess an electronic structure that is mainly dominated by the $Rh_2$ core. For example, in $Rh_2(\mu\text{-}O_2CCH_3)_4$ the HOMO and LUMO are $\pi^*$ and $\sigma^*$ orbitals, respectively. The $\pi^*$ orbitals are formed by the out-of-phase interaction of the $d_{xz}$ and $d_{yz}$ metal orbitals, while the $\sigma^*$ orbital is originated from the rhodium $d_{z2}$ orbitals.[163,164] In our group, however, we have observed that some dirhodium complexes can have LUMO orbitals localized on the ligands and not on the metal centers.[44] It is evident that the nature of the frontier orbitals is important to understand the reaction between dirhodium-dppz complexes and sulphur-containing compounds such as glutathione.

**DFT calculations on the model complex $[Rh_2(\mu\text{-}O_2CCH_3)_2(dppz)(bpy)(H_2O)_2]^{2+}$**

DFT calculations were performed on the model complexes $Rh_2(\mu\text{-}O_2CCH_3)_4$ and $[Rh_2(\mu\text{-}O_2CH)_2(dppz)(bpy)(H_2O)_2]^{2+}$ and the results are summarized in Figure III.6 and Figure III.7.

In the parent complex $Rh_2(\mu\text{-}O_2CCH_3)_4$, the frontier orbitals of the $Rh_2(\mu\text{-}O_2CCH_3)_4$ complex are dominated by the metal-metal interaction. The electronic configuration of the $Rh_2$ core is as follows: $\sigma^2\pi^4\delta^2\pi^{*2}\delta^{*2}\sigma^{*0}\delta^{*0}$, with a net single bond

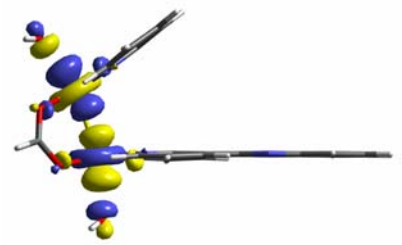

**LUMO + 2 (166), -0.09957 eV**

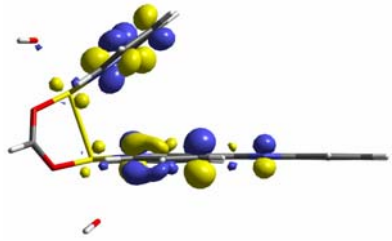

**LUMO + 1 (165), - 0.10080 eV**

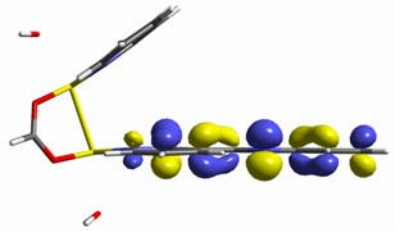

**LUMO (164), - 0.10749 eV**

**Figure III.6.** Illustration of the 0.04 contour surface diagrams for the DFT calculated three lowest unoccupied MOs for the model complex $[Rh_2(\mu\text{-}O_2CH)_2(dppz)(bpy)(H_2O)_2]^{2+}$.

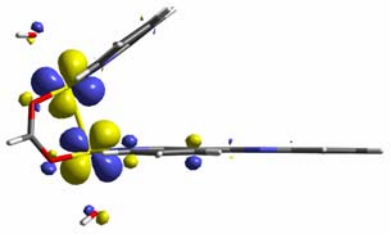

**HOMO (163), - 0.24640 eV**

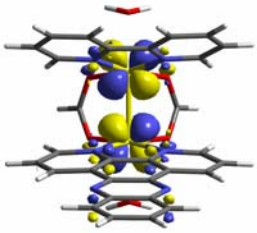

**HOMO – 1 (162), - 0.24718 eV**

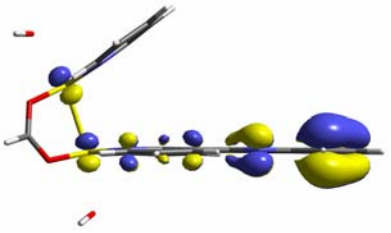

**HOMO – 2 (161), - 0.24846 eV**

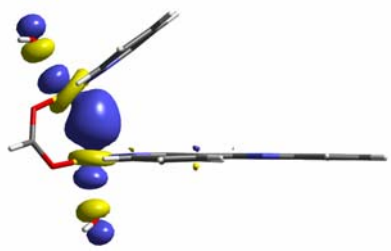

**HOMO – 3 (160), - 0.25153 eV**

**Figure III.7.** Illustration of the 0.04 contour surface diagrams for the DFT calculated four highest occupied MOs for the model complex $[Rh_2(\mu\text{-}O_2CH)_2(dppz)(bpy)(H_2O)_2]^{2+}$.

between the two rhodium atoms. The HOMO and LUMO orbitals of the $Rh_2(\mu\text{-}O_2CCH_3)_4$ molecule are the $\pi^*$ and $\sigma^*$ orbitals, respectively. The $\sigma$ and $\sigma^*$ bonds originated from the interaction between the rhodium $d_{z2}$ orbitals, whereas the $\pi$ and $\pi^*$ orbitals correspond to the overlap of the $d_{xz}$ and $d_{yz}$ metal orbitals. In addition, the positive and negative overlap between the two rhodium $d_{xy}$ orbitals form the $\delta$ and $\delta^*$ orbitals. The $d_{x2-y2}$ orbitals participate in the metal-ligand $\sigma$ bonds, and they are not as involved as the other metal orbitals in the metal-metal interaction. Note that the $\delta^*$ orbital is higher in energy than the $\pi^*$ orbital, a fact that can be explained by the interaction between the rhodium $d_{xy}$ orbitals and the $O_\pi$ orbitals that raise the energy of the $\delta^*$ orbital.

For the model complex $[Rh_2(\mu\text{-}O_2CH)_2(dppz)(bpy)(H_2O)_2]^{2+}$, two bridging ligands are replaced by two diimine molecules, dppz and bpy, each one on a different rhodium atom. The $\delta$ and $\delta^*$ orbitals are further stabilized with respect to the other orbitals, and the $\pi$ and $\pi^*$ orbitals are no longer doubly degenerate due the lower symmetry of the complex. As a consequence of the stabilization of the $\delta^*$ orbital, the HOMO in the model complex is a Rh-Rh $\pi^*$ orbital. The $[Rh_2]^{4+}\sigma^*$ orbital does not appear as the LUMO of the system. In addition, located between the $\pi^*_{[Rh\text{-}Rh]}$ (HOMO) and $\sigma^*_{[Rh\text{-}Rh]}$ orbitals are two ligand-based orbitals. The LUMO is a $\pi^*$ orbital of the dppz ligand, and the second-lowest unoccupied orbital (SLUMO) has predominantly bpy and dppz character.

**TD-DFT calculations on the model complex $[Rh_2(\mu\text{-}O_2CCH_3)_2(dppz)(bpy)(H_2O)_2]^{2+}$**

TD-DFT calculations were performed on the model complex $[Rh_2(\mu\text{-}O_2CH)_2(dppz)(bpy)(H_2O)_2]^{2+}$ and the results are summarized in Table III.3.

**Table III.3** Results of TD-DFT calculation on model complex $[Rh_2(\mu\text{-}O_2CCH_3)_2(dppz)(bpy)(H_2O)_2]^{2+}$

| Excited State | $\lambda$, nm ($f$) | Major contributions |
|---|---|---|
| 1 | 558.66 (0.0002) | 162 → 166 |
| 2 | 551.45 (0.0014) | 163 → 166 |
| 3 | 419.44 (0.0007) | 159 → 166 |
| 4 | 401.85 (0.0002) | 162 → 164 |
| | | 162 → 165 |
| 5 | 397.50 (0.0435) | 163 → 164 |
| | | 163 → 165 |
| 6 | 387.90 (0.1138) | 160 → 166 |
| | | 163 → 164 |
| 7 | 379.97 (0.0020) | 162 → 164 |

The optical spectra of $Rh_2$-dppz complexes in different solvents consist of a weak ($\varepsilon \approx 350$ $M^{-1}cm^{-1}$) low-energy band in the 550 - 600 nm region. The next feature is a shoulder that appears at ~430 nm with an $\varepsilon \approx 4000$ $M^{-1}cm^{-1}$. Stronger bands appear at ~400 nm ($\varepsilon \approx 15000$ $M^{-1}cm^{-1}$) and ~290 nm ($\varepsilon \approx 60000$ $M^{-1}cm^{-1}$). It must be highlighted, that the peak at 400 nm, as noted earlier, is very important for the DNA photocleavage properties of these complexes.

The lowest energy band, appearing at ~580 nm, is similar to the lowest energy transition in the parent molecule $Rh_2(\mu\text{-}O_2CCH_3)_4$. This peak has been previously

assigned to a $\pi^*_{[Rh\text{-}Rh]} \rightarrow \sigma^*_{[Rh\text{-}Rh]}$ transition. The TD-DFT calculations indicate that this band involves transitions from orbitals 162 (HOMO-1) and 163 (HOMO), which are $\pi^*_{[Rh\text{-}Rh]}$ in character, to the orbital 166 (LUMO), the $\sigma^*_{[Rh\text{-}Rh]}$ orbital.

In the case of the band appearing at ~400 nm, the results on the model complex $[Rh_2(\mu\text{-}O_2CCH_3)_2(dppz)(bpy)(H_2O)_2]^{2+}$ indicate that it belongs to a metal-to-ligand charge transfer (MLCT) band. The major contribution to this MLCT band is from the transitions arising from the HOMO $\pi^*_{[Rh\text{-}Rh]}$ orbital (163) to the LUMO (164) and LUMO+1 (165) orbitals (Table III.3). This band also has a minor contribution from transitions from one of the $\pi^*_{[Rh\text{-}Rh]}$ orbitals (162) to the ligand-based LUMO (164) and LUMO+1 (165) orbitals. It should be noted that this band appears in dirhodium complexes containing other diimine ligands, *e.g*; bpy, phen. Pruchnik *et al*., used the Fenske-Hall molecular-orbital method to study these complexes and also assigned this band to a charge-transfer transition, although the electron was said to originate from the $\sigma_{[Rh\text{-}Rh]}$ orbital.[165] The difference with respect to the present calculation is attributed to the different methods used.

**DNA photocleavage in the presence of glutathione**

As shown in Figures III.8 and III.9, both **6** and **7** are able to photocleave plasmid DNA upon absorption of photons in the visible region ($\lambda_{irr} \geq 395$ nm, 20 min). The control lanes in Figures III.8 and III.9 (Lane 1), which contain only 100 μM pUC18 plasmid alone in the dark, show the position of the undamaged supercoiled pUC18 plasmid with a small amount of nicked, circular DNA as an impurity. Irradiation of 100 μM pUC18 in the presence of 20 μM

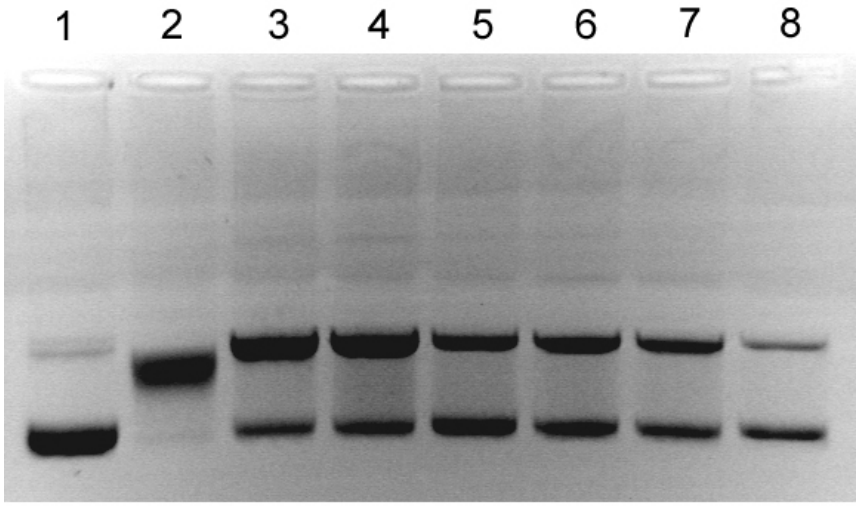


**Figure III.8.** Ethidium bromide stained agarose gel (2%) of 100 μM pUC18 plasmid, showing the photocleavage ($\lambda_{irr}$ > 395 nm, 20 min) by 20 μM metal complex in 5 mM Tris, 50 mM NaCl, pH = 7.5. Lane 1: plasmid, dark; Lane 2: plasmid + **6** + 50 μM glutathione, irr.; Lane 3: plasmid + **6** + 50 μM glutathione, irr.; Lane 4: plasmid + **6** + 100 μM glutathione, irr.; Lane 5: plasmid + **6** + 200 μM glutathione, irr.; Lane 6, plasmid + **6** + 300 μM glutathione, irr.; Lane 7: plasmid + **6** + 400 μM glutathione, irr.; Lane 8: plasmid + **6** + 500 μM glutathione, irr.

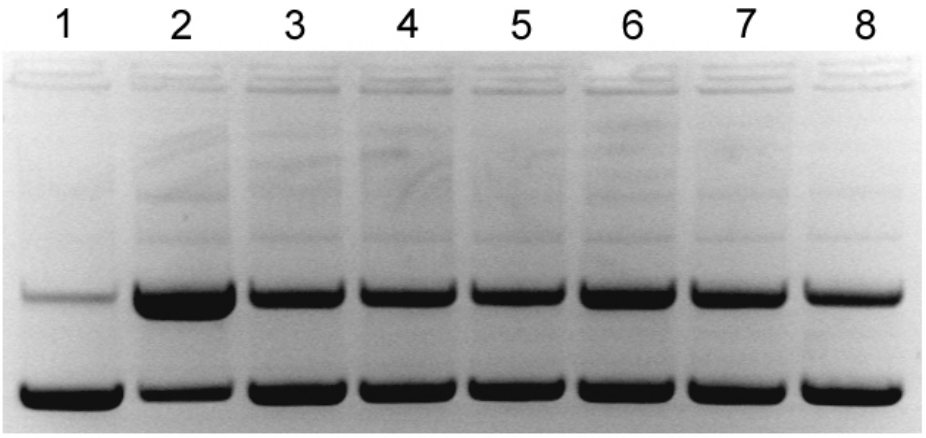


**Figure III.9.** Ethidium bromide stained agarose gel (2%) of 100 μM pUC18 plasmid, showing the photocleavage ($\lambda_{irr}$ > 395 nm, 20 min) by 20 μM metal complex in 5 mM Tris, 50 mM NaCl, pH = 7.5. Lane 1: plasmid, dark; Lane 2: plasmid + **7** + 50 μM glutathione, irr.; Lane 3: plasmid + **7** + 50 μM glutathione, irr.; Lane 4: plasmid + **7** + 100 μM glutathione, irr.; Lane 5: plasmid + **7** + 200 μM glutathione, irr.; Lane 6, plasmid + **7** + 300 μM glutathione, irr.; Lane 7: plasmid + **7** + 400 μM glutathione, irr.; Lane 8: plasmid + **7** + 500 μM glutathione, irr.

**6** and **7** ($\lambda_{irr} \geq 395$ nm, 20 min) results in the formation of nicked DNA, as shown in Lanes 2 of Figures III.8 and III.9. Lanes 3-8 show the effect of the addition of increasing amounts of glutathione (2.5 – 25 equivalents, 50 – 500 μM) on the ability of **6** and **7** to photocleave supercoiled pUC18 plasmid. As it can be observed, increasing the concentration of glutathione decreases the amount of cleaved DNA. This inhibition is not complete though, and even at quantities as high as 25 equivalents, compounds **6** and **7** are still active. A plausible explanation for this behavior is that glutathione reduces the metal complexes, and the compounds in this reduced state cannot transfer the electron from the dirhodium core to the ligand as efficiently as they can in their original oxidation state.

**Single-cell electrophoresis experiments**

The single-cell gel electrophoresis (SCGE) assay, also known as the comet assay, is a rapid and sensitive technique for detecting DNA damage at the level of individual cells.[158,166,167] The types of DNA damage that can be observed with this method are DNA single- and double-strand breaks, alkali labile sites, DNA-protein crosslinks, among others.[158,166,167] In the experiment, the cells are embedded in agarose gel and lysed under mild alkaline conditions to remove cellular proteins. During the electrophoresis, undamaged DNA migrates slowly and close to the nucleoid, whereas broken DNA fragments migrates away from the nucleoid, giving the appearance of a comet tail.

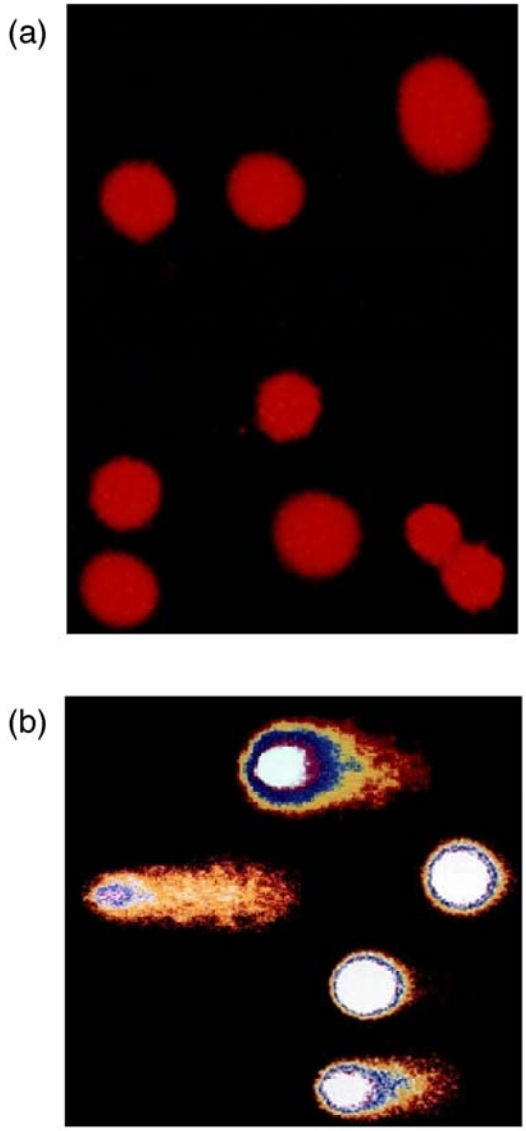


**Figure III.10.** Single cell electrophoresis of human skin cells exposed to 120 μM **7** for 30 min then (a) kept in the dark for 30 min and (b) irradiated with visible light for 30 min; the red color indicates stained DNA.

Single-cell electrophoresis experiments were performed in the presence of 120 μM **7** in the dark and under irradiation conditions with visible light in order to investigate if photolysis results in DNA damage (Figure III.10). Human skin fibroblasts contain glutathione in levels in the range of 5 - 10 nmol/$10^8$ cells (~ 50 – 100 μM) and represent an ideal model to study the effect of glutathione on the ability of these complexes to cleave DNA after irradiation.[168] When the human skin cells are exposed to **7** for 1 h in the dark, the stained DNA remains within the cells (Figure III.10a). In contrast, upon irradiation (30 min, 400-700 nm, 5 J/$cm^2$), approximately half of the cells exhibit a "comet tail" indicative of the presence of damaged DNA in the cells (Figure III.10b). This indicates that despite the presence of glutathione in the cells, compound **7** has the ability to cause damage to DNA localized in the cell nucleus. It is important to note, that in a study of hematoporphyrin, it was observed that this compound does not show comet tails either with or without irradiation.[169] From these results, it was concluded that the reactive species generated by photo-activated hematoporphyrin were unable to reach nuclear DNA.[169] In the case of compound **7**, it is possible that either the molecule itself or its photo-generated products are able to penetrate the nucleus and damage the DNA found in the interior.

*Concluding Remarks*

Glutathione reacts with $[Rh_2(\mu\text{-}O_2CCH_3)_2(dppz)_2]^{2+}$ (**6**), and $[Rh_2(\mu\text{-}O_2CCH_3)_2(dppz)(bpy)]^{2+}$ (**7**) producing a reduced complex that re-oxidizes to the original compound. Likewise, ethanol is also capable of reducing **6** and **7** under $N_{2(g)}$, and the process is reversed by exposing the solutions to air. The EPR spectrum of the reduced complex **7** is a broad, featureless isotropic signal ($g \approx 1.99$) that resembles those observed for other dirhodium complexes wherein the electron is delocalized onto the ligand. DFT calculations on the model complex $[Rh_2(\mu\text{-}O_2CH)_2(dppz)(bpy)\ (H_2O)_2]^{2+}$ show that, indeed, the LUMO and LUMO + 1 orbitals are mainly ligand in character, and it is concluded that the electron added upon reduction is delocalized onto the dppz ligand(s). The addition of glutathione in the photocleavage studies result in a decrease activity of the complexes, although it does not inhibit it completely. Compounds **6** and **7** can tolerate up to 25 equivalents of glutathione and still be capable of induce DNA cleavage upon irradiation. In this chapter it was also shown that compound **7** can damage DNA in human skin cells as observed in the single cell electrophoresis experiments.

# CHAPTER IV

# DIRHODIUM(II,II) COMPLEXES: UNDERSTANDING THEIR *IN VITRO* ACTIVITY*

## *Introduction*

Medicinal inorganic chemistry is an area of bioinorganic chemistry that is still in its infancy. The topic is at the interface between medicine and chemistry but differs from medicinal organic chemistry in two aspects: firstly, medicinal inorganic chemistry makes use of many more elements, and secondly it is less developed than its organic counterpart. Medicinal inorganic chemistry has witnessed some outstanding successes, most notably cisplatin for treatment of cancer and gadolinium complexes in magnetic resonance imaging (MRI) applications,[170-175] but there are many new promising applications to pursue.[176,177]

Therapeutic applications of inorganic compounds depend greatly not only on the metal ions themselves but also on the ligands bound to them. Ligands are useful for mediating the bioavailability of metal ions, they can deliver the compounds to certain tissues or organs, and more importantly they can modify the reactivity of the metal centers.[177-179] Therefore, studies aimed at the understanding of the effect of ligands and substitutents on a particular metal ion are important if improved therapeutic effectiveness is to be achieved.

---

* Reprinted in part from "Dirhodium (II,II) Complexes: Molecular Characteristics that Affect in Vitro Activity" Angeles-Boza, A. M.; Chifotides, H. T.; Aguirre, J. D.; Chouai, A.; Fu, P. K.-L.; Dunbar, K. R.; Turro, C. *J. Med. Chem.* **2006**, *49*(23), 6841-6847; 

Recent studies of various dirhodium compounds have indicated that there is a correlation between their molecular characteristics including the ligand environment and their cytotoxic behavior.[42,54-58] An important factor that likely affects the biological properties of these compounds is their ability to react with the cellular target(s), which includes the lability of the groups bound to the dirhodium core, and the presence of open coordination sites. Evidence of the importance of these factors can be found from the reactions of dirhodium compounds with single-stranded oligonucleotides containing dipurine sites. In these reactions the following order of reactivity was observed $Rh_2(O_2CCH_3)_4$ << *cis*-$[Rh_2(O_2CCH_3)_2(CH_3CN)_6](BF_4)_2$ < $Rh_2(O_2CCF_3)_4$, which correlates with the lability of the equatorial groups.[55] Furthermore, a recent study showed that the extent of interstrand cross-link formation by dirhodium compounds of a DNA fragment containing 123 base pairs also correlates with the lability of the leaving groups.[56] In this part of the thesis an evaluation of the type and lability of the equatorially bound groups to the dirhodium core on the cytotoxicity of the complexes towards human skin cells has been uundertaken. The determination of some general correlations between the molecular characteristics of these compounds and their cytotoxic behavior has been established. These findings are aimed at improving the design of more effective dirhodium compounds as potential drugs and PDT agents.

*Experimental Section*

**Materials**

The ligands dipyrido[3,2-*a*:2',3'-*c*]phenazine (dppz) and benzodipyrido[3,2-*a*:2',3'-*c*]phenazine (dppn) were synthesized according to reported procedures.[103;177] The dirhodium complexes $Rh_2(O_2CCH_3)_4$ (**1**), $Rh_2(O_2CCF_3)_4$ (**2**), $[Rh_2(O_2CCH_3)_2(phen)_2]^{2+}$ (**3**), $[Rh_2(O_2CCF_3)_2(phen)_2]^{2+}$ (**4**), $[Rh_2(\mu\text{-}O_2CCH_3)_2(\eta^1\text{-}O_2CCH_3)(dppz)(MeOH)]^{+}$ (**5**), $[Rh_2(O_2CCH_3)_2(dppz)_2]^{2+}$ (**6**), and $[Rh_2(O_2CCH_3)_2(dppz)(bpy)]^{2+}$ (**7**) were synthesized as reported in Chapter II. The starting material $RhCl_3 \cdot nH_2O$ was purchased from Pressure Chemicals and used as received. The compounds 2,2'-bipyridine (bpy), 1,10-phenanthroline (phen), 2,3-diaminonaphthalene were purchased from Acros. The compounds 9-ethylguanine (9-EtGuaH), sodium phosphate (dibasic, anhydrous) and NaCl were purchased from Sigma. The deuterated solvents $D_2O$-$d_2$, $CD_3COCD_3$-$d_6$, $CD_3OD$-$d_4$, and $C_6D_6$-$d_6$ were purchased from Aldrich.

*Synthesis of $[Rh_2(\mu\text{-}O_2CCF_3)_2(dppz)_2](O_2CCF_3)_2$* ***(8)***

A solution of $Rh_2(\mu\text{-}O_2CCF_3)_4$ (126.3 mg, 0.19 mmol) in $CH_3CN$ (16 mL) was treated with solid dppz (108.2 mg, 0.38 mmol) and the suspension was heated to reflux for 16 h. After this time period, the red mixture was cooled to room temperature, the solution was filtered and the red solid washed with $CH_3CN$. Yield = 206.7 mg, 89%. ESI-MS: *m/z* 499.2 ($[Rh_2(\mu\text{-}O_2CCF_3)_2(dppz)_2]^{2+}$). $^1$H NMR: ($CD_3OD/CDCl_3$) $\delta$ (ppm) 9.35 (d, 4H, dppz), 8.95 (d, 4H, dppz), 8.45 (m, 4H, dppz), 8.25 (m, 4H, dppz), 8.10 (m, 4H, dppz). Anal. Calcd for $C_{44}H_{20}N_8O_8F_{12}Rh_2 \cdot H_2O$: C, 42.60; H, 1.79; N, 9.03. Found: C, 42.64; H, 1.75; N, 8.98.

*Synthesis of [$Rh_2(\mu$-$O_2CCH_3)_2(\eta^1$-$O_2CCH_3)$(dppn)($CH_3OH$)]($O_2CCH_3$)* ***(10)***

A suspension of dppn (90 mg, 0.39 mmol) and $Rh_2(\mu$-$O_2CCH_3)_4(CH_3OH)_2$ (171 mg, 0.39 mmol) in acetone (15 mL) was stirred at room temperature under $N_2$ for 48 h. The resulting green precipitate was filtered and washed with acetone (3 x 5 mL). The solid was suspended in $CH_3OH$ (50 mL) and stirred at room temperature for 24 h. The resulting green solution was filtered, concentrated under reduced pressure to 2 mL, and the product was precipitated by addition of $Et_2O$. The green solid was collected by filtration, washed with $Et_2O$, and dried under vacuum (93 mg, 40%). $^1$H-NMR ($CD_3OD/CDCl_3$, 1:1 v:v) $\delta$ (ppm): 9.77 (d, 1H), 9.12 (s, 1H), 8.86 (dd, 1H), 8.35 (d, 1H), 8.15 (dd, 1H), 7.76 (dd, 1H), 2.49 (s, 3H, $CH_3CO_2$), 2.45 (s, 3H, $CH_3CO_2$), 2.02 (s, 3H, $CH_3CO_2$), 1.23 (s, 3H, $CH_3CO_2$); ESI-MS *m/z* 715 (100%, [$Rh_2(\mu$-$O_2CCH_3)_2$(dppn)($O_2CCH_3$)]$^+$).

*Synthesis of [$Rh_2(\mu$-$O_2CCH_3)_2$(dppn)$_2$]($O_2CCH_3)_2$* ***(11)***

A mixture of dppn (100 mg, 0.30 mmol) and $Rh_2(\mu$-$O_2CCH_3)_4(CH_3OH)_2$ (76.2 mg, 0.15 mmol) in $CH_3CN$ (10 mL) was heated under nitrogen for 24 h. After cooling, the precipitate was collected by filtration, washed with $CH_3CN$ (3 x 5 mL), and dried overnight under vacuum to provide a red solid (144 mg, 87%). $^1$H NMR ($CD_3OD$) $\delta$ (ppm): 9.03 (d, 1H), 8.62 (d, 1H), 8.08 (s, 1H), 7.73 (t, 1H), 7.60 (d, 1H), 7.41 (dd, 1H), 2.60 (s, 6H, $CH_3CO_2$), 1.73 (s, 6H, $CH_3CO_2$); MS *m/z* 494 (100%, [$Rh_2(\mu$-$O_2CCH_3)_2$(dppn)$_2$]$^{2+}$); Anal. Calcd for $C_{52}H_{36}N_8O_8Rh_2 \cdot 4H_2O$: C, 52.97; H, 3.76; N, 9.51. Found: C, 53.07; H, 3.42; N, 10.16.

*Synthesis of cis-[$Rh_2(\mu\text{-}O_2CCH_3)_2(dppn)(bpy)](O_2CCH_3)_2$* ***(12)***

Following the procedure described for *cis*-[$Rh_2(\mu\text{-}O_2CCH_3)_2(dppn)_2](O_2CCH_3)_2$, a mixture of **8** (270 mg, 0.35 mmol) and bpy (55 mg, 0.35 mmol) in $CH_3CN$ (10 mL) was heated under $N_2$ for 24 h to produce a dark red solid (173 mg, 42%). $^1$H NMR ($CD_3OD$) $\delta$ (ppm): 9.42 (d, 1H), 9.05 (s, 1H), 8.61 (d, 1H), 8.32 (d, 1H), 8.27 (dd, 1H), 7.78-7.68 (m, 3H), 7.53 (t, 1H), 7.31 (t, 1H), 2.57 (s, 6H, $CH_3CO_2$), 1.75 (s, 6H, $CH_3CO_2$); ESI-MS *m/z* 406 (100%, $[Rh_2(\mu\text{-}O_2CCH_3)_2(dppn)_2]^{2+}$); Anal. Calcd for $C_{52}H_{36}N_8O_8Rh_2 \cdot 4H_2O$: C, 47.90; H, 4.02; N, 8.38. Found: C, 47.96; H, 3.54; N, 8.69.

*Synthesis of [$Rh_2((\mu\text{-}O_2CCF_3)_2(CH_3CN)_6](BF_4)_2$* ***(13)***

To a 10 mL solution of $Rh_2(\mu\text{-}O_2CCF_3)_4$ (0.27 g, 0.61 mmol) in $CH_3CN/CH_2Cl_2$ (1/1) was slowly added a solution of 1.0 M $Et_3OBF_4$ in $CH_2Cl_2$ (1.4 mL). The solution was stirred at r.t. for 12 h. The volume was reduced to 4 mL under vacuum. The solid was recovered by filtration on a sintered glass frit and washed several times with cold $CH_3CN$. The crude purple product was redissolved in 7 mL of $CH_3CN$ and stored at -10 °C for 24 hours. Purple microcrystals of $[Rh_2((\mu\text{-}O_2CCF_3)_2(CH_3CN)_6](BF_4)_2$ were isolated by filtration and the product was dried under vacuum for 4 h. Yield = 0.32 g (60.1 %).$^1$H NMR ($CD_3CN$) $\delta$ (ppm): 2.46 (s, 12H), 1.96 (s, 6H).

*Synthesis of N,N'-di-p-fluoroformamidine ($DPh^FFH$)*

P-fluoroaniline (56.8 ml, 0.6 mol) was treated with ethylorthoformate (50.0 ml, 0.3 mol). The mixture was heated to reflux and the ethanol formed in the reaction was removed by distillation. The white solid that formed was dissolved in hot toluene and the

solution was stored for 48 h. White crystals of *N,N'*-di-*p*-fluoroformamidine were isolated by filtration. The product was recrystallized from toluene an additional time, and the white product was isolated by suction filtration and dried under vacuum for 12 h. Yield = 66.7 g (96.2 %). $^1$H NMR ($CDCl_3$) $\delta$ (ppm): 8.03 (s, 1H), 7.01 (s, 4H), 6.98 (s, 4H), 6.29 (s, 1H).

*Synthesis of [Rh(cod)(DPh$^F$F)]$_2$*

The compound [Rh(cod)(DPh$^F$F)]$_2$ was prepared by a modification of the literature method. The KDPh$^F$F salt was prepared *in situ* by stirring a toluene solution (25.0 mL) of *N,N'*-di-*p*-fluoroformamidine (292.8 mg, 1.26 mmol) with KOBu$^t$ (141.2 g, 1.26 mmol) for 30 minutes. To this solution was added a toluene solution of [Rh(cod)Cl]$_2$ (310.7 mg, 0.63 mmol). The mixture was stirred for 12 h. at r.t. and the resulting orange solution was filtered and concentrated to *ca.* 5 mL. Addition of hexanes produced an orange solid that was isolated by filtration in 83% yield (462 mg).

*Synthesis of [Rh$_2$(DPh$^F$F)$_2$(CH$_3$CN)$_6$](BF$_4$)$_2$* ***(14)***

The compound [Rh$_2$(DPh$^F$F)$_2$(CH$_3$CN)$_6$](BF$_4$)$_2$ was prepared by a modification of the literature method. A solution of [Rh(cod)Cl]$_2$ (124.5 mg, 0.14mmol) in $CH_2Cl_2$/acetonitrile (1/1, 40 mL) was treated with $AgBF_4$ (112.1 mg, 0.58 mmol) in the absence of light. The mixture was stirred at r.t. for 6 h., and subsequently refluxed for 24 h, after which time visible Ag metal deposits were present. The mixture was filtered through a Celite plug, concentrated to ~8 mL under reduced pressure, treated with 12 mL of diethyl ether, and finally chilled to -10 °C. A red mycrocrystalline solid was collected by suction filtration, washed with diethyl ether and dried *in vacuo*. Yield = 115.2 mg

(75.6 %). $^{1}$H NMR ($CD_3CN$) $\delta$ (ppm): 7.51 (t, 1H, NCHN), 7.11 (m, 4H, Ar-H), 7.02 (m, 4H, Ar-H), 2.54 (s, 12H, *eq*-$CH_3CN$), 1.96 (s, 6H, *ax*-$CH_3CN$).

*Synthesis of* $[Rh_2(\mu\text{-}DPh^FF)_2(phen)_2(CH_3CN)_2](BF_4)_2$ ***(15)***

A solution of $[Rh_2(DPh^FF)_2(CH_3CN)_6](BF_4)_2$ **(14)** (130.9 mg, 0.12mmol) in acetonitrile (60 mL) was treated with 1,10-phenanthroline (43.4 mg, 0.24 mmol). The mixture was refluxed for 24 h, after which time the volume was reduced to 10 mL under reduced pressure and layered with diethyl ether until a dark red solid appeared. The solid was recovered by filtration on a sintered glass frit and washed several times with diethyl ether. The product was dried under vacuum for ~10 h. Yield = 0.12 g (77.9 %). $^{1}$H NMR ($CD_3CN$) $\delta$ (ppm): 8.58 (dd, 4H, phen), 8.30 (t, 2H, NCHN), 8.14 (dd, 4H, phen), 7.67 (s, 4H, phen), 7.44 (dd, 4H, phen), 7.11 (m, 4H, Ar-H), 7.02 (m, 4H, Ar-H), 1.96 (s, 6H, *ax*-$CH_3CN$).

*Synthesis of* $[Rh_2(\mu\text{-}DPh^FF)_2(dppz)(CH_3CN)_4](BF_4)_2$ ***(16)***

A solution of $[Rh_2(DPh^FF)_2(CH_3CN)_6](BF_4)_2$ **(14)** (100.5 mg, 0.09 mmol) in acetonitrile (50 mL) was treated with dppz (25.4 mg, 0.09 mmol). The mixture was refluxed for 24 h, after which time the volume was reduced to 20 mL under reduced pressure and layered with diethyl ether until a red solid appeared. The solid was recovered by filtration on a sintered glass frit and washed several times with diethyl ether. The product was dried under vacuum overnight. Yield = 0.107 g (92.1%). $^{1}$H NMR ($CD_3CN$) $\delta$ (ppm): 9.15 (d, 2H, dppz), 8.78 (d, 2H, dppz), 8.35 (m, 2H, dppz),

8.29 (t, 2H, NCHN), 8.18 (m, 2H, dppz), 8.10 (m, 2H, dppz), 7.13 (m, 4H, Ar-H), 7.04 (m, 4H, Ar-H), 2.51 (s, 6H, *eq*-$CH_3CN$), 1.96 (s, 6H, *ax*-$CH_3CN$).

*Synthesis of* $[Rh_2(DPh^FF)_2(dppz)_2(CH_3CN)_2](BF_4)_2$ ***(17)***

A solution of $[Rh_2(DPh^FF)_2(CH_3CN)_6](BF_4)_2$ **(14)** (120.0 mg, 0.11mmol) in acetonitrile (60 mL) was treated with dppz (64.9 mg, 0.23 mmol). The mixture was refluxed for 24 h and the volume was reduced to 20 mL under reduced pressure. The red solid was recovered by filtration on a sintered glass frit and washed several times with cold acetonitrile (3 × 10 mL) and diethyl ether (2 × 10 mL). The product was dried under vacuum overnight. Yield = 0.149 g (90.8 %). $^1$H NMR ($CD_3CN$) $\delta$ (ppm): 9.01 (d, 4H, dppz), 8.77 (d, 4H, dppz), 8.41 (m, 4H, dppz), 8.29 (t, 2H, NCHN), 8.16 (m, 4H, dppz), 8.11 (m, 4H, dppz), 7.13 (m, 4H, Ar-H), 7.04 (m, 4H, Ar-H), 2.51 (s, 6H, *eq*-$CH_3CN$), 1.96 (s, 6H, *ax*-$CH_3CN$).

**Methods**

*X-ray Crystallographic Studies*

***X-ray Structural Study of*** $[Rh_2(\mu\text{-}DPh^FF)_2(dppz)(CH_3CN)_4](BF_4)_2$ ***(16).*** For the X-ray crystallographic analysis, a red prismatic crystal of **16** (approximate dimensions: 0.31 x 0.22 x 0.19 $mm^3$) was selected. The crystal was coated with Paratone oil, transferred to a nylon loop, and placed in a cold $N_2$ stream at 110(2) K. A total of 46,455 reflections were collected in the range $1.65^o \leq \theta \leq 27.51^o$. The structure was solved and refined in the space group *P*-1. The final refinement cycle was based on 16,345 unique reflections (11,457 with $F_\sigma^2 > 2\sigma(F_\sigma^2)$), 897 parameters, and 34

restraints ($R1$ = 0.0719, $wR2$ = 0.1653). The maximum and minimum peaks in the final difference Fourier map corresponded to 1.329 and –1.696 e/Å$^3$, respectively, with a goodness-of-fit value of 1.081.

*Ligand Exchange Kinetics*

***Reaction of $Rh_2(O_2CCH_3)_4(H_2O)_2$ with 9-EtGH.*** In a typical reaction, a slurry of 9-EtGuaH (25mg, 0.14 mmol) in $H_2O$ (5 mL) was added to a solution of $Rh_2(O_2CCH_3)_4(H_2O)_2$ (30 mg, 0.063 mmol) in 5 mL of $H_2O$. The reaction solution was heated at a constant temperature (± 3 ºC) for a few days during which time its color gradually changed from aqua to emerald green. Small aliquots (200 μL) were removed from the reaction solution at various time intervals (depending on the rate of the reaction at the particular temperature), lyophilized several times, redissolved in $D_2O$-$d_2$ and monitored by $^1$H NMR spectroscopy to determine the progress of the reaction. The areas of the H8 protons of the reaction product $Rh_2(O_2CCH_3)_2$(9-EtGua)$_2$ **(***head-to-head* and *head-to-tail* isomers**)** in each sample were integrated against the area of the H8 proton of the unreacted 9-EtGuaH.

***Reaction of $Rh_2(O_2CCF_3)_4$ with 9-EtGH.*** In a typical reaction, a slurry of 9-EtGH (25mg, 0.14 mmol) in $H_2O$ (5 mL) was added to a solution of $Rh_2(O_2CCF_3)_4$ (46 mg, 0.070 mmol) in 5 mL of $H_2O$. The reaction solution was heated at a constant temperature (± 3 ºC) for several hours during which time its color gradually changed from blue to emerald green. Small aliquots (350 μL) were removed from the reaction solution at various time intervals (depending on the rate of the reaction at the particular temperature), lyophilized a few times and redissolved in exactly 450 μL of $(CD_3)_2CO$-$d_6$.

To each sample, a precise amount of $C_6D_6$-$d_6$ (1.5 μL) was added and the sample was monitored by $^1$H NMR spectroscopy. The area of the H8 protons of $[Rh_2(O_2CCF_3)_2(9\text{-EtGuaH})_2](O_2CCF_3)_2$ in each sample was integrated against the area of the internal $C_6D_6$-$d_6$. Sampling of the reaction was discontinued when the integration area of the H8 protons (from the product) remained constant with respect to the integration area of the internal $C_6D_6$-$d_6$. The internal $C_6D_6$-$d_6$ had to be added to the NMR sample because, although $[Rh_2(O_2CCF_3)_2(9\text{-EtGuaH})_2](O_2CCF_3)_2$ is readily soluble in $(CD_3)_2CO$-$d_6$, 9-EtGuaH is not (to monitor the unreacted amount). The $^1$H NMR spectra of the reaction aliquots could not be monitored in $D_2O$-$d_2$, because $[Rh_2(O_2CCF_3)_2(9\text{-EtGuaH})_2](O_2CCF_3)_2$ is not completely soluble in $D_2O$-$d_2$. Efforts to monitor the progress of the reaction by $^{19}$F NMR spectroscopy were not successful because the resonances of the free and bound trifluoroacetate ($CF_3CO_2^-$) are very close, making the integration values unreliable. Monitoring the substitution reactions of the acetate and trifluoroacetate bridging groups with other reagents, e.g., HCOOH or $Na_2CO_3$ was not possible, because the reactions with dirhodium trifluoroacetate are complete within minutes and thus not possible to monitor by NMR spectroscopy.

*In Vitro Cytotoxicity Measurements*

Human skin fibroblasts (Hs-27) were obtained from the American Type Culture Collection, cell line CRL-1634 (Manassas). Cells were cultured in Dulbecco's modified Eagle medium, containing 10% fetal bovine serum (Life Technologies), 50 μg/mL gentamicin, 4.5 mg/ml glucose, and 4 mM L-glutamine (Invitrogen Life Technology). Cell cultures were incubated in a humidified atmosphere containing 5% $CO_2$ at 37 $^oC$.

For assessing the cytotoxicity and photocytotoxicity of different compounds, subconfluent (50% - 80% confluent) monolayers of Hs-27 in 60 mm culture dishes were used. The monolayers were washed twice with phosphate-buffered saline (PBS) to ensure that the culture dishes were free of any culture medium, fresh PBS containing different concentrations of each compound were added to cover the fibroblasts. After this procedure, the cells were removed from the dishes by trypsinization, seeded into 24-well culture dishes, and incubated for 2 to 4 days or until the untreated control group reached confluence. N-lauroyl sarcosine (200 μL, 40 mM) was then added to each well and the cells were allowed to lyse for at least 15 min. Quantitative determination of the protein content in each well was undertaken using Peterson's Modification of the Micro-Lowry Method (Sigma reagent kit), where the lysate was treated with 200 μL Lowry reagent for 20 min and then with 100 μL Folin-Ciocalteau phenol reagent for 30 min or until color developed. A portion of the contents (200 μL) of each well was transferred to a 96-well plate for absorbance determination using a multiwell plate reader (Dynatech Laboratory). The absorbance at 630 nm was monitored, which is proportional to the total protein content and the number of cells in each well.

**Instrumentation**

The $^{1}$H-NMR spectra for the synthesis of the complexes were recorded on a Varian spectrometer at 300 MHz. The $^{1}$H-NMR spectra for the kinetics studies were recorded at 20 ºC on a 500 MHz Varian Inova spectrometer with a 5 mm switchable probehead. The $^{1}$H-NMR spectra for the dirhodium tetraacetate and trifluoroacetate reactions with 9-EtGuaH were referenced to the residual proton impurities of the

deuterated solvents $D_2O$-$d_2$ and $(CD_3)_2CO$-$d_6$, respectively. The $^1$H-NMR spectra for the compounds **8**, and **10**-**13** were referenced to the residual proton impurities of the deuterated solvents $CD_3OD$-$d_4$ and $CD_3OD$-$d_4$/$CD_3Cl$, respectively. Absorption spectra were recorded in a UV-1601PC Shimadzu spectrophotometer. Mass spectra were acquired on a PE SCIEX QSTAR Pulsar electrospray ionization mass spectrometer at Texas A&M University. Elemental analyses were performed by Atlantic Microlab Inc., P.O. Box 2288, Norcross, GA 30091.

## *Results and Discussion*

### Syntheses

The cytotoxicities of the dirhodium compounds **1**-**16** have been studied with respect to their structural features. The compounds $Rh_2(\mu\text{-}O_2CCH_3)_4$ (**1**), $Rh_2(\mu\text{-}O_2CCF_3)_4$ (**2**), $[Rh_2(\mu\text{-}O_2CCH_3)_2(phen)_2]^{2+}$ (**3**), and $[Rh_2(\mu\text{-}O_2CCF_3)_2(phen)_2]^{2+}$ (**4**) were previously reported. $[Rh_2(\mu\text{-}O_2CCH_3)_2(\eta^1\text{-}O_2CCH_3)(dppz)(MeOH)]^+$ (**5**), $[Rh_2(\mu\text{-}O_2CCH_3)_2(dppz)_2]^{2+}$ (**6**), and $[Rh_2(\mu\text{-}O_2CCH_3)_2(dppz)(bpy)]^{2+}$ (**7**) were synthesized as detailed in Chapter II. The synthetic routes for the newly synthesized dirhodium(II,II) complexes **8**, **10**-**17** are outlined in Schemes IV.1 and IV.2.

**Scheme IV.1.** Synthetic routes used to prepare compounds **8**, **10** - **12**, and **16**.

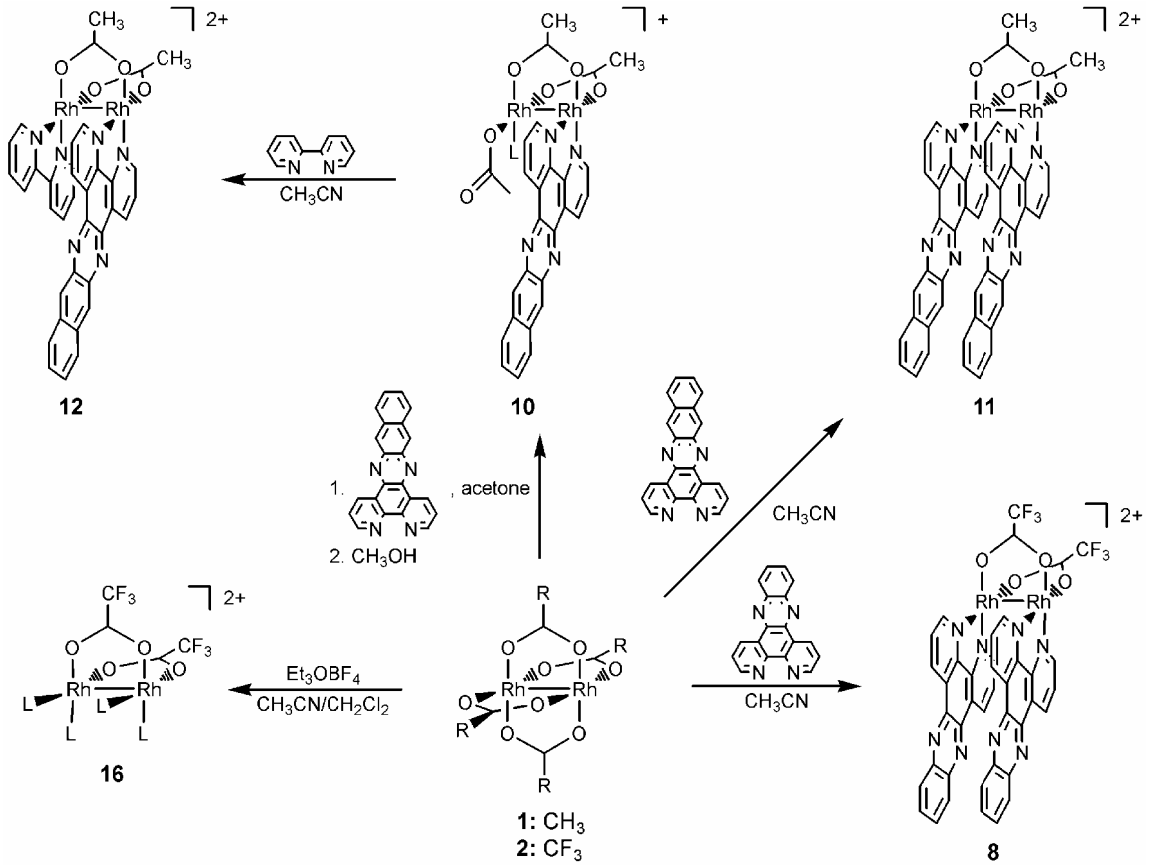

**Scheme IV.2.** Synthetic routes used to prepare compounds **14-17**.

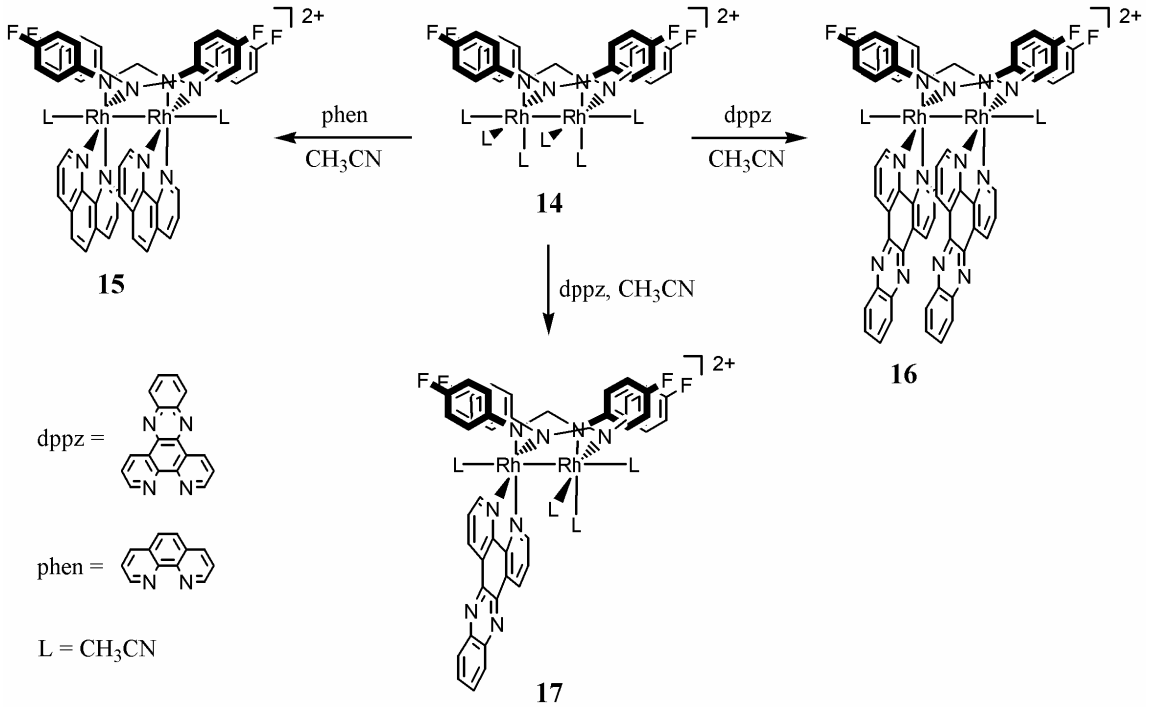

The ligand dppn was introduced into compounds **10-12** due to its higher lipophilicity as compared to dppz. Heating **1** with two equivalents of dppn in refluxing $CH_3CN$ yields **11** (87%) as a red solid. The reaction temperature and time are critical for the formation of **11**. If the reaction is performed at lower temperatures or for shorter time periods, a mixture of the mono and bis dirhodium complexes are obtained. Compound **10** is synthesized at a 40% yield by the reaction of **1** with 1 eq of dppn. The intermediate product $Rh_2(\mu\text{-}O_2CCH_3)_2(\eta^2\text{-}O_2CCH_3)(\eta^1\text{-}O_2CCH_3)$(dppn) in the reaction possesses a chelating acetate ion, which occupies eq/ax positions of one rhodium atom.[43] This intermediate exhibits low solubility in both polar and non-polar solvents; it is converted, however, into the more soluble product **10**, by stirring a slurry of the insoluble compound in methanol until a clear green solution is obtained. In the last step, one acetate group is displaced by methanol. Compound **10** is reacted with one equivalent of 2,2'-bipyridine in acetonitrile to produce **12** in a 42% yield.

It is well-known that formamidinato ligands are less labile than the carboxylato ligands. For this reason, compounds **14-16** were synthesized so they could be compared to their acetato analogues. Compound **14** is synthesized by reacting $[Rh(cod)(DPh^FF)]_2$, which does not contain a Rh-Rh bond, with an excess of $AgBF_4$. The oxidation of the rhodium atoms from the oxidation state +1 to the +2 state results in the formation of **14**, which contains a Rh-Rh bond, and in which the cyclooctadiene ligands have been displaced by acetonitrile molecules due to the strong trans effect exerted by the N atoms of the formamidinato ligands. Compound **14** serves as the starting material for the preparation of **15** and **16**, as shown in Scheme IV.2. Compound **15** is readily prepared by

reacting **14** with two equivalents of 1,10-phenanthroline in acetonitrile. This complex exhibits a high solubility in $CH_3CN$ but is poorly soluble in $H_2O$. Likewise, compounds **16** and **17** can be prepared by displacing either two or four *eq*-$CH_3CN$ ligands from **14** with one or two dppz molecules, respectively. These compounds are also soluble in $CH_3CN$, but not very soluble in water. As compared to their acetato counterparts, compounds **14**-**16** are more lipophilic.

Crystals suitable for X-ray crystallography were grown from a solution of **16** in $CH_3CN$ in the presence of toluene. The molecular structure of the complex consists of a dinuclear $Rh_2$(II,II) core with two formamidato bridging ligands in a *cis* disposition, a chelating dppz ligand coordinated to one Rh atom, and two acetonitrile molecules bound to the other rhodium center. The axial positions are occupied by acetonitrile molecules (Figure IV.1). The Rh-Rh distance in **16**, 2.581(1) Å, is similar to that found for $[Rh_2(\mu\text{-DTolF})_2(bpy)(CH_3CN)_4](BF_4)_2$ (2.5783(3) Å) (DtolF = *N*,*N*'-di-p-tolylformamidinate), although slightly shorter than that found for $[Rh_2(\mu\text{-DTolF})_2(bpy)(CH_3CN)_3](BF_4)_2$ (2.638(3) Å), which contains only one axial ligand. The Rh-$N_{dppz}$ bonds, 2.032(3) to 2.043(3) Å, are longer to those found in **6a**, (2.005(4) to 2.016(4) Å), and **6b**, (1.995(7) to 2.018(7) Å), but they are similar to the Rh-$N_{bpy}$ reported for $[Rh_2(\mu\text{-DTolF})_2(bpy)(CH_3CN)_4](BF_4)_2$ (2.035(2) Å and 2.051(2) Å). This lengthening is attributed to the stronger *trans* influence of the formamidinato ligand as compared to the acetato ligands. Selected crystal parameters for compounds **16** are listed in Table IV.1. A summary of selected bond distances and angles for compound **16** is listed in Tables IV.2 and IV.3, respectively.

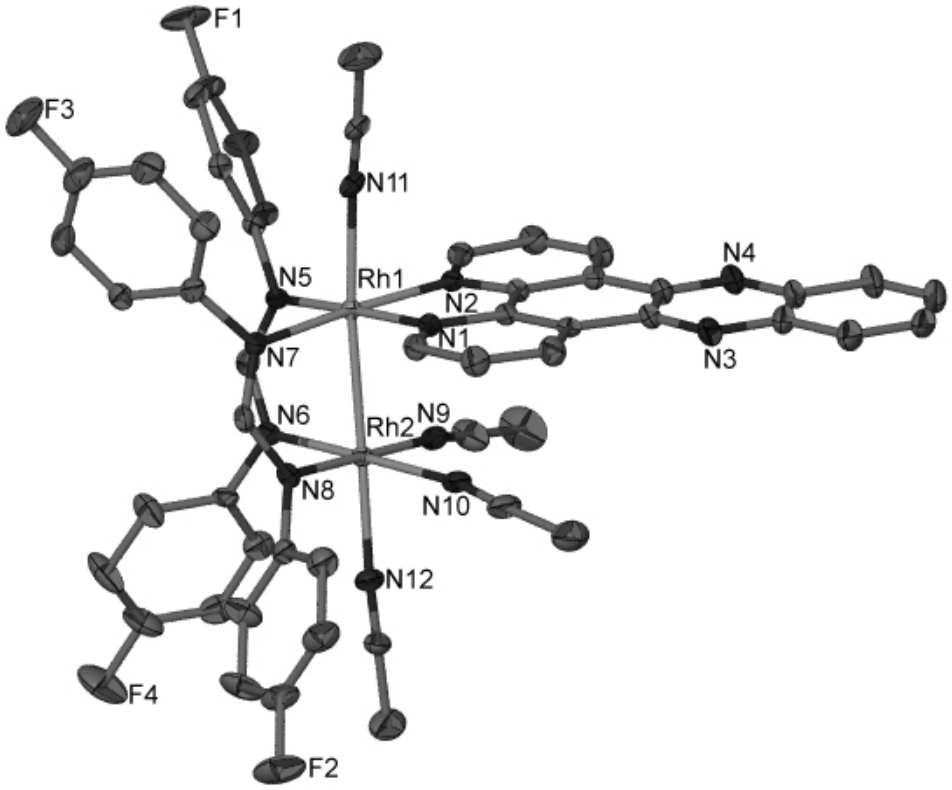


**Figure IV.1.** Thermal ellipsoid plot at the 50% probability level of the cation in **16**.

**Table IV.1.** Crystal data and structural refinement parameters for compound **16**.

| | |
|---|---|
| Empirical formula | $C_{76.50}H_{68}B_2F_{12}N_{12}Rh_2$ |
| Formula weight | 1610.87 |
| Temperature | 100(2) K |
| Wavelength | 0.71073 Å |
| Crystal system | Triclinic |
| Space group | *P*-1 |
| a | 11.667(2) Å |
| b | 13.105(3) Å |
| C | 25.238(5) Å |
| α | 78.80(3) ° |
| β | 84.52(3) ° |
| γ | 72.52(3) ° |
| Volume | 3607.5(12) $Å^3$ |
| Z | 2 |
| Density (calculated) | 1.483 $Mg/m^3$ |
| Crystal size | 0.31 x 0.22 x 0.19 $mm^3$ |
| Theta range for data collection | 1.65 to 27.51°. |
| Reflections collected | 16345 |
| Independent reflections | 11457 [R(int) = 0.0719] |
| Data / restraints / parameters | 11457 / 34 / 897 |
| Goodness-of-fit on $F^2$ | 1.081 |
| Final R indices [I>2sigma(I)] | R1 = 0.0719, wR2 = 0.1653 |
| R indices (all data) | R1 = 0.1106, wR2 = 0.1790 |

$R_1 = \Sigma||F_o| - |F_c||/\Sigma|F_o|$; $wR_2 = [\Sigma[w(F_0^2-F_c^2)^2]/\Sigma[w(F_0^2)^2]]^{1/2}$

**Table IV.2.** Selected bond distances (Å) for compound **16**.

| | Bond Distances (Å) |
|---|---|
| Rh(1)-Rh(2) | 2.582(1) |
| Rh(1)-N(1) | 2.026(8) |
| Rh(1)-N(2) | 2.041(7) |
| Rh(1)-N(5) | 2.045(8) |
| Rh(1)-N(7) | 2.049(7) |
| Rh(1)-N(11) | 2.222(9) |
| Rh(2)-N(9) | 2.031(8) |
| Rh(2)-N(10) | 2.025(9) |
| Rh(2)-N(6) | 2.021(8) |
| Rh(2)-N(8) | 2.030(8) |
| Rh(2)-N(12) | 2.171(9) |

**Table IV.3.** Selected bond angles (°) for compound **16**.

| | Bond Angles (°) |
|---|---|
| N(11)-Rh(1)-Rh(2) | 174.4(2) |
| N(12)-Rh(2)-Rh(1) | 179.1(2) |
| N(2)-Rh(2)-Rh(1) | 92.7(2) |
| N(1)-Rh(1)-Rh(2) | 90.5(2) |
| N(5)-Rh(1)-N(7) | 88.0(3) |
| N(1)-Rh(1)-N(7) | 94.6(3) |
| N(1)-Rh(1)-N(2) | 80.7(3) |
| N(6)-Rh(2)-N(8) | 90.3(3) |
| N(9)-Rh(2)-N(10) | 90.0(3) |

**Effect of substituent on bridging ligands**

In order to explore the effect of the bridging ligand on the cytotoxicity of the dirhodium complexes **2**, **4**, **8** (which represent the trifluoroacetate analogs of **1**, **3**, **6**, respectively) were synthesized (Figure IV.2). Compounds **1-4**, **6**, and **8** were evaluated for their capability to inhibit cell growth *in vitro* using human skin fibroblasts (Hs-27) and the $LC_{50}$ values (concentration required to kill 50% of the cells) are listed in Table IV.4. The $LC_{50}$ values of the acetate derivatives **1**, **3**, and **6** were found to be 15 ± 2, 290 ± 15, and 135 ± 8, respectively, and those for the trifluoroacetate analogs **2**, **4**, and **8** were 7.7 ± 0.5, 152 ± 7, and 58 ± 3, respectively. The $LC_{50}$ values for each complex with acetate bridging ligands is, in each case, twice the magnitude of that of its trifluoroacetate counterpart. Since the charge and the lipophilicity of the other ligands within the subsets of dirhodium complexes **1**/**2**, **3**/**4** and **6**/**8** are the same, the observed differences in the cytotoxicities were investigated with respect to the relative labilities of the acetate vs the trifluoroacetate leaving groups. Differences in the reactivity of complexes **1** and **2** with short oligonucleotides and double-stranded DNA have already been reported and correlated with the different labilities of the two leaving groups, $CH_3CO_2^-$ as compared to $CF_3CO_2^-$.[56,57]

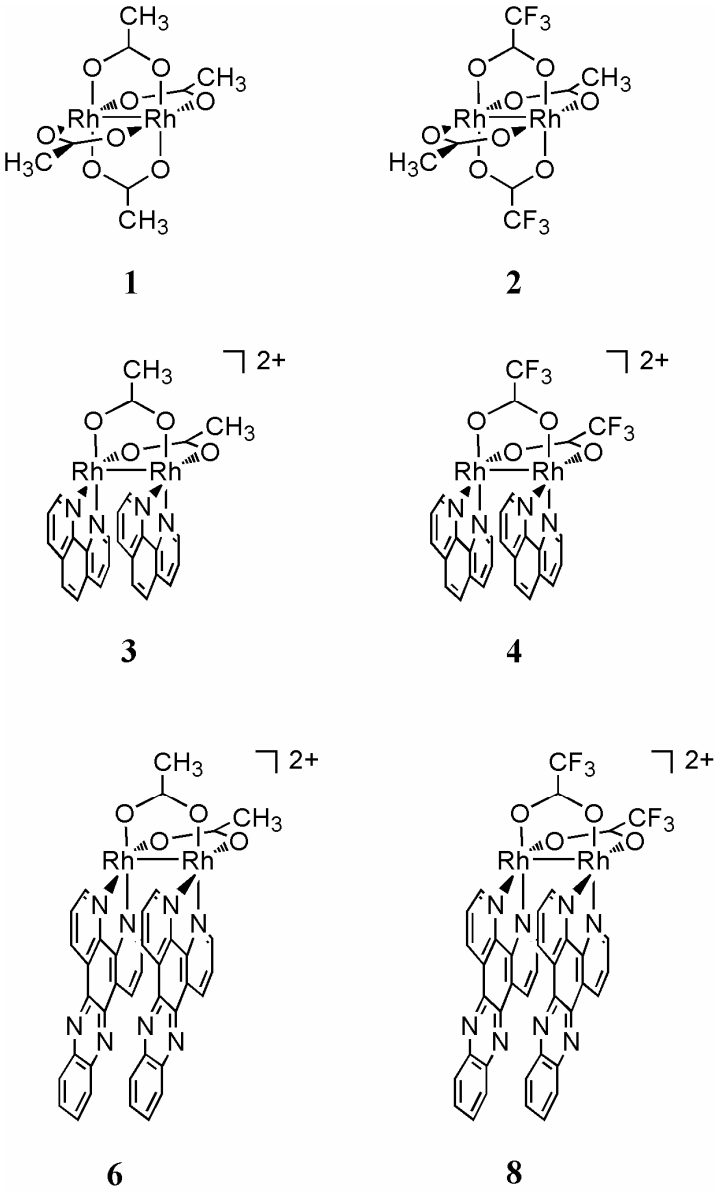


**Figure IV.2.** Schematic representations of compounds **1** - **4**, **6**, and **8**.

**Table IV.4.** Cytotoxicity ($LC_{50}$) values for complexes **1-4**, **6**, and **8**.

| Complex | | $LC_{50}$ (μM)[a] |
|---|---|---|
| $Rh_2(\mu\text{-}O_2CCH_3)_4$ | **1** | 15 ± 2 |
| $Rh_2(\mu\text{-}O_2CCF_3)_4$ | **2** | 7.7 ± 0.5 |
| $[Rh_2(\mu\text{-}O_2CCH_3)_2(phen)_2]^{2+}$ | **3** | 290 ± 15 |
| $[Rh_2(\mu\text{-}O_2CCF_3)_2(phen)_2]^{2+}$ | **4** | 152 ± 7 |
| $[Rh_2(\mu\text{-}O_2CCH_3)_2(dppz)_2]^{2+}$ | **6** | 135 ± 8 |
| $[Rh_2(\mu\text{-}O_2CCF_3)_2(dppz)_2]^{2+}$ | **8** | 58 ± 3 |

[a] Hs-27 human skin cells exposed to each compound for 30 min in the dark.

**Ligand exchange kinetics**

The substitution reactions of **1** and **2** with 9-EtGuaH were performed at various temperatures between 40 and 75 ºC in order to gain insight into the relative lability of acetate and trifluoroacetate bridging ligands in dirhodium complexes. At each temperature, the product concentration follows pseudo-first order kinetics according to the equation:

$$[C] = [C_o](1 - e^{-k_T t}) \qquad \text{(Eq. 1)}$$

where [C] is the product concentration, $[C_o]$ is the initial concentration of the reagent, $k_T$ is the rate of the reaction at a certain temperature T, and $t$ represents reaction time. By fitting the experimental data points for **1** and **2** at each temperature T, the rate $k_T$ for each reaction at a certain temperature T is derived. For example, at 60 ºC, the product formed as a function of time and the corresponding fits to Eq. 1 for the reactions of **1** and **2** are shown in Figures IV.3 and IV.4, respectively.

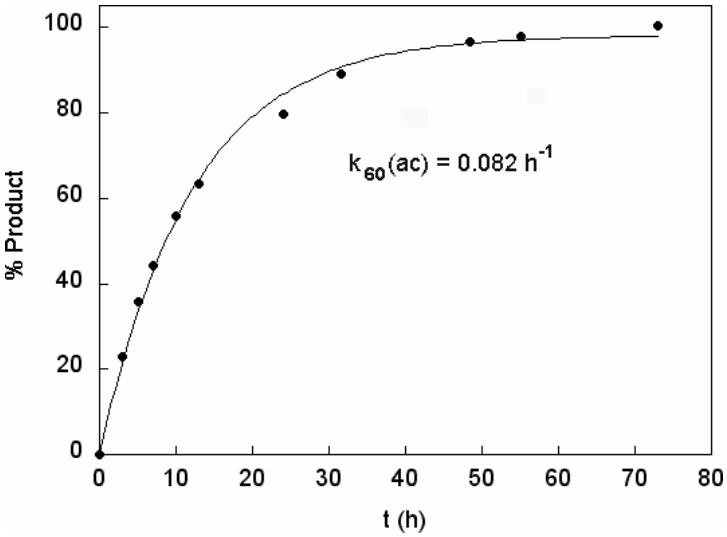


**Figure IV.3.** Plot of the % product from the reaction of dirhodium tetraacetate with 9-EtGuaH, as a function of time (t) at 60 ºC ($k_{60}$ (ac) = 0.082 $h^{-1}$).

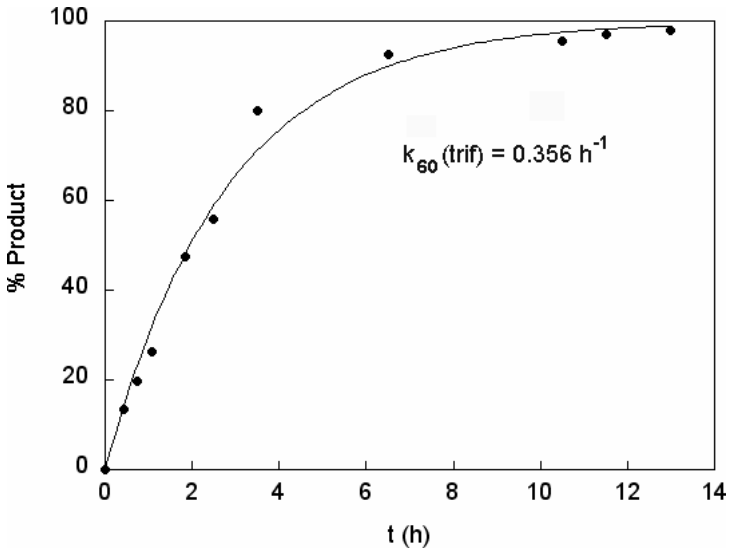


**Figure IV.4.** Plot of the % product from the reaction of dirhodium trifluoroacetate with 9-EtGuaH, as a function of time (t) at 60 ºC ($k_{60}$ (trif) = 0.356 $h^{-1}$).

Using fits of eq 1 as described above, the rate constant $k_T$ was determined for each reaction of **1** and **2** conducted at a given temperature T. For each complex, the plots of $k_T$ against 1/T resulted in a straight line and were subsequently fit to Eq. 2, with a slope equal to $– E_a/R$:

$$\ln k_T = \ln A – E_a(\mathbf{n}) / RT \quad \text{(Eq. 2)}$$

where $E_a(\mathbf{n})$ is the activation energy of complex **n** and A represents the pre-exponential factor of the reaction. The least squares best fits to eq 2 for the reactions of **1** and **2** with 9-EtGuaH afford activation energy values of $E_a(\mathbf{1})$ = 69 ± 4 kJ/mol and $E_a(\mathbf{2})$ = 35 ± 2 kJ/mol, respectively.

The 2:1 ratio of the acetate vs. the trifluoroacetate activation energies (for the systems under investigation) is in accord with the greater lability of the trifluoroacetate vs. the acetate group due to the lower basicity of $CF_3CO_2^-$ ($pK_b$ 13.5) as compared to $CH_3CO_2^-$ ($pK_b$ 9.2).[178] This 2:1 ratio of the activation energies for acetate/trifluoroacetate compounds **1** and **2** correlates well with the difference in the $LC_{50}$ values of the acetate derivatives **1**, **3** and **6** being half as cytotoxic as the trifluoroacetate derivatives **2**, **4** and **8** (Table IV.4). Since the trifluoroacetate groups are substituted by the same nucleophile easier than the acetate ligand, the dirhodium compounds **2**, **4** and **8** react faster than the acetate analogs **1**, **3** and **6** with biomolecules within cells, and thus the lability of the leaving groups accounts for the higher toxicity of the trifluoroacetate derivatives.

It is notable that a relationship exists between the ligand exchange kinetics and the *in vitro* toxicity for other classes of compounds, which bind covalently to DNA.[182] For example, the response toxic level for cisplatin and carboplatin against Sarcoma 180 cells of 9 and 150 mg/kg, respectively, correlates well with the greater lability of $Cl^-$ vs. the chelating $C_6H_6O_4^{2-}$ group, rendering cisplatin more toxic than carboplatin.[183] Likewise, in a series of diamine platinum(II) compounds, the complexes with chloride or oxalate leaving groups are cytotoxic against ovarian cancer cell lines at much lower concentrations than their congeners with the 1,1´-cyclobutanedicarboxylato leaving groups (for the same carrier ligand).[184] The importance of the lability of the ligands has also been demonstrated in a series of platinum-amine complexes, in which the aqua derivatives of the series are the most toxic as compared to the tetramino complexes without labile ligands, which are the least toxic.[185] Likewise in the series *cis*-$Pt(NH_3)_2X_2$ with various groups X, it is shown that the Pt-X bond strength has a substantial influence on the intrinsic reactivity of the compounds (*e.g.*, complexes with the strongly bound isocyanate ($-SCN^-$) and nitrite ($-NO_2$) ligands show no antitumor potential).[186] Additionally, in the series of compounds $[PtCI(R´R´´SO)(diam)]NO_3$ (diam = bidentate amine such as 1,2-diaminocyclohexane (dach) or 1,1-bis(aminomethyl)cyclohexane (damch) and R´R´´SO substituted sulfoxides such as dimethyl ($Me_2SO$), methyl phenyl (MePhSO), methyl benzyl (MeBzSO), diphenyl ($Ph_2SO$), and dibenzyl sulfoxide ($Bz_2SO$)), the presence of the more labile $Ph_2SO$ sulfoxide group renders the platinum compounds more toxic than complexes with other sulfoxide groups.[187]

**Effect of accessibility of coordination sites**

The role of the lability of the equatorial ligands is also nicely demonstrated by comparing the cytotoxicities of compounds **5** and **10** (Figure IV.5) with those of **7** and **12**, as well as **6** and **11** (Figure IV.6), respectively (Table IV.5). Complexes **5** and **10** are eight and four times more cytotoxic than **7** and **12**, respectively, and their toxicities are five and seven times greater than those measured for **6** and **11**. The greater toxicities of **5** and **10** relative to the other complexes is attributed to the presence of solvent molecules and monodentate acetate groups in the equatorial positions of one rhodium atom. These ligands are more labile than the diimine bpy, dppz and dppn ligands occupying the same equatorial positions in **6, 11, 7**, and **12**. The labile solvent molecules and the monodentate acetate groups in **5** and **10** provide potential 'open sites' accessible for nucleophilic substitution, as opposed to these sites being occupied by the chelating N-N diimine ligands in **6**, **11**, **7** and **12**, which reduces the reactivity of the latter.[43] This is supported by the fact that the dirhodium compound *cis*-$[Rh_2(\mu\text{-}O_2CCH_3)_2(\eta^1\text{-}O_2CCH_3)(bpy)(CH_3OH)]^+$ with an analogous structure to **10**, **11** has been shown to react with biologically relevant molecules such as 9-EtGuaH.[188] In addition, the partially solvated complexes $[Rh_2(\mu\text{-}O_2CCF_3)_2(CH_3CN)_4]^{2+}$ (**13**) and $[Rh_2(DPh^FF)_2(CH_3CN)_4]^{2+}$ (**14**) are highly toxic, as determined by their low $LC_{50}$ values (<5 μM), whereas the complexes $[Rh_2(\mu\text{-}O_2CCF_3)_2(phen)_2]^{2+}$ (**4**), $[Rh_2(\mu\text{-}O_2CCF_3)_2(dppz)_2]^{2+}$ (**8**), $[Rh_2(\mu\text{-}DPh^FF)_2(phen)_2]^{2+}$ (**15**) and $[Rh_2(\mu\text{-}DPh^FF)_2(dppz)_2]^{2+}$ (**17**) containing diimine ligands instead of the labile acetonitrile molecules are less cytotoxic. Similarly, the higher toxicity of **1** as compared

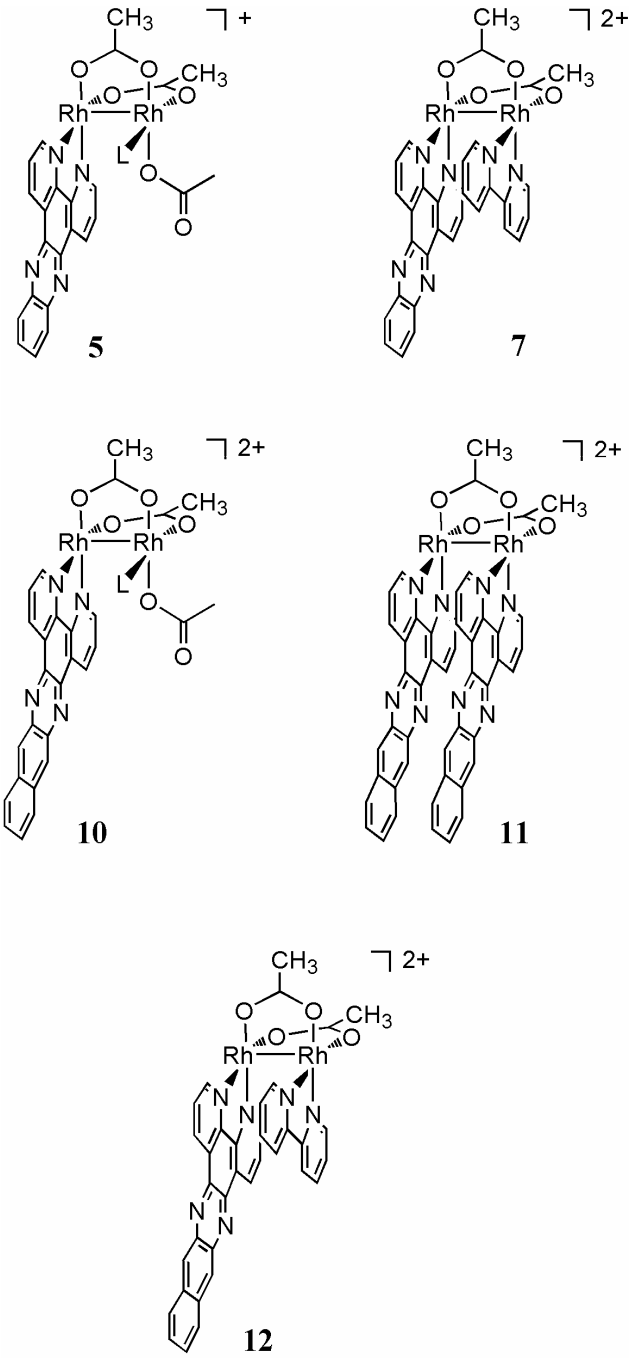


**Figure IV.5.** Schematic representations of compounds **5**, **7**, and **10 – 12** (L = $CH_3OH$).

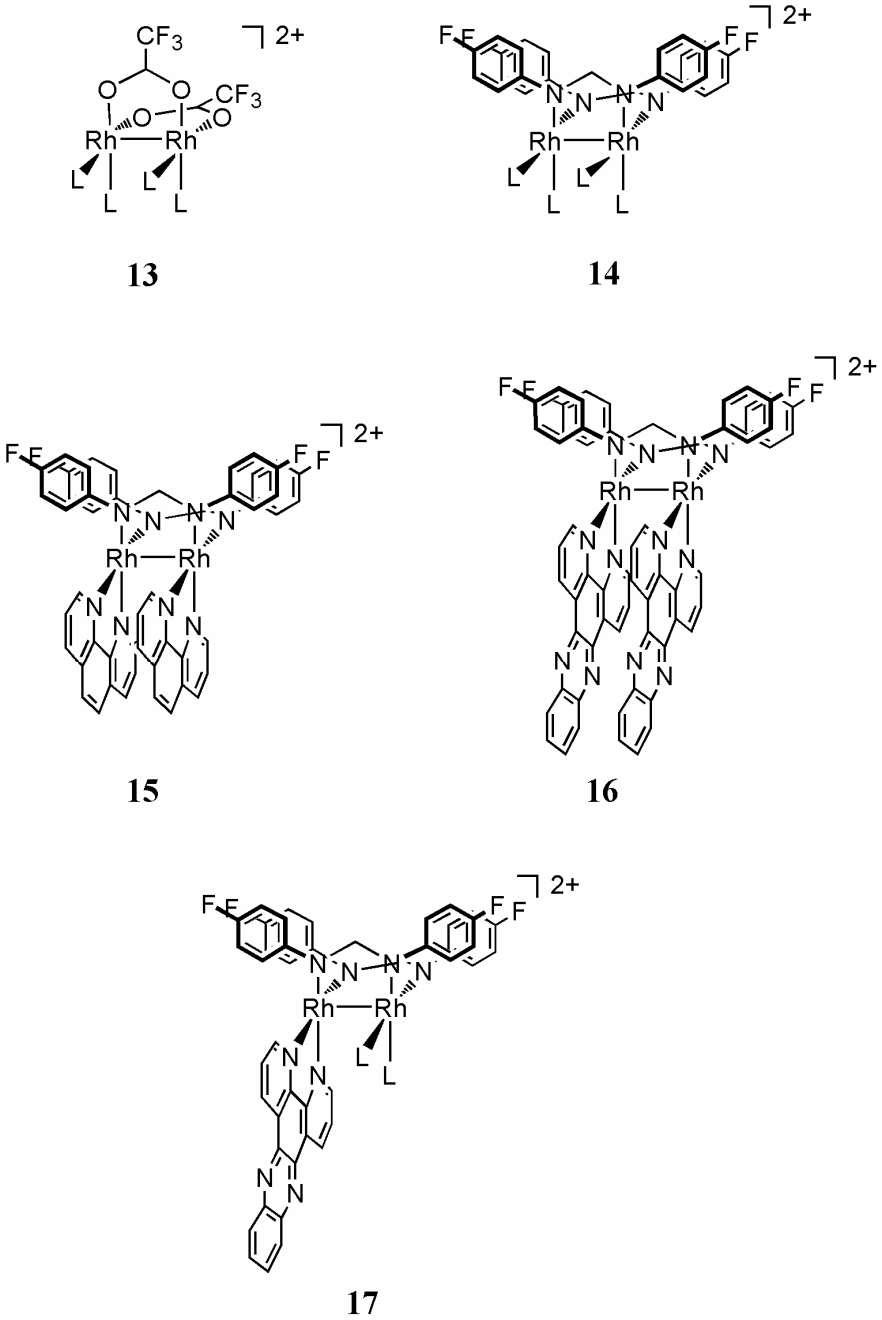


**Figure IV.6.** Schematic representations of compounds **13 – 17** (L = $CH_3CN$).

to **3** and **6** may be attributed to the greater lability of the carboxylate groups as compared to the chelating N-N diimine groups (phen and dppz for **3** and **6**, respectively). A two to three-fold decrease in the cytotoxicity of $Rh_2(\mu\text{-}O_2CCH_3)_4$ towards human oral carcinoma KB cell lines has also been observed upon substituting two acetate groups with 2,2´-bpy and 1,10-phen.[38]

**Table IV.5.** Cytotoxicity ($LC_{50}$) values for complexes **5**, **7**, **10**-**17**.

| Complex | | $LC_{50}$ (μM)[a] |
|---|---|---|
| $[Rh_2(\mu\text{-}O_2CCH_3)_2(\eta^1\text{-}O_2CCH_3)(dppz)(MeOH)]^+$ | **5** | 27 ± 2 |
| $[Rh_2(\mu\text{-}O_2CCH_3)_2(dppz)(bpy)]^{2+}$ | **7** | 208 ± 10 |
| $[Rh_2(\mu\text{-}O_2CCH_3)_2(\eta^1\text{-}O_2CCH_3)(dppn)(MeOH)]^+$ | **10** | 51 ± 5 |
| $[Rh_2(\mu\text{-}O_2CCH_3)_2(dppn)_2]^{2+}$ | **11** | 384 ± 24 |
| $[Rh_2(\mu\text{-}O_2CCH_3)_2(dppn)(bpy)]^{2+}$ | **12** | 200 ± 20 |
| $[Rh_2(\mu\text{-}O_2CCF_3)_2(CH_3CN)_4]^{2+}$ | **13** | < 5 |
| $[Rh_2(\mu\text{-}DPh^FF)_2(CH_3CN)_4]^{2+}$ | **14** | < 5 |
| $[Rh_2(\mu\text{-}DPh^FF)_2(phen)_2]^{2+}$ | **15** | 25 ± 2 |
| $[Rh_2(\mu\text{-}DPh^FF)_2(CH_3CN)_2(dppz)]^{2+}$ | **16** | n.a. |
| $[Rh_2(\mu\text{-}DPh^FF)_2(dppz)_2]^{2+}$ | **17** | 79 ± 4 |

[a] Hs-27 human skin cells exposed to each compound for 30 min in the dark.

*Concluding Remarks*

The collective studies presented in this chapter indicate that the toxicity of the complexes synthesized is related to the lability of the leaving groups on the dirhodium core. The kinetic results for the activation energies for acetate/trifluoroacetate compounds **1** and **2** (2:1 ratio) correlate well with the $LC_{50}$ values of the acetate derivatives **1**, **3**, and **6** being half as cytotoxic as the trifluoroacetate derivatives **2**, **4**, and **8** and underscore the importance of the ligand lability/*in vitro* toxicity relationship. Additional evidence of the effect of the ligand lability and the accessibility of the equatorial sites of these dirhodium molecules is provided by comparing the toxicities of compounds **5** and **10** with those of **7** and **12**, respectively. The labile solvent molecules and the monodentate acetate groups in **5** and **10** easily provide potential "open sites" accessible for nucleophilic substitution, as opposed to these sites being occupied by non-labile groups that reduce the reactivity of the complexes. Further examples of this effect are found in the toxicity of compounds **13** and **14**, which are several times more toxic than their analogues containing diimine ligands instead of acetonitrile molecules that can be easily displaced. Thus, the labile equatorial groups play a critical role in the toxicity of these complexes in vitro, which is expected to be related to the antitumor activity of similar dirhodium compounds. Careful tailoring of groups surrounding the dirhodium core in these complexes is expected to lead to more effective and less toxic drugs.

# CHAPTER V

## GENERATION OF NEW DIRHODIUM(II,II) DPPZ COMPLEXES

### *Introduction*

Given the research outlined in the previous chapters, we considered a next logical step to be the synthesis and study of other sub-families of complexes in which the acetato ligands are replaced by other bridging ligands; in particular we are interested in those that are less labile than acetate since they might show a lower cytotoxicity. Unfortunately, the chemistry of dirhodium complexes containing diimine ligands with bridging ligands other than acetate is not well developed.[189] Only one example of substitution reactions of the tetrakis-trifluoroacetamidodirhodium complexhas been reported and there are no examples of such chemistry for the acetamido derivative.[189] A plausible reason for this situation is the fact that the acetamidato and trifluoroacetamidato ligands are much less easily substituted than their acetato counteparts. One way to overcome this problem is to use a starting material containing two diimine ligands already bound to the dimetal core and then replace the existing bridging groups by the desired ligands.

In his search for a high yield synthesis of $Rh_2^{4+}$(aq), Taube and co-workers developed a procedure for the synthesis of $[Rh_2(CO_3)_4]^{4-}$.[190] Although they were never able to use this complex for its initial purpose, namely the synthesis of the fully hydrated $Rh_2^{4+}$ complex, the compound later proved to be a convenient starting material for the synthesis of other $Rh_2$(II,II) carboxylates.[191] Roos et al., have demonstrated that the carbonato bridged complex readily reacts with various carboxylic acids to produce tetracarboxylate species in high yields.[191]

In this chapter, the syntheses of dirhodium diimine complexes containing carbonato bridging ligands, which can be used to prepare trifluoroamidato, pyrrolidinonato and trifluoroacetato bridged $Rh_2$(II,II)-dppz complexes is described.

## *Experimental Section*

### Materials

All reactions were carried out under nitrogen using standard Schlenk-line techniques. The reagents $RhCl_3$, 1,10-phenanthroline, 2-pyrrolidinone, sodium acetate, sodium chloride, $NaBF_4$ and $Na_2CO_3$ were purchased from Aldrich and used without further purification. The compounds $Rh_2(\mu\text{-}O_2CCH_3)_4$ (**1**),[105] $[Rh_2(\mu\text{-}O_2CCH_3)_2(phen)_2](O_2CCH_3)_2$ (**3**),[44] $[Rh_2(\mu\text{-}O_2CCH_3)_2(dppz)_2](O_2CCH_3)_2$ (**6**), and dppz were synthesized by previously reported methods.[106]

*Synthesis of cis-$Rh_2(\mu\text{-}O_2CO)_2(phen)_2(H_2O)_2$* ***(18)***

A red slurry of $[Rh_2(\mu\text{-}O_2CCH_3)_2(phen)_2][O_2CCH_3]_2$ (0.103 g, 0.13 mmol) in $H_2O$ (25 ml) was added to a 1.0 M solution (30 ml) of $Na_2CO_3$ in $H_2O$ and the mixture refluxed for 1 h under $N_{2(g)}$, during which time the red slurry changed to a brown solution. The solution was concentrated to 7 ml and acetone was added (10 mL). The product was recovered by filtration and recrystallized from a $H_2O$/acetone (1/1) solution. Yield: 76.1 mg (81%). ESI-MS: *m/z* 686.9 ($[Rh_2(\mu\text{-}O_2CO)_2(phen)_2] + H^+$). Anal. Calc. for $Rh_2C_{26}N_4O_{10}H_{24}$ ($Rh_2(\mu\text{-}O_2CO)_2(phen)_2(H_2O)_2 \cdot 2H_2O$): C, 41.18; H, 3.19; N, 7.39. Found: C, 40.99; H, 3.34; N, 7.34 %. $^1$H NMR (300 MHz) in $CD_3OD$, δ / ppm (mult., int.): 8.65 (d, 4H), 8.13 (dd, 4H), 7.62 (s, 4H), 7.54 (dd, 4H).

*Synthesis of cis-$Rh_2(\mu\text{-}HNCOCF_3)_2(phen)_2(Cl)_2$* ***(19)***

A brown solution of $[Rh_2(\mu\text{-}O_2CO)_2(phen)_2(H_2O)_2$ (0.103 g, 0.14 mmol) in $H_2O/CH_3OH$ (3/7, 60 ml), was heated with trifluoroacetamide (0.130 g, 1.15 mmol) under nitrogen. It was stirred for 15 minutes, and 0.1 M HCl (2.8 ml) was added dropwise. The mixture was refluxed for 24 h, after which time the solution was concentrated to ~20 mL and the dark red product recovered by vacuum filtration and recrystallized from methanol. Yield: 89.2 mg (74%). Anal. Calc. for $Rh_2C_{28}N_6O_2H_{18}F_6Cl_2$: C, 39.05; H, 2.11; N, 9.76. Found: C, 39.27; H, 2.43; N, 9.51 %. $^1$H NMR (300 MHz) in $CD_3OD$, δ / ppm (mult., int.): 8.78 (d, 2H), 8.65 (d, 2H), 8.45 (m, 4H), 7.96 (s, 2H), 7.88 (s, 2H), 7.74 (m, 4H), 6.57 (br, 2H).

*Synthesis of cis-$Rh_2(\mu\text{-}O_2CO)_2(dppz)_2(H_2O)_2$* ***(20)***

A red slurry of $[Rh_2(\mu\text{-}O_2CCH_3)_2(dppz)_2][O_2CCH_3]_2$ (0.163 g, 0.16 mmol) in 100 mL of $H_2O/CH_3OH$ (4/1) was added to a 1 M solution (35 ml) of $Na_2CO_3$ in $H_2O$ and the mixture refluxed under nitrogen for 1 h, during which time the color of the reaction mixture changed from red to brown. The volume was reduced to c.a. 30 mL and the product was recovered by filtration as a brown powder. The compound was recrystallized from a $H_2O$/MeOH (1/2) solution. Yield: 108.2 mg (73%). ESI-MS: *m/z* 891.0 ($[Rh_2(\mu\text{-}O_2CO)_2(dppz)_2] + H^+$). Anal. Calc. for $Rh_2(\mu\text{-}O_2CO)_2(dppz)_2(H_2O)_2 \cdot 2.5H_2O$: C, 46.98; H, 3.01; N, 11.53. Found: C, 47.04; H, 2.79; N, 11.71 %. $^1$H NMR (300 MHz) in $CD_3OD$, δ / ppm (mult., int.): 8.15 (m, 4H), 8.41 (m, 4H), 8.65 (m, 4H), 9.24 (d, 4H), 9.95 (d, 4H).

*Synthesis of cis-$Rh_2(\mu\text{-}HNCOCF_3)_2(dppz)_2(Cl)_2$* ***(21)***

A brown solution of $[Rh_2(\mu\text{-}O_2CO)_2(dppz)_2(H_2O)_2$ (0.083 g, 0.09 mmol) in $H_2O/CH_3OH$ (3/7, 60 ml) was reacted with trifluoroacetamide (0.085 g, 0.75 mmol) under nitrogen and stirred for 15 minutes, after which time 0.1 M HCl (1.8 mL) was added dropwise. The mixture was refluxed for 24 h, the solution was concentrated to ~20 mL and the red product was collected by filtration and finally recrystallized from methanol. Yield: 74.8 mg (78%). Anal. Calc. for $[Rh_2(\mu\text{-}HNCOCF_3)_2(dppz)_2(Cl)_2]$: C, 45.09; H, 2.08; N, 13.15. Found: C, 44.94; H, 2.11; N, 13.10 %. $^1$H NMR (300 MHz) in $CD_3OD$, δ / ppm (mult., int.): 9.13 (d, 2H), 9.06 (d, 2H), 8.90 (m, 4H), 8.55 (m, 4H), 8.28 (m, 4H), 8.14 (m, 4H), 6.65 (br, 2H).

*Synthesis of cis-$Rh_2(pyro)_2(dppz)_2(Cl)_2$* ***(22)***

A brown solution of $Rh_2(\mu\text{-}O_2CO)_2(dppz)_2(H_2O)_2$ (82.2 mg, 0.09 mmol) in $H_2O/CH_3OH$ (3/7, 60 mL), was reacted with 2-pyrrolidinone (62.1 mg, 0.72 mmol), and the reaction mixture was stirred for 15 minutes, followed by the dropwise addition of 0.1 M HCl (1.8 mL). The mixture was refluxed under nitrogen for 36 h, after which the solution was concentrated to ~40 mL and the red product was collected by filtration. Yield: 49.1 mg (54%). $^1$H NMR (300 MHz) in $CDCl_3/CD_3OD$ (1:1 v:v), δ / ppm (mult., int., assignment): 2.68 (m, 4H, pyrro), 2.75 (t, 4H, pyrro), 4.21 (t, 4H, pyrro), 7.24 (m, 4H, dppz), 8.77 (d, 2H, dppz), 9.02 (d, 2H, dppz), 9.25 (t, 2H, dppz), 8.41 (m, 4H, dppz), 9.72 (t, 2H, dppz), 9.99 (m, 4H, dppz).

*Synthesis of cis-$[Rh_2(\mu\text{-}O_2CCF_3)_2(phen)_2](O_2CCF_3)_2$* ***(4)***

$Rh_2(\mu\text{-}O_2CO)_2(phen)_2(H_2O)_2$ (0.075 g, 0.11 mmol) was treated with trifluoroacetic acid (10 mL) and the mixture stirred at r.t. under nitrogen for 15 minutes. The solvent was evaporated under vacuum and the product dissolved in acetonitrile. The red microcrystalline product was recovered after the addition of hexanes. Yield: 101.9 mg (91%). $^1$H NMR (300 MHz) in $CD_3OD$, δ / ppm (mult., int.): 8.29 (d, 4H), 8.06 (dd, 4H), 7.44 (s, 4H), 7.32 (dd, 4H).

*Synthesis of cis-$[Rh_2(\mu\text{-}O_2CCF_3)_2(dppz)_2](O_2CCF_3)_2$* ***(8)***

$Rh_2(\mu\text{-}O_2CO)_2(dppz)_2(H_2O)_2$ (118.3 mg, 0.14 mmol) was treated with trifluoroacetic acid (15 mL) and the mixture was stirred at r.t. under nitrogen for 15 minutes. The solvent was evaporated under vacuum and the product was dissolved in acetonitrile. A red microcrystalline product was recovered after the addition of

hexanes. Yield: 159.2 mg (93%). $^1$H NMR (300 MHz) in $CD_3OD$, δ / ppm (mult., int.): 9.35 (m, 4H), 8.95 (m, 4H), 8.45 (m, 4H), 8.25 (d, 4H), 8.10 (d, 4H).

**Methods**

*X-ray Crystallographic Studies*

***X-ray Structural Study of cis-$Rh_2(\mu$-$HNCOCF_3)_2(phen)_2(Cl)_2$ (19).*** For the X-ray crystallographic analysis, a red prismatic crystal of **19** (approximate dimensions: 0.24 x 0.22 x 0.18 $mm^3$) was selected. The crystal was grown from a solution of **19** in $CH_3CN/CH_3OH$ layered with diethyl ether. The crystal was coated with Paratone oil, transferred to a nylon loop, and placed in a cold $N_2$ stream at 110(2) K. An indexing of the preliminary diffraction patterns indicated that the crystal was monoclinic. A total of 12,871 reflections were collected in the range $1.82 \leq \theta \leq 28.29°$. The data collection covered approximately a hemisphere of reciprocal space, by a combination of three sets of exposures; each set had a different $\phi$ angle for the crystal and each exposure covered 0.3º in $\Omega$. Crystal decay, which was monitored by analyzing duplicate reflections, was found to be less than 1%, therefore, no decay correction was applied. During the final cycles of refinement, all atoms with the exception of hydrogen were refined anisotropically. The structure of **19** was solved and refined in the space group C 1 2/*c*1.

***X-ray Structural Study of cis-$Rh_2(pyro)_2(dppz)_2(Cl)_2$ (22).*** For the X-ray crystallographic analysis, a red plate crystal of **22** (approximate dimensions: 0.20 x 0.15 x 0.08 $mm^3$) was selected. The crystal was grown from a solution of **19** in $CH_3CN$/benzene layered with diethyl ether in the presence of $NaBF_4$. The crystal was coated with Paratone oil, transferred to a nylon loop, and placed in a cold $N_2$ stream at

110(2) K. An indexing of the preliminary diffraction patterns indicated that the crystal was monoclinic. A total of 18,539 reflections were collected in the range $1.50 \leq \theta \leq 23.32°$. Hydrogen atoms belonging to methylene groups were placed in regions of maximum electron density around the methylene C atoms. The structure was solved and refined in the space group *P*-1. The final refinement cycle was based on 18,539 unique reflections (6,247 with $F_\sigma^2 > 2\sigma(F_\sigma^2)$), 588 parameters, and 0 restraints ($R1 = 0.0561$, $wR2 = 0.1362$). The maximum and minimum peaks in the final difference Fourier map corresponded to 2.712 and –0.813 e/Å$^3$, respectively, with a goodness-of-fit value of 1.038.

***X-ray Structural Study of cis-[Rh$_2$($\mu$-O$_2$CCF$_3$)$_2$(dppz)$_2$](O$_2$CCF$_3$)$_2$ (8).*** For the X-ray crystallographic analysis, a red block crystal of **8** (approximate dimensions: 0.34 x 0.23 x 0.14 mm$^3$) was selected. The crystal was coated with Paratone oil, transferred to a nylon loop, and placed in a cold $N_2$ stream at 110(2) K. An indexing of the preliminary diffraction patterns indicated that the crystal was monoclinic. A total of 39,468 reflections were collected in the range $1.78 \leq \theta \leq 27.61°$. The structure was solved and refined in the space group *P*-1. The final refinement cycle was based on 10,042 unique reflections (5,151 with $F_\sigma^2 > 2\sigma(F_\sigma^2)$), 684 parameters, and 24 restraints ($R1 = 0.0871$, $wR2 = 0.2040$). The maximum and minimum peaks in the final difference Fourier map corresponded to 0.993 and –1.017 e/Å$^3$, respectively, with a goodness-of-fit value of 1.017.

**Instrumentation**

The $^1$H NMR spectra of the complexes were recorded on a Unity-300 NMR spectrometer. Absorption measurements were performed on a Schimadzu UVPC-3001 spectrophotometer. X-ray diffraction data were collected on a Bruker APEX CCD diffractometer with graphite monochromated Mo-$K_\alpha$ radiation ($\lambda$ = 0.71073 Å). The frames were integrated with the Bruker SAINT software,[110] and a semi-empirical absorption correction using multiple-measured reflections was applied using SADABS.[111] The structures were solved and refined using X-SEED,[112] a graphical interface to SHELX97.[113]

*Results and Discussion*

**Synthesis**

The synthetic routes for the newly synthesized dirhodium(II,II) complexes **8**, and **18**-**22** are outlined (Schemes V.1 and V.2). When $[Rh_2(\mu\text{-}O_2CCH_3)_2(phen)_2][O_2CCH_3]_2$ in distilled water is added to an aqueous solution of $Na_2CO_3$ and refluxed for 1 h, the complex $Rh_2(\mu\text{-}O_2CO)_2(phen)_2(H_2O)_2$ (**18**) is formed. Compound **18** is soluble in $H_2O$ and $CH_3OH$, sparingly soluble in $CH_3CN$ and $C_2H_5OH$ and insoluble in $CHCl_3$ and $CH_2Cl_2$. The ESI mass spectrum of **18** exhibits a parent ion peak, $[Rh_2(\mu\text{-}O_2CO)_2(phen)_2] + H^+$ , at m/z = 687.3, and the $^1$H-NMR (300 MHz) spectrum in $CD_3OD$ shows resonances at δ / ppm (mult., int.) 8.65 (dd, 4H), 8.13 (dd, 4H), 7.62 (s, 4H), 7.54 (dd, 4H) with no features in the aliphatic region. The observed $^1$H-NMR aromatic peaks resemble that of the parent dirhodium complex containing two phenanthroline ligands, although they are shifted downfield by ~1 ppm.

**Scheme V.1.** Synthetic routes for the syntheses of compounds **4**, **18**, and **19**.

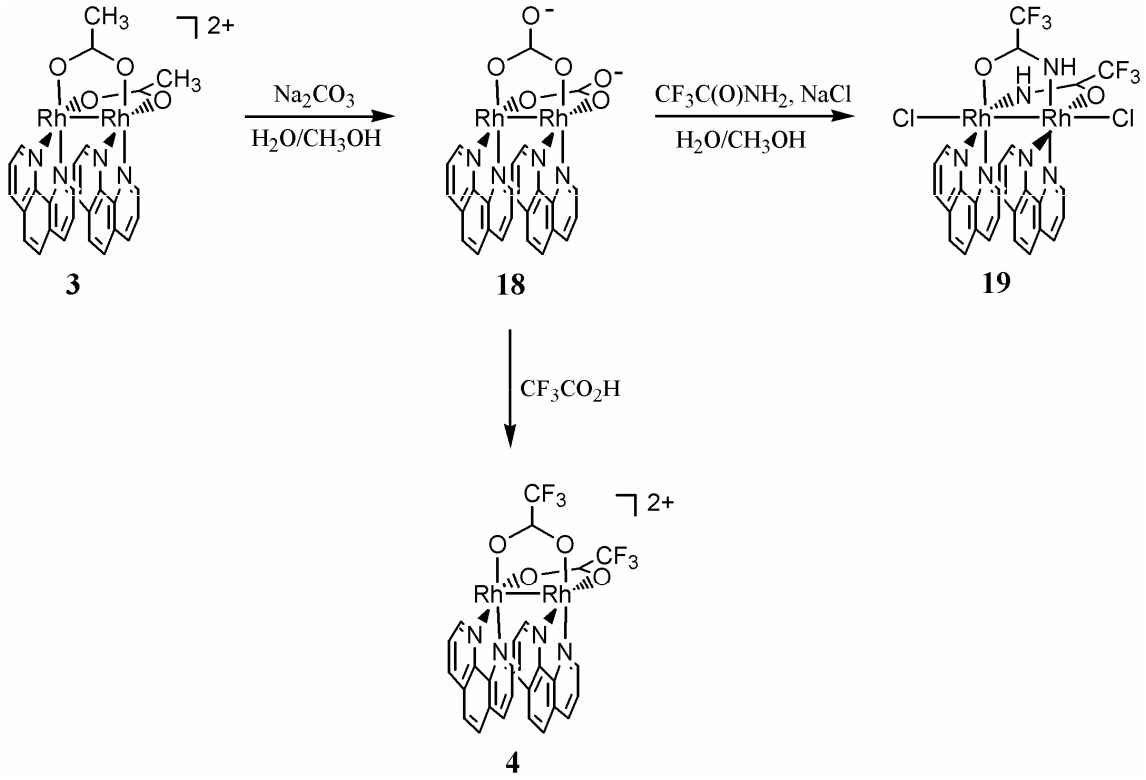

**Scheme V.2.** Synthetic routes for the syntheses of compounds **8**, **20** - **22**.

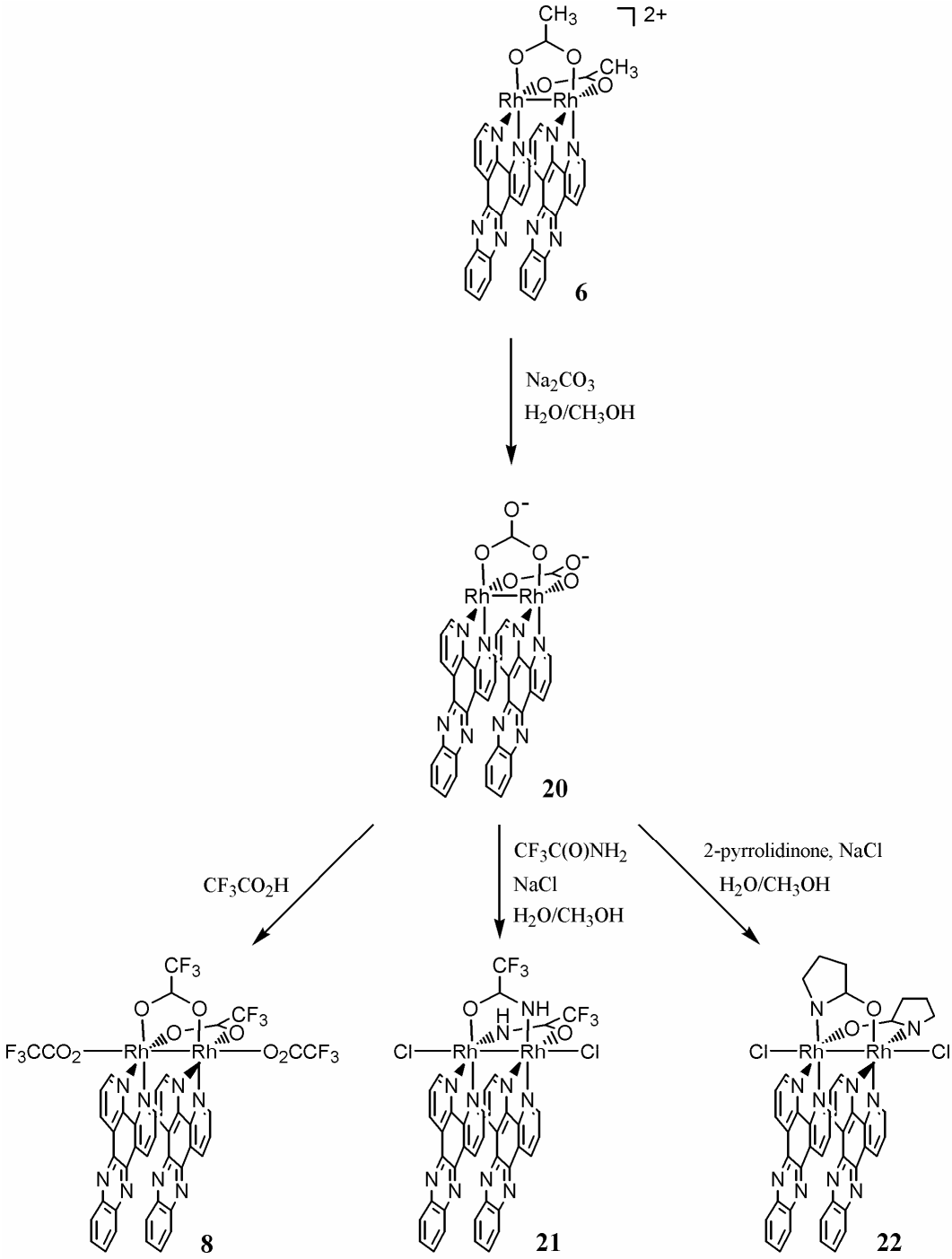

In the case of $[Rh_2(\mu\text{-}O_2CCH_3)_2(dppz)_2][O_2CCH_3]_2$, the reaction with $Na_2CO_3$(aq) under conditions used for the bis-phenanthroline analogue produces the expected complex in low yields, a result that is most likely due to the low solubility of the starting material in $H_2O$. The addition of methanol to the reaction mixture increases the yield of $Rh_2(\mu\text{-}O_2CO)_2(dppz)_2(H_2O)_2$ (**20**) to 73%. The $^1$H NMR (300 MHz) spectrum in $CD_3OD$ contains resonances peaks at δ / ppm (mult., int.) 9.95 (d, 4H), 9.24 (d, 4H), 8.65 (m, 4H), 8.41 (m, 4H), and 8.15 (m, 4H). The spectrum is very similar to that of $[Rh_2(\mu\text{-}O_2CCH_3)_2(dppz)_2][O_2CCH_3]_2$ (**6**), with the difference being that in the case of **20** the resonances appear at lower fields. These results indicate that the structure of **20** must be similar to that of **6**, and that the dirhodium core remains intact in the product.

The presence of two carbonato ligands bound to the bis-diimine dirhodium unit offers the possibility of facile access to other similar complexes. Roos et al., have shown that the tetracarbonato complex quickly reacts within 20-40 minutes with 8 equivalents of the desired carboxylic acid in water at 80-90° C.[191] Based on this information, a reasonable course of action is to react the bis-carbonato bis-diimine dirhodium species with an excess of acetamido ligand.

Reactions of $Rh_2(\mu\text{-}O_2CO)_2(phen)_2(H_2O)_2$ **(18)** with an excess of trifluoroacetamide (8 eq.) in a $H_2O$/MeOH (3/7) mixture under nitrogen produces the amidato derivative $Rh_2(\mu\text{-}HNCOCF_3)_2(phen)_2(Cl)_2$ (**19**) in a good yield. During the reaction, an intensely colored blue product is formed in both cases. Attempts to isolate this compound proved to be unsuccessful since, upon cooling, the reactions

turn red and **19** is the only product recovered. This color has been previously observed in reactions involving the preparation of related bis-diimine dirhodium derivatives in the presence of methanol and it has been determined that is due to the formation of reduced $Rh_2$(I,II) species that form chains in the solid state.[156-158]

Similarly, **20** was treated with trifluoroacetamide to produce $Rh_2(\mu\text{-}HNCOCF_3)_2(dppz)_2(Cl)_2$ (**21**) in good yield (78%). As mentioned above, a blue color appears during the reaction that turns red-brown when the reaction is exposed to air or when the solution is cooled. When **20** is treated with 2-pyrrolidinone in water/methanol (3/7), the compound $Rh_2(pyro)_2(dppz)_2(Cl)_2$, (**22**), is recovered in moderate yield (54%).

It is possible to convert the carbonato ligands into better leaving groups by protonation. By treating both **18** and **20** with neat trifluoroacetic acid**,** it is possible to isolate $[Rh_2(\mu\text{-}O_2CCF_3)_2(phen)_2](O_2CCF_3)_2$ (**4**), and $[Rh_2(\mu\text{-}O_2CCF_3)_2(dppz)_2](O_2CCF_3)_2$ (**8**). The reaction proceeds to near completion at room temperature and the red products are obtained in approximately 15 minutes.

**X-Ray crystallography**

The molecular structure of **19**, as revealed by X-ray crystallography, consists of a central $Rh_2$ core coordinated to two trifluoroamidato ligands in a *cis* disposition and two chelating phen molecules in the remaining equatorial positions. The rhodium atoms are further coordinated to two chloride anions at the axial sites. The structure of **19** is shown in Figure V.1. The Rh-Rh distance of 2.614(1) Å is comparable to the analogous distance obtained for the closely related compound $Rh_2(\mu\text{-}HNCOCF_3)_2(phen)_2(C_5H_5N)_2$, 2.612(1) Å,[189] but longer than the Rh-Rh distances in acetato counterparts.[44] The Rh-Cl bonds deviate slightly from the axis formed by the rhodium-rhodium bond at an angle of 172.2°.

The bonds to the oxygen atoms of the bridging amidato ligands are longer than those to the nitrogen atoms (2.059(4) and 2.024(4) Å respectively). The lengths of the Rh-$N_{phen}$ bonds are affected by the different *trans* influence of the nitrogen and oxygen atoms on the bridging ligands; those *trans* to oxygen have a mean distance of 2.003(4) Å, while those *trans* to nitrogen are at an average distance of 2.031(4) Å. These distances are shorter than the those reported for the related complex $Rh_2(\mu\text{-}HNCOCF_3)_2(phen)_2(C_5H_5N)_2$ (Rh-$N_{phen}$ *trans* to O, 2.020(6); Rh-$N_{phen}$ trans to NH, 2.040(5) Å).[186] The two phen moieties are found in a staggered arrangement about the Rh-Rh bond with a torsion angle of 13.8°, similar to the one observed for the aforementioned di-cation which exhibits an angle of 15.8°.[189] Selected crystal crystal parameters, bond distances and angles for compound **19** are listed in Tables V.1, V.2, and V.3.

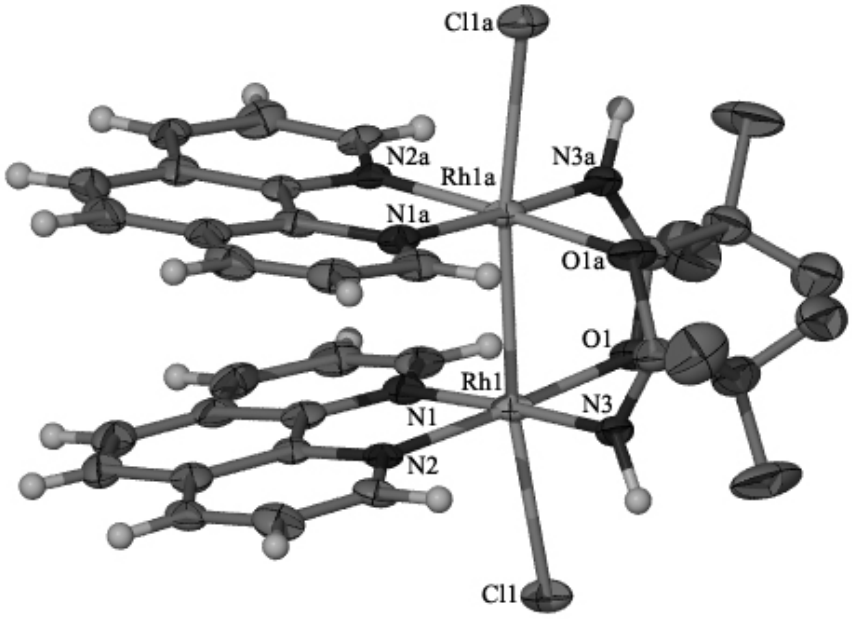


**Figure V.1.** Thermal ellipsoid plot at the 50% probability level of compound **19**.

The structure of $Rh_2(pyro)_2(dppz)_2(Cl)_2$ (**22**), is shown in Figure V.2. The molecular structure consists of a dinuclear $Rh_2(II,II)$ core with two chelating dppz ligands coordinated to each Rh atom, and two bridging pyrrolidinonato ligands occupying the remaining equatorial sites. The complex exhibits a head-to-tail arrangement of the bridging ligands, similar to that observed for compound **19**. The octahedral coordination around the rhodium atoms is completed by a pair of $Cl^-$ ions bound to the axial positions. The Rh-Rh bond distance is 2.612(12) Å, which is longer than the Rh-Rh bond observed for the $Rh_2(pyro)_4(Hpyro)_2$ complex (2.445(1) Å).[192] This increase in the metal-metal bond distance may be related to the presence of the $Cl^-$ ligands in the axial positions which are known to cause such an increase, the ocurrence of the two dppz ligands that push the two rhodium atoms further apart in order to avoid repulsive π interactions, or more likely a combination of both factors.[189,193] The Rh-Cl interactions are slightly off the axis formed by the two metal atoms and form angles of 175.93(5)° and 176.05(6)° with the dirhodium axis, respectively. Selected crystal parameters, bond distances and angles for compound **19** are listed in Tables V.4, V.5, and V.6.

**Table V.1.** Crystal data and structural refinement parameters for compound **19**.

| | |
|---|---|
| Empirical formula | $C_{28}H_{18}Cl_2F_6N_6O_2Rh_2$ |
| Formula weight | 861.20 |
| Temperature | 100(2) K |
| Wavelength | 0.71073 Å |
| Crystal system | Monoclinic |
| Space group | P21 |
| a | 19.310(4) Å |
| b | 14.880(3) Å |
| C | 14.690(3) Å |
| α | 90° |
| β | 118.00(3)° |
| γ | 90° |
| Volume | 3726.8(13) $Å^3$ |
| Z | 4 |
| Density (calculated) | 1.535 $Mg/m^3$ |
| Crystal size | 0.24 x 0.22 x 0.18 $mm^3$ |
| Theta range for data collection | 1.82 to 28.29°. |
| Reflections collected | 12871 |
| Independent reflections | 4302 [R(int) = 0.0500] |
| Data / restraints / parameters | 4302 / 208 / 0 |
| Goodness-of-fit on $F^2$ | 0.927 |
| Final R indices [I>2sigma(I)] | R1 = 0.0647, wR2 = 0.1496 |
| R indices (all data) | R1 = 0.0983, wR2 = 0.1634 |

$R_1 = \Sigma||F_o| - |F_c||/\Sigma|F_o|$; $wR_2 = [\Sigma[w(F_0^2-F_c^2)^2]/\Sigma[w(F_0^2)^2]]^{1/2}$

**Table V.2.** Selected bond distances (Å) for compound **19**.

| | Bond Distances (Å) |
|---|---|
| Rh(1)-Rh(2) | 2.614(1) |
| Rh(1)-N(1) | 2.031(4) |
| Rh(1)-N(2) | 2.003(4) |
| Rh(1)-N(3) | 2.024(4) |
| Rh(1)-O(1) | 2.058(4) |
| Rh(1)-Cl(1) | 2.540(2) |

**Table V.3.** Selected bond angles (°) for compound **19**.

| | Bond Angles (°) |
|---|---|
| N(1)-Rh(1)-N(2) | 82.1(2) |
| N(2)-Rh(1)-N(3) | 94.9(2) |
| N(3)-Rh(1)-O(1) | 90.9(2) |
| O(1)-Rh(1)-N(1) | 92.1(2) |
| Cl(1)-Rh(1)-Rh(1a) | 172.24(4) |
| N(1)-Rh(1)-Cl(1) | 88.4(1) |
| N(2)-Rh(1)-Cl(1) | 91.1(1) |
| N(3)-Rh(1)-Cl(1) | 90.5(1) |
| O(1)-Rh(1)-Cl(1) | 88.9(1) |

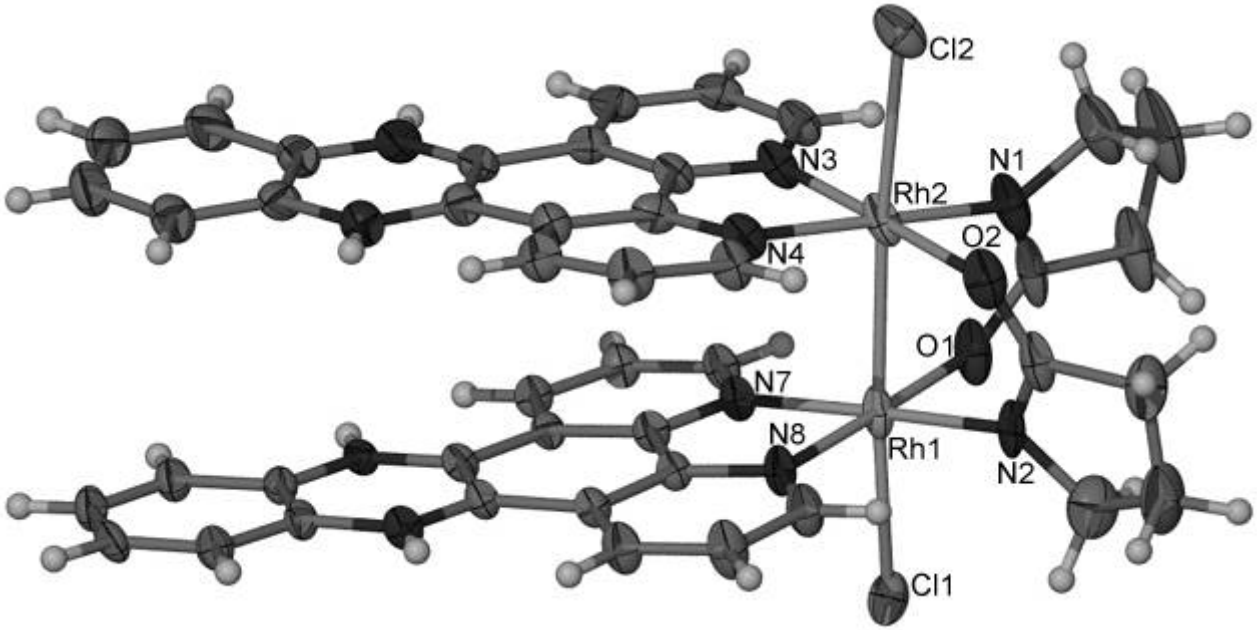


**Figure V.2.** Thermal ellipsoid plot at the 50% probability level of compound **22**.

**Table V.4.** Crystal data and structural refinement parameters for compound **22**.

| | |
|---|---|
| Empirical formula | $C_{47}H_{38}Cl_2N_{11}O_3Rh_2$ |
| Formula weight | 1081.60 |
| Temperature | 100(2) K |
| Wavelength | 0.71073 Å |
| Crystal system | Triclinic |
| Space group | P-1 |
| a | 12.45(3) Å |
| b | 13.16(6) Å |
| C | 14.32(6) Å |
| α | 98.2(1)° |
| β | 105.0(1)° |
| γ | 100.1(1)° |
| Volume | 2186(15) $Å^3$ |
| Z | 2 |
| Density (calculated) | 1.643 $Mg/m^3$ |
| Crystal size | 0.20 x 0.15 x 0.08 $mm^3$ |
| Theta range for data collection | 1.50 to 23.32°. |
| Reflections collected | 18539 |
| Independent reflections | 6247 [R(int) = 0.0500] |
| Data / restraints / parameters | 6247 / 588 / 0 |
| Goodness-of-fit on $F^2$ | 1.038 |
| Final R indices [I>2sigma(I)] | R1 = 0.0561, wR2 = 0.1362 |
| R indices (all data) | R1 = 0.0778, wR2 = 0.1480 |

$R_1 = \Sigma||F_o| - |F_c||/\Sigma|F_o|$; $wR_2 = [\Sigma[w(F_0^2-F_c^2)^2]/\Sigma[w(F_0^2)^2]]^{1/2}$

**Table V.5.** Selected bond distances (Å) for compound **22**.

| | Bond Distances (Å) |
|---|---|
| Rh(1)-Rh(2) | 2.612(12) |
| Rh(1)-N(2) | 2.027(10) |
| Rh(1)-O(1) | 2.059(7) |
| Rh(1)-N(7) | 2.032(9) |
| Rh(1)-N(8) | 2.001(7) |
| Rh(1)-Cl(1) | 2.557(12) |
| Rh(2)-N(1) | 2.023(8) |
| Rh(2)-O(2) | 2.056(10) |
| Rh(2)-N(3) | 1.995(10) |
| Rh(2)-N(4) | 2.044(8) |
| Rh(2)-Cl(2) | 2.561(12) |

**Table V.6.** Selected bond angles (°) for compound **22**.

| | Bond Angles (°) |
|---|---|
| O(1)-Rh(1)-N(2) | 88.0(3) |
| N(2)-Rh(1)-N(8) | 94.4(3) |
| N(8)-Rh(1)-N(7) | 80.9(3) |
| Cl(1)-Rh(1)-N(8) | 88.8(2) |
| O(2)-Rh(2)-N(1) | 86.9(2) |
| N(1)-Rh(2)-N(3) | 95.0(3) |
| N(3)-Rh(2)-N(4) | 80.8(2) |
| Cl(2)-Rh(2)-N(3) | 89.8(2) |
| Rh(1)-Rh(2)-Cl(2) | 176.06(6) |

The molecular structure of **8**, determined by X-ray crystallographic methods, consists of a dinuclear $Rh_2$(II,II) core with a chelating dppz ligands coordinated to each Rh atom in a *syn* disposition, and two bridging trifluoroacetato groups occupying the remaining equatorial sites. A trifluoroacetate ligand and a $CH_3CN$ group coordinated at the axial positions completes an irregular octahedral coordination sphere about each Rh atom. The structure of **8** is shown in Figure V.3. The Rh-Rh distance in **8**, 2.567(1) Å, is comparable to the one reported for $[Rh_2(O_2CCF_3)_2(bpy)_2]^{2+}$, 2.570(6) Å. When compared to the analogous bis-acetato complex, a lengthening of the metal-metal bond (2.5519(6) Å) is observed, a situation that also occurs with other acetate-trifluoroacetate pairs. The lengths of the Rh-$O_{eq}$ bonds in **8**, which range from 2.056(6) to 2.063(6) Å, are also longer than the analogous acetato complex (2.009(4)-2.051(3) Å). The Rh-$N_{dppz}$ bonds, 1.988(7) to 2.011(7) Å, are shorter (2.005(4) to 2.016(4) Å). The internal twist angle from the eclipsed geometry of 10.6° in **8** is smaller than that observed for the bis-acetate analogue (13°). Selected crystal parameters, bond distances and angles for compound **19** are listed in Tables V.7, V.8, and V.9.

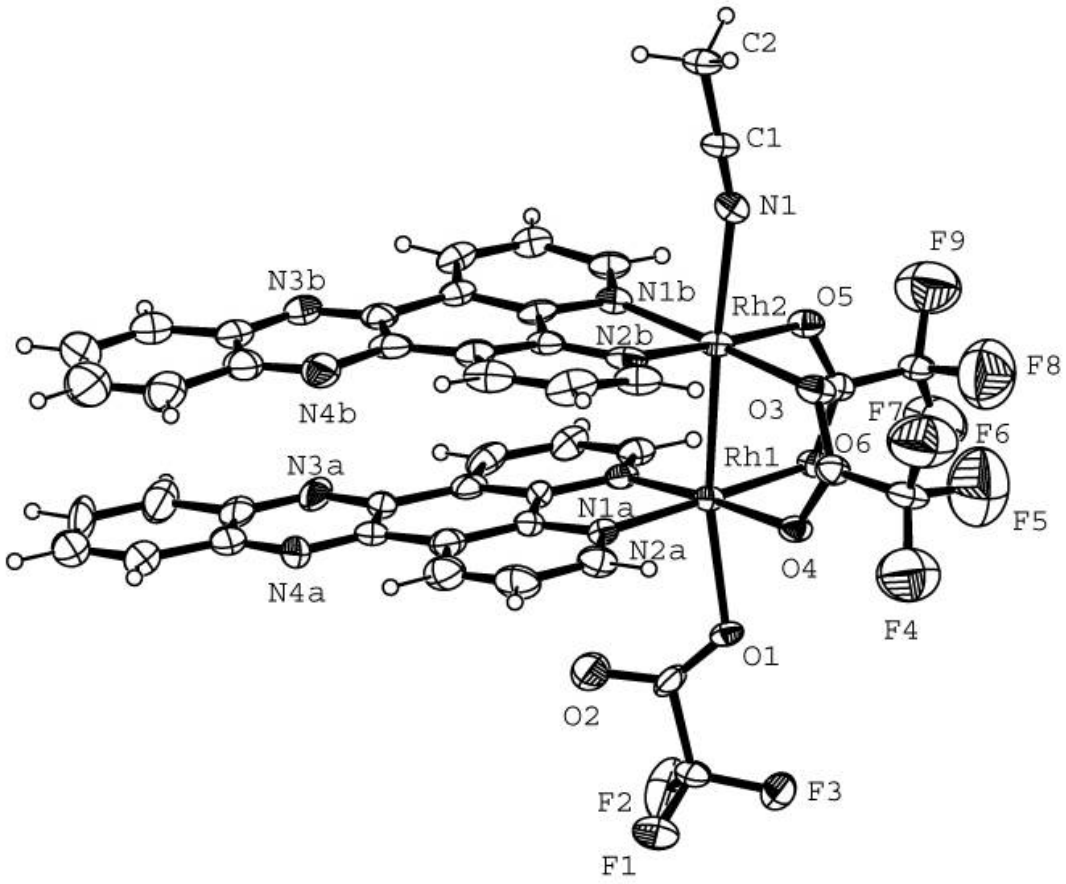


**Figure V.3.** Thermal ellipsoid plot at the 50% probability level of compound **8**.

**Table V.7.** Crystal data and structural refinement parameters for compound **8**.

| | |
|---|---|
| Empirical formula | $C_{47}H_{26}BF_{13}N_9O_6Rh_2$ |
| Formula weight | 1276.40 |
| Temperature | 100(2) K |
| Wavelength | 0.71073 Å |
| Crystal system | Monoclinic |
| Space group | C2/c |
| a | 51.678(10) Å |
| b | 11.735(2)Å |
| C | 15.943(3) Å |
| $\alpha$ | 90.00 ° |
| $\beta$ | 106.32(3)° |
| $\gamma$ | 90.00° |
| Volume | 9279(3) $Å^3$ |
| Z | 8 |
| Density (calculated) | 1.827 $Mg/m^3$ |
| Crystal size | 0.34 x 0.23 x 0.14 $mm^3$ |
| Theta range for data collection | 1.78 to 27.61°. |
| Reflections collected | 39468 |
| Independent reflections | 10042 [R(int) = 0.0500] |
| Data / restraints / parameters | 10042 / 684 / 28 |
| Goodness-of-fit on $F^2$ | 1.017 |
| Final R indices [I>2sigma(I)] | R1 = 0.0871, wR2 = 0.2040 |
| R indices (all data) | R1 = 0.1710, wR2 = 0.2534 |

$R_1 = \Sigma||F_o| - |F_c||/\Sigma|F_o|$; $wR_2 = [\Sigma[w(F_0^2-F_c^2)^2]/\Sigma[w(F_0^2)^2]]^{1/2}$

**Table V.8.** Selected bond distances (Å) for compound **8**.

| | Bond Distances (Å) |
|---|---|
| Rh(1)-Rh(2) | 2.567(1) |
| Rh(1)-N(1a) | 2.006(7) |
| Rh(1)-N(2a) | 1.988(7) |
| Rh(1)-O(4) | 2.058(5) |
| Rh(1)-O(6) | 2.063(6) |
| Rh(1)-O(1) | 2.249(5) |
| Rh(2)-N(1b) | 2.011(7) |
| Rh(2)-N(2b) | 2.008(7) |
| Rh(2)-O(3) | 2.056(6) |
| Rh(2)-O(5) | 2.063(6) |
| Rh(2)-N(1) | 2.279(7) |

**Table V.9.** Selected bond angles (°) for compound **8**.

| | Bond Angles (°) |
|---|---|
| Rh(1)-Rh(2)-N(1) | 176.6(2) |
| Rh(2)-Rh(1)-O(1) | 170.1(2) |
| O(6)-Rh(1)-O(4) | 87.3(2) |
| O(6)-Rh(1)-N(1a) | 94.5(3) |
| O(4)-Rh(1)-N(2a) | 96.4(3) |
| O(5)-Rh(2)-O(3) | 87.8(2) |
| O(5)-Rh(2)-N(1b) | 96.0(3) |
| O(3)-Rh(2)-N(2b) | 94.3(3) |

## *Concluding Remarks*

The results of this study demonstrate that the carbonato-bridged complexes of the $Rh_2(\mu\text{-}O_2CO)_2(diimine)_2(H_2O)_2$-type are useful precursors for the preparation of dirhodium-diimine compounds. The reactions of $Rh_2(\mu\text{-}O_2CO)_2(diimine)_2(H_2O)_2$ (diimine = dppz, phen) with trifluoroacetamide, 2-pyrrolidinone, and trifluoroacetic acid lead to products in which the carbonato ligands have been displaced from the dirhodium core. The compounds described in this chapter lay the synthetic groundwork for a new series of dirhodium complexes that contain the interesting dppz ligand and bridging ligands other than acetate.

# CHAPTER VI

# CONCLUSIONS

The discovery of new molecules for the treatment of diseases is obviously of tantamount importance in the field of medicinal chemistry. Once the activity of a particular compound is noted, however, it is also important to understand the structure/activity relationship of the new molecules, so they can be modified to obtain molecules with improved pharmacological properties as compared to the parent compound(s). In this dissertation, a new family of dirhodium complexes containing the electron acceptor ligand dipyrido[3,2-a:2′,3′-c]phenazine (dppz) was reported along with their chemical, physical and biological properties. Of particular interest is the understanding of the relationship between the reactivity of the metal complexes and their cytotoxicity in the dark as well as after irradiation.

In Chapter II, the synthesis and characterization of the new dirhodium complexes *cis*-$[Rh_2(\mu\text{-}O_2CCH_3)_2(\eta^1\text{-}O_2CCH_3)(dppz)(MeOH)]^+$ (**5**), $[Rh_2(\mu\text{-}O_2CCH_3)_2(dppz)_2]^{2+}$ (**6**), $[Rh_2(\mu\text{-}O_2CCH_3)_2(dppz)(bpy)]^{2+}$ (**7**), and $[Rh_2(\mu\text{-}O_2CCF_3)_2(dppz)_2]^{2+}$ (**8**) was reported. All of these complexes photocleave pUC18 plasmid DNA *in vitro* under irradiation with visible light, resulting in the nicked, circular form. A comparison of the phototocleavage properties of ds-DNA of **5** and **6** revealed that **5** is more reactive, a fact that is attributed to the intercalative ability of the former compound. The presence of the dppz ligand is important for the photocleavage activity of these complexes, since other dirhodium caraboxylate compounds that do not contain this ligand are not able to cleave DNA after irradiation.

The toxicity of dirhodium dppz complexes ligand towards human skin cells increases when the cell cultures are irradiated with visible light. In contrast, the photocytotoxicity of those complexes that do not contain the dppz ligand do not differ from their cytotoxicity properties in the dark. The mono-substituted compound, **5**, does not significantly increase its cytotoxicity upon irradiation., whereas greater differences were observed for compounds **6**, **7** and **8** which increase their cytotoxicity from two to five times when irradiated with visible light. In particular, compound **7** shows an increase in its cytotoxicity upon irradiation similar to that of the clinically used photodynamic therapy drug hematoporphyrin.

An interesting fact encountered in these studies is that dirhodium complexes containing the dppz ligand can photocleave DNA in the absence of oxygen as well as in the presence of oxygen. Although less photocleavage is observed under anaerobic conditions, it is apparent that there are two pathways that are operative. It is plausible that the role of molecular oxygen in the reactivity of these molecules is the reoxidation of the dirhodium-dppz molecules, thereby rendering the photocleavage of DNA catalytic. As reported in Chapter III, compounds **6** and **7** are reduced in the presence of ethanol to form a blue compound which reverts to the original complex upon exposure to air. If one considers the photocleavage mechanism proposed by Turro *et al*.,[194] for dirhodium tetraacetate in the presence of an external electron acceptor (Figure VI.1), it is obvious that if a similar mechanism is invoked for the dirhodium-dppz complexes, the cycle cannot be closed without the assistance of an oxidizing agent (Figure VI.2). From

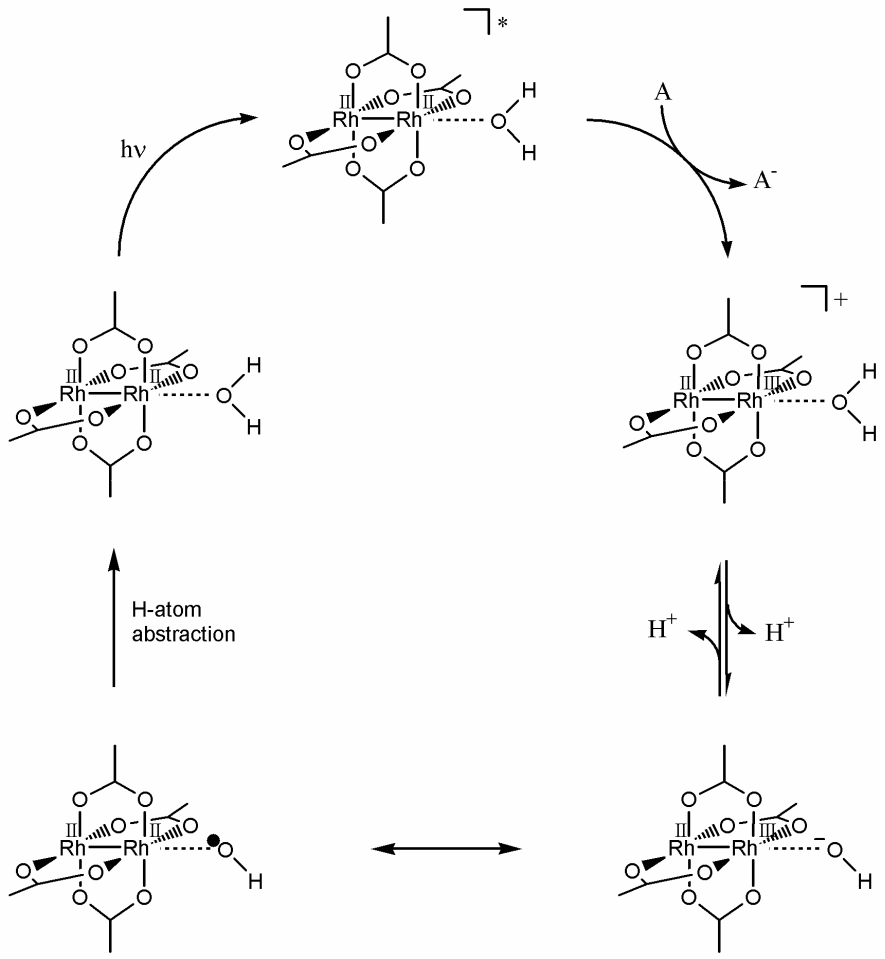


**Figure VI.1.** Proposed mechanism for the photocatalytic generation of hydroxyl radical from dirhodium tetraacetate (ref. 194).

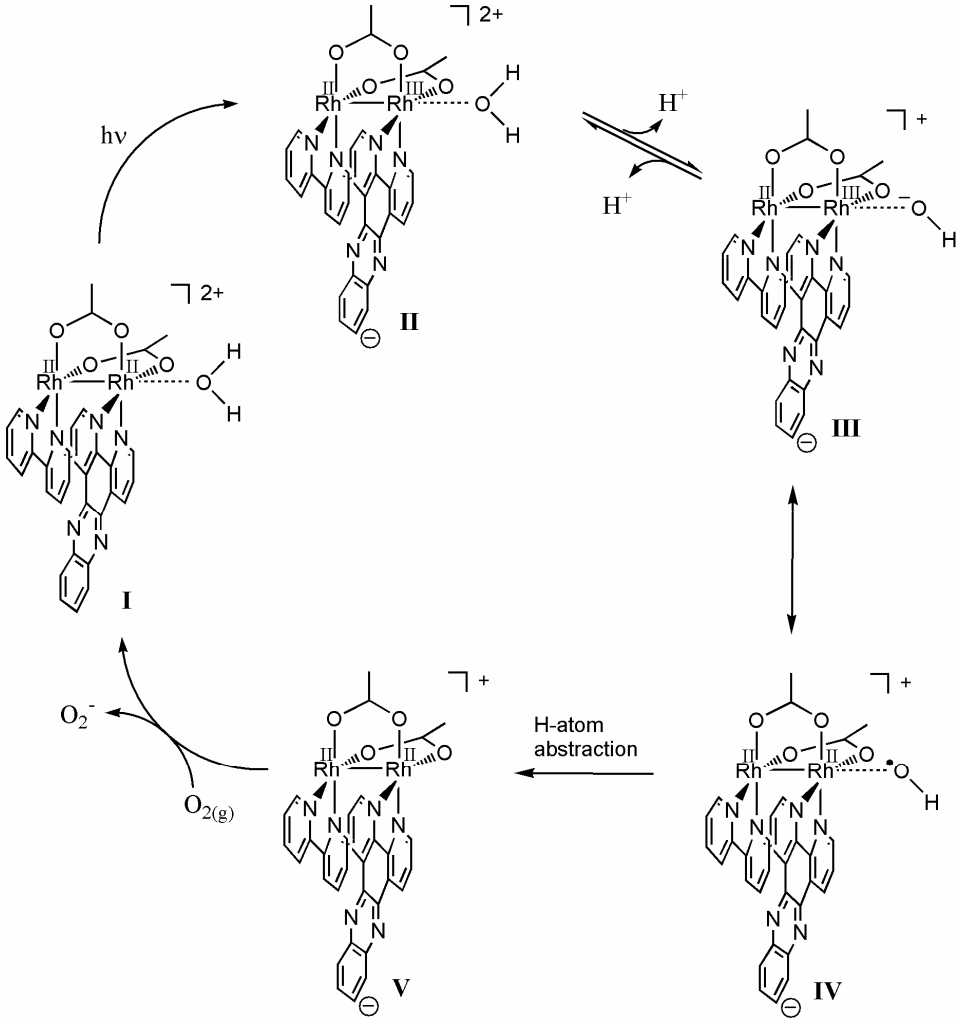


**Figure VI.2.** Proposed mechanism for the photocatalytic generation of hydroxyl radical from a dirhodium-dppz complex.

the reactions of these complexes with ethanol it can be concluded that oxygen will lead to the re-oxidation of species **V** into **I** (Figure VI.2).

The work described in Chapter III describes reactivity studies of dirhodium-dppz complexes with glutathione, an important molecule in the deactivation of metal-based drugs due to its high concentration (millimolar) in the cellular milieu. Compounds **6** and **7** are reacte with glutathione to produce a blue compound that is reminiscent of the blue color obtained in the reduction reactions with alcohols. The product formed in the reaction with glutathione also reoxidizes to the original complex. An EPR spectrum of the product formed in the reaction of complex **7** with glutathione consists of a broad isotropic signal similar to the spectra obtained for one-electron reduced dirhodium complexes containing polypyridyl ligands, where the added electron is found delocalized on the aromatic ligands. DFT calculations indicate that the LUMO and LUMO + 1 orbitals in compound **7** are ligand-based $\pi^*$ orbitals, a fact that corroborates the conclusion that the extra electron is located on the ligands as in the case of the aforementioned dirhodium complexes.

In addition, Chapter III also reports results from single-cell electrophoresis experiments of cells treated with compound **7**. As depicted in Figure III.6a, in the absence of light, **7** does not damage nuclear DNA. If the cell culture containing **7** is irradiated, however, a comet tail appears which accounts for cellular DNA damage (Figure III.6b). Hematoporphyrin, the key ingredient of Photofrin®, does not damage DNA, as observed previously in a similar experiment. This implies that, despite the abundance of other reactive compounds in the cell, compound **7** (or the species

generated after activation), is capable of reaching the cellular nucleus and causes damage to nuclear DNA.

Chapter IV discusses the molecular characteristics that affect the *in vitro* activity of dirhodium complexes. It was observed that the lability of the groups coordinated to the dirhodium complexes is a significant factor that influences the toxicity of the complexes. In the case of acetate and trifluoroacetate derivatives, the reactivity ratios for ligand displacement in compounds **1** and **2** (2:1 ratio) correlate well with the $LC_{50}$ values of the acetate derivatives with **1**, **3**, and **6** being half as cytotoxic as the trifluoroacetate derivatives **2**, **4**, and **8**. In addition, the presence of labile solvent molecules and the monodentate acetate groups in **5**, **10**, **13** and **14** provide potential "open sites" accessible for nucleophilic substitution, as opposed to these sites being occupied by non-labile groups such as bpy that reduce the reactivity of the complexes. Clearly, the labile equatorial groups play a critical role in the toxicity of dirhodium(II,II) complexes *in vitro*.

A large cytotoxicity/photocytotoxicity ratio is an important property in compounds for PDT applications. From the data in Chapter IV, it is plausible to suggest that in order to decrease the cytotoxicity of the dirhodium-dppz complexes in the dark, the acetato bridging ligands should be replaced by less labile groups. The results of Chapter V demonstrate that the carbonato-bridged complexes of the $[Rh_2(\mu\text{-}O_2CO)_2(diimine)_2(H_2O)_2\ ]^{2+}$ type are useful precursors to access new dirhodium-diimine compounds. These compounds react with trifluoroacetamide, 2-pyrrolidinone, and trifluoroacetic acid to form products in which the carbonato ligands have been displaced

from the dirhodium core. Chapter V lays the synthetic groundwork for a new series of dirhodium complexes that contain the interesting dppz ligand and bridging ligands other than acetate.

## REFERENCES


1. Chabner, B. A.; Roberts, T. G. *Nature Rev. Cancer* **2005**, *5*, 65-72.

2. Futreal, P. A.; Coin, L.; Marshall, M.; Down, T.; Hubbard, T.; Wooster, R.; Rahman, N.; Stratton, M. R. *Nature Rev. Cancer* **2004**, *4*, 177-183.

3. Suarez, H. G. *Anticancer Res.* **1989**, *9*, 1331-1343.

4. Povirk, L. F.; Shuker, D. E. *Mutation Research-Rev. Gen. Toxicol.* **1994**, *318*, 205-226.

5. Souhami, R. L. *Quarterly J. Med.* **1994**, *87*, 195-197.

6. (a) Hurley, L. H. *Nature Rev. Cancer* **2002**, *2*, 188-200. (b) Jordan, M. A.; Wilson, L. *Nature Rev. Cancer* **2004**, *4*, 253-265.

7. Neidle, S.; Thurston, D. E. *Nature Reviews Cancer* **2005**, *5*, 285-296.

8. Thurston, D. E. *British J. Cancer* **1999**, *80*, 65-85.

9. Schultz, E. M.; Sprague, J. M. *J. Am. Chem. Soc.* **1948**, *70*, 48-52.

10. Suggitt, M.; Bibby, M. C. *Clin. Cancer Res.* **2005**, *11*, 971-981.

11. Holbeck, S. L. *Eur. J. Cancer* **2004**, *40*, 785-793.

12. Monga, M.; Sausville, E. A. *Leukemia* **2002**, *16*, 520-526.

13. Brown, J. M. *Oncology Res.* **1997**, *9*, 213-215.

14. Anderson, A. C. *Chem. Biol.* **2003**, *10*, 787-797.

15. Suggitt, M.; Bibby, M. C. *Clin. Cancer Res.* **2005**, *11*, 971-981.

16. Pizzorno, G.; Davis, S. J.; Hartigan, D. J.; Russello, O. *Biochem. Pharmacol*. **1994**, *47*(11), 1981-1988.

17. Agrawal, K. C.; Booth, B. A.; Michaud, R. L.; Moore, E. C.; Sartorelli, A. C. *Biochem. Pharmacol*. **1974**, *23*(17), 2421-2429.

18. Rosenberg, B.; Vancamp, L.; Krigas, T. *Nature* **1965**, *205*, 698-699.

19. Rosenberg, B.; Vancamp, L.; Trosko, J. E.; Mansour, V. H. *Nature* **1969**, *222*, 385-386.

20. McKeage, M. J.; Higgins, J. D.; Kelland, L. R. *British J. Cancer* **1991**, *64*, 788-792.

21. McKeage, M. J. *Exp. Opin. Invest. Drugs* **2005**, *14*, 1033-1046.

22. Ang, W. H.; Khalaila, I.; Allardyce, C. S.; Juillerat-Jeanneret, L.; Dyson, P. J. *J. Am. Chem. Soc.* **2005**, *127*, 1382-1383.

23. Farrell, N.; Ha, T. T. B.; Souchard, J. P.; Wimmer, F. L.; Cros, S.; Johnson, N. P. *J. Med. Chem.* **1989**, *32*, 2240-2241.

24. Farrell, N. *Cancer Invest.* **1993**, *11*, 578-589.

25. Farrell, N. *J. Inorg. Biochem.* **2001**, *86*, 45-51.

26. Farrell, N. *Met. Ions Biol. Syst.* **2004**, *42*, 251-296.

27. Alessio, E.; Mestroni, G.; Bergamo, A.; Sava, G. *Curr. Top. Med. Chem.* **2004**, *4*, 1525-1535.

28. Clarke, M. J. *Coord. Chem. Rev.* **2002**, *232*, 69-93.

29. Kratz, F.; Schutte, M. T. *Cancer J. - France* **1998**, *11*, 176-182.

30. Iwamoto, M.; Mukundan, S.; Marzilli, L. G. *J. Am. Chem. Soc.* **1994**, *116*, 6238-6244.

31. Takahara, P. M.; Frederick, C. A.; Lippard, S. J. *J. Am. Chem. Soc.* **1996**, *118*, 12309-12321.

32. Guo, M. L.; Sun, H. Z.; McArdle, H. J.; Gambling, L.; Sadler, P. J. *Biochemistry* **2000**, *39*, 10023-10033.

33. Guo, M. L.; Guo, Z. J.; Sadler, P. J. *J. Biol. Inorg. Chem.* **2001**, *6*, 698-707.

34. Caruso, F.; Rossi, M. *Met. Ions Biol. Syst.* **2004**, *42*, 353-384.

35. Chifotides, H. T.; Dunbar, K. R. *Acc. Chem. Res.* **2005**, *38*, 146-156.

36. Bear, J. L.; Gray, H. B.; Rainen, L.; Chang, I. M.; Howard, R.; Serio, G.; Kimball, A. P. *Cancer Chem. Rep. Part 1* **1975**, *59*, 611-620.

37. Erck, A.; Rainen, L.; Whileyman, J.; Chang, I. M.; Kimball, A. P.; Bear, J. *Proc. Soc. Exp. Biol. Med.* **1974**, *145*, 1278-1283.

38. Fimiani, V.; Ainis, T.; Cavallaro, A.; Piraino, P. *J. Chemother.* **1990**, *2*, 319-326.

39. Pruchnik, F.; Dus, D. *J. Inorg. Biochem.* **1996**, *61*, 55-61.

40. Esposito, B. P.; Zyngier, S. B.; De Souza, A. R.; Najjar, R. *Metal-Based Drugs* **1997**, *4*, 333-338.

41. Esposito, B. P.; Zyngier, S. B.; Najjar, R.; Paes, R. P.; Ueda, S. M. Y.; Barros, J. C. *Metal-Based Drugs* **1999**, *6*, 17-18.

42. Howard, R. A.; Sherwood, E.; Erck, A.; Kimball, A. P.; Bear, J. L. *J. Med. Chem.* **1977**, *20*, 943-946.

43. Crawford, C. A.; Matonic, J. H.; Streib, W. E.; Huffman, J. C.; Dunbar, K. R.; Christou, G. *Inorg. Chem.* **1993**, *32*, 3125-3133.

44. Crawford, C. A.; Matonic, J. H.; Huffman, J. C.; Folting, K.; Dunbar, K. R.; Christou, G. *Inorg. Chem.* **1997**, *36*, 2361-2371.

45. Perlepes, S. P.; Huffman, J. C.; Matonic, J. H.; Dunbar, K. R.; Christou, G. *J. Am. Chem. Soc.* **1991**, *113*, 2770-2771.

46. Aoki, K.; Salam, M. A. *Inorg. Chim. Acta* **2002**, *339*, 427-437.

47. Farrell, N. *J. Inorg. Biochem.* **1981**, *14*, 261-265.

48. Crawford, C. A.; Day, E. F.; Saharan, V. P.; Folting, K.; Huffman, J. C.; Dunbar, K. R.; Christou, G. *Chem. Comm.* **1996**, 1113-1114.

49. Catalan, K. V.; Mindiola, D. J.; Ward, D. L.; Dunbar, K. R. *Inorg. Chem.* **1997**, *36*, 2458-2460.

50. Catalan, K. V.; Hess, J. S.; Maloney, M. M.; Mindiola, D. J.; Ward, D. L.; Dunbar, K. R. *Inorg. Chem.* **1999**, *38*, 3904-3913.

51. Chifotides, H. T.; Koshlap, K. M.; Perez, L. M.; Dunbar, K. R. *J. Am. Chem. Soc.* **2003**, *125*, 10703-10713.

52. Chifotides, H. T.; Koshlap, K. M.; Perez, L. M.; Dunbar, K. R. *J. Am. Chem. Soc.* **2003**, *125*, 10714-10724.

53. Chifotides, H. T.; Dunbar, K. R. *Chem.-Eur. J.* **2006**, *12*, 6458-6468.

54. Asara, J. M.; Hess, J. S.; Lozada, E.; Dunbar, K. R.; Allison, J. *J. Am. Chem. Soc.* **2000**, *122*, 8-13.

55. Chifotides, H. T.; Koomen, J. M.; Kang, M. J.; Tichy, S. E.; Dunbar, K. R.; Russell, D. H. *Inorg. Chem.* **2004**, *43*, 6177-6187.

56. Dunham, S. U.; Chifotides, H. T.; Mikulski, S.; Burr, A. E.; Dunbar, K. R. *Biochemistry* **2005**, *44*, 996-1003.

57. Sorasaenee, K.; Fu, P. K. L.; Angeles-Boza, A. M.; Dunbar, K. R.; Turro, C. *Inorg. Chem.* **2003**, *42*, 1267-1271.

58. Chifotides, H. T.; Fu, P. K. L.; Dunbar, K. R.; Turro, C. *Inorg. Chem.* **2004**, *43*, 1175-1183.

59. Bradley, P. M.; Bursten, B. E.; Turro, C. *Inorg. Chem.* **2001**, *40*, 1376-1379.

60. Fu, P. K. L.; Bradley, P. M.; Turro, C. *Inorg. Chem.* **2001**, *40*, 2476-2477.

61. Lutterman, D. L.; Turro, C. Personnal communication. Department of Chemistry, Ohio State University, Columbus, Ohio.

62. Broxterman, H. J.; Georgopapadakou, N. *Drug Resist. Upd.* **2001**, *4*, 197-209.

63. Goldie, J. H. *Cancer Metast. Rev.* **2001**, *20*, 63-68.

64. Heringova, P.; Woods, J.; Mackay, F. S.; Kasparkova, J.; Sadler, P. J.; Brabec, V. *J. Med. Chem.* **2006**, *49*, 7792-7798.

65. Karukstis, K. K.; Perelman, L. A.; Wong, W. K. *Langmuir* **2002**, *18*, 10363-10371.

66. Fuertes, M. A.; Alonso, C.; Perez, J. M. *Chem. Rev.* **2003**, *103*, 645-662.

67. Cohen, S. M.; Lippard, S. J. *Prog. Nucleic Acid Res. Mol. Biol., Vol 67* **2001**, *67*, 93-130.

68. Dougherty, T. J. *Proc. Am. Assoc. Cancer Res.* **1984**, *25*, 408-410.

69. Dougherty, T. J. *Adv. Exp. Med. Biol.* **1985**, *193*, 313-328.

70. Dougherty, T. J. *Lasers Surg. Med.* **1985**, *5*, 140.

71. Dougherty, T. J. *Lasers Surg. Med.* **1988**, *8*, 177.

72. Young, S. W.; Woodburn, K. W.; Wright, M.; Mody, T. D.; Fan, Q.; Sessler, J. L.; Dow, W. C.; Miller, R. A. *Photochem. Photobiol.* **1996**, *63*, 892-897.

73. Stilts, C. E.; Nelen, M. I.; Hilmey, D. G.; Davies, S. R.; Gollnick, S. O.; Oseroff, A. R.; Gibson, S. L.; Hilf, R.; Detty, M. R. *J. Med. Chem.* **2000**, *43*, 2403-2410.

74. Sessler, J. L.; Mallouk, T. E.; Maiya, B. G.; Hemmi, G.; Harriman, A. *Abstracts of Papers of the American Chemical Society* **1989**, *197*, 248-ORGN.

75. Kessel, D.; Dougherty, T. J. *Rev. Cont. Pharm.* **1999**, *10*, 19-24.

76. Ho, Y. K.; Missert, J. R.; Dougherty, T. J. *Photochem. Photobiol.* **1991**, *54*, 83-87.

77. Dougherty, T. J. *Clin. Chest Med.* **1985**, *6*, 219-236.

78. Dougherty, T. J. *Sem. Surg. Onc.* **1989**, *5*, 6-16.

79. Derosa, M. C.; Crutchley, R. J. *Coord. Chem. Rev.* **2002**, *233*, 351-371.

80. Friedman, A. E.; Chambron, J. C.; Sauvage, J. P.; Turro, N. J.; Barton, J. K. *J. Am. Chem. Soc.* **1990**, *112*, 4960-4962.

81. Holmlin, R. E.; Dandliker, P. J.; Barton, J. K. *Angew. Chem.-Int. Ed.* **1997**, *36*, 2715-2730.

82. Mcmillin, D. R.; Liu, F.; Meadows, K. A.; Aldridge, T. K.; Hudson, B. P. *Coord. Chem. Rev.* **1994**, *132*, 105-112.

83. Olson, E. J. C.; Hu, D.; Hormann, A.; Jonkman, A. M.; Arkin, M. R.; Stemp, E. D. A.; Barton, J. K.; Barbara, P. F. *J. Am. Chem. Soc.* **1997**, *119*, 11458-11467.

84. Stoeffler, H. D.; Thornton, N. B.; Temkin, S. L.; Schanze, K. S. *J. Am. Chem. Soc.* **1995**, *117*, 7119-7128.

85. Turro, C.; Bossmann, S. H.; Jenkins, Y.; Barton, J. K.; Turro, N. J. *J. Am. Chem. Soc.* **1995**, *117*, 9026-9032.

86. Copeland, K. D.; Lueras, A. M. K.; Stemp, E. D. A.; Barton, J. K. *Biochemistry* **2002**, *41*, 12785-12797.

87. Peyratout, C. S.; Aldridge, T. K.; Crites, D. K.; Mcmillin, D. R. *Inorg. Chem.* **1995**, *34*, 4484-4489.

88. Turro, N. J.; Barton, J. K. *J. Biol. Inorg. Chem.* **1998**, *3*, 201-209.

89. Lewis, F. D.; Wu, T. F.; Zhang, Y. F.; Letsinger, R. L.; Greenfield, S. R.; Wasielewski, M. R. *Science* **1997**, *277*, 673-676.

90. Delaney, S.; Pascaly, M.; Bhattacharya, P. K.; Han, K.; Barton, J. K. *Inorg. Chem.* **2002**, *41*, 1966-1974.

91. Brauns, E. B.; Murphy, C. J.; Berg, M. A. *J. Am. Chem. Soc.* **1998**, *120*, 2449-2456.

92. Brauns, E. B.; Madaras, M. L.; Coleman, R. S.; Murphy, C. J.; Berg, M. A. *Phys. Rev. Lett.* **2002**, *88*, 158101-158104.

93. Gearheart, L. A.; Somoza, M. M.; Rivers, W. E.; Murphy, C. J.; Coleman, R. S.; Berg, M. A. *J. Am. Chem. Soc.* **2003**, *125*, 11812-11813.

94. Kang, J. S.; Lakowicz, J. R.; Piszczek, G. *Arch. Pharm. Res.* **2002**, *25*, 143-150.

95. Fu, P. K. L.; Bradley, P. M.; van Loyen, D.; Durr, H.; Bossmann, S. H.; Turro, C. *Inorg. Chem.* **2002**, *41*, 3808-3810.

96. Thomas, A. M.; Neelakanta, G.; Mahadevan, S.; Nethaji, M.; Chakravarty, A. R. *Eur. J. Inorg. Chem.* **2002**, 2720-2726.

97. Dhar, S.; Reddy, P. A. N.; Nethaji, M.; Mahadevan, S.; Saha, M. K.; Chakravarty, A. R. *Inorg. Chem.* **2002**, *41*, 3469-3476.

98. Collins, J. G.; Aldrich-Wright, J. R.; Greguric, I. D.; Pellegrini, P. A. *Inorg. Chem.* **1999**, *38*, 5502-5509.

99. Arounaguiri, S.; Maiya, B. G. *Inorg. Chem.* **1996**, *35*, 4267-4272.

100. Mcfadyen, W. D.; Wakelin, L. P. G.; Roos, I. A. G.; Hillcoat, B. L. *Biochem. J.* **1987**, *242*, 177-183.

101. Onfelt, B.; Lincoln, P.; Norden, B. *J. Am. Chem. Soc.* **1999**, *121*, 10846-10847.

102. Breiner, K. M.; Daugherty, M. A.; Oas, T. G.; Thorp, H. H. *J. Am. Chem. Soc.* **1995**, *117*, 11673-11679.

103. Kalsbeck, W. A.; Gingell, D. M.; Malinsky, J. E.; Thorp, H. H. *Inorg. Chem.* **1994**, *33*, 3313-3316.

104. Carter, P. J.; Breiner, K. M.; Thorp, H. H. *Biochemistry* **1998**, *37*, 13736-13743.

105. Winkhaus, G.; Ziegler, P. *Z. Anorg. Allg. Chem.* **1967**, *350*, 51-57.

106. Dickeson, J. E.; Summers, L. A. *Aust. J. Chem.* **1970**, *23*, 1023-1027.

107. Nair, R. B.; Cullum, B. M.; Murphy, C. J. *Inorg. Chem.* **1997**, *36*, 962-965.

108. Pyle, A. M.; Rehmann, J. P.; Meshoyrer, R.; Kumar, C. V.; Turro, N. J.; Barton, J. K. *J. Am. Chem. Soc.* **1989**, *111*, 3051-3058.

109. Peterson, G. L. *Anal. Biochem.* **1977**, *83*, 346-356.

110. *SAINT*, version 6.34; Bruker AXS Inc.: Madison, WI, 2001.

111. *SADABS*, version 2.03; Bruker AXS Inc.: Madison, WI, 2002.

112. Barbour, L. J. *J. Supra. Chem.* **2007**, *1*, 189-191.

113. Sheldrik, G. M. *SHELX, Programs for Solving and Refining Crystal Structures*; University of Göttingen: Göttingen, Germany, 2007.

114. Kornhauser, A.; Wamer, W. G.; Lambert, L. A. In *Dermatotoxicology*; Marzulli, F. N.; Maibach, H. I., Eds.; Taylor and Francis: Washington, DC, 2002; pp 189-230.

115. Chambron, J. C.; Sauvage, J. P.; Amouyal, E.; Koffi, P. *Nouveau Journal de Chimie-New Journal of Chemistry* **1985**, *9*, 527-529.

116. Liu, J. G.; Zhang, Q. L.; Shi, X. F.; Ji, L. N. *Inorg. Chem.* **2001**, *40*, 5045.

117. Calligaris, M.; Campana, L.; Mestroni, G.; Tornatore, M.; Alessio, E. *Inorg Chim Acta* **1987**, *127*, 103-112.

118. Hunter, C. A.; Sanders, J. K. M. *J. Am. Chem. Soc.* **1990**, *112*, 5525-5534.

119. Nair, R. B.; Teng, E. S.; Kirkland, S. L.; Murphy, C. J. *Inorg. Chem.* **1998**, *37*, 139-141.

120. Felthouse, T. R. *Prog. Inorg. Chem.* **1982**, *29*, 73-166.

121. Miskowski, V. M.; Dallinger, R. F.; Christoph, G. G.; Morris, D. E.; Spies, G. H.; Woodruff, W. H. *Inorg. Chem.* **1987**, *26*, 2127-2132.

122. Jones, G.; Vullev, V. I. *J. Phys. Chem. A* **2001**, *105*, 6402-6406.

123. Bilakhiya, A. K.; Tyagi, B.; Paul, P.; Natarajan, P. *Inorg. Chem.* **2002**, *41*, 3830-3842.

124. Jockusch, S.; Turro, N. J.; Tomalia, D. A. *Macromol.* **1995**, *28*, 7416-7418.

125. Slavnova, T. D.; Chibisov, A. K.; Gorner, H. *J. Phys. Chem. A* **2002**, *106*, 10985-10990.

126. Wang, M. M.; Dilek, I.; Armitage, B. A. *Langmuir* **2003**, *19*, 6449-6455.

127. Wang, M. M.; Silva, G. L.; Armitage, B. A. *J. Am. Chem. Soc.* **2000**, *122*, 9977-9986.

128. Kang, M.; Chouai, A.; Chifotides, H. T.; Dunbar, K. R. *Angew. Chem.-Int. Ed.* **2006**, *45*, 6148-6151.

129. Fu, P. K. L.; Bradley, P. M.; Turro, C. *Inorg. Chem.* **2003**, *42*, 878-884.

130. Suh, D.; Oh, Y. K.; Chaires, J. B. *Proc. Biochem.* **2001**, *37*, 521-525.

131. Paoletti, C.; Lepecq, J. B.; Lehman, I. R. *J. Mol. Biol.* **1971**, *55*, 75-84.

132. Tang, T. C.; Huang, H. J. *Electroanal.* **1999**, *11*, 1185-1190.

133. Sitlani, A.; Long, E. C.; Pyle, A. M.; Barton, J. K. *J. Am. Chem. Soc.* **1992**, *114*, 2303-2312.

134. Brennaman, M. K.; Alstrum-Acevedo, J. H.; Fleming, C. N.; Jang, P.; Meyer, T. J.; Papanikolas, J. M. *J. Am. Chem. Soc.* **2002**, *124*, 15094-15098.

135. Dyer, J.; Blau, W. J.; Coates, C. G.; Creely, C. M.; Gavey, J. D.; George, M. W.; Grills, D. C.; Hudson, S.; Kelly, J. M.; Matousek, P.; McGarvey, J. J.; McMaster, J.; Parker, A. W.; Towrie, M.; Weinstein, J. A. *Photochem. Photobiol. Sc.* **2003**, *2*, 542-554.

136. Pourtois, G.; Beljonne, D.; Moucheron, C.; Schumm, S.; Kirsch-De Mesmaeker, A.; Lazzaroni, R.; Bredas, J. L. *J. Am. Chem. Soc.* **2004**, *126*, 683-692.

137. Cervantes, G.; Marchal, S.; Prieto, M. J.; Perez, J. M.; Gonzalez, V. M.; Alonso, C.; Moreno, V. *J. Inorg. Biochem.* **1999**, *77*, 197-203.

138. Featherstone, J.; Dykes, P. J.; Marks, R. *Skin Pharm.* **1991**, *4*, 169-174.

139. Sandman, K. E.; Fuhrmann, P.; Lippard, S. J. *J. Biol. Inorg. Chem.* **1998**, *3*, 74-80.

140. Gharehbaghi, K.; Szekeres, T.; Yalowitz, J. A.; Fritzer-Szekeres, M.; Pommier, Y. G.; Jayaram, H. N. *Life Sc.* **2000**, *68*, 1-11.

141. Quiroga, A. G.; Ranninger, C. N. *Coord. Chem. Rev.* **2004**, *248*, 119-133.

142. Bear, J. L.; Gray, H. B., Jr.; Rainen, L.; Chang, I. M.; Howard, R. A.; Serio, G.; Kimball, A. P. *Cancer Chem. Rep., Part 1* **1975**, *59*(3), 611-20.

143. Howard, R. A.; Spring, T. G.; Bear, J. L. *Cancer Res.* **1976**, *36*(12), 4402-4405.

144. Das, K.; Bear, J. L. *Inorg. Chem.* **1976**, *15*(9), 2093-2095.

145. Sorasaenee, K.; Galan-Mascaros, J. R.; Dunbar, K. R. *Inorg. Chem.* **2002**, *41*(2), 433-436.

146. Sorasaenee, K.; Galan-Mascaros, J. R.; Dunbar, K. R. *Inorg. Chem.* **2003**, *42*(3), 661-663.

147. Chin T. A.; Templeton D. M. *Toxicol.* **1993**, *77*(1-2), 145-156.

148. Reedijk, J. *Chem. Rev.* **1999**, *99*, 2511.

149. Zak F.; Turanek J.; Kroutil A.; Sova P.; Mistr A; Poulova A.; Mikolin P.; Zak Z.; Kasna A.; Zaluska D.; Neca J.; Sindlerova L.; Kozubik A. *J. Med. Chem.* **2004**, *47*(3), 761-763.

150. Christoph G. G.; Tolbert, M. *ACA* **1980**, Ser. 2, *7*, 39.

151. Hess, J. H. M. Sc. Thesis, Michigan State University, 1998.

152. Frisch, M. J.; Trucks, G. W.; Schlegel, H. B.; Scuseria, G. E.; Robb, M. A.; Cheeseman, J. R.; Zakrzewski, V. G.; Montgomery, J. A.; Stratmann, R. E.; Burant, J. C.; Dapprich, S.; Millam, J. M.; Daniels, A. D.; Kudin, K. N.; Strain, M. C.; Farkas, O.; Tomasi, J.; Barone, V.; Cossi, M.; Cammi, R.; Mennucci, B.; Pomelli, C.; Adamo, C.; Clifford, S.; Ochterski, J.; Petersson, G. A.; Ayala, P. Y.; Cui, Q.; Morokuma, K.; Malick, D. K.; Rabuck, A. D.; Raghavachari, K.; Foresman, J. B.; Cioslowski, J.; Ortiz, J. V.; Stefanov, B. B.; Liu, G.; Liashenko, A.; Piskorz, P.; Komaromi, I.; Gomperts, R.; Martin, R. L.; Fox, D. J.; Keith, T.; Al-Laham, M. A.; Peng, C. Y.; Nanayakkara, A.; Gonzalez, C.; Challacombe, M.; Gill, P. M. W.; Johnson, B. G.; Chen, W.; Wong, M. W.; Andres, J. L.; Head-Gordon, M.; Replogle, E. S.; Pople J. A. *Gaussian 98*, revision A.7; Gaussian, Inc.: Pittsburgh, PA, 1998.

153. Becke, A. D. *J. Chem. Phys*. **1993**, *98*, 5648-5652.

154. Lee, C.; Yang, W.; Parr, R. G. *Phys. Rev. B* **1988**, *37*, 785.

155. Andrae, D.; Häussermann, U.; Dolg, M.; Stoll, H.; Preuss, H. *Theor. Chim. Acta* **1990**, *77*, 123-141.

156. Cossi, M.; Barone, V.; Cammi, R.; Tomasi, J. *Chem. Phys. Lett.* **1996**, *255*, 327-335.

157. Miertus, S.; Scrocco, E.; Tomasi, J. *Chem. Phys.* **1981**, *55*, 117-129.

158. Speit, G.; Hartmann, A. In *Methods Molecular Biology; DNA Repairs Protocols*; Henderson, D. S., Ed.; Humana Press: New York, 1999;Vol. 113, pp 203-212.

159. Pruchnik, F. P.; Jakimowicz, P.; Ciunik, Z.; Stanislawek, K.; Oro, L. A.; Tejel, C.; Ciriano, M. A. *Inorg. Chem. Comm.* **2001**, 4(1), 19-22.

160. Pruchnik, F. P.; Jakimowicz, P.; Ciunik, Z. *Inorg. Chem. Comm.* **2001**, 4(12), 726-729.

161. Pruchnik, Florian P.; Jutarska, Anna; Ciunik, Zbigniew; Pruchnik, Miroslaw. *Inorg. Chim. Acta* **2004**, 357(10), 3019-3026.

162. Bear, J. L.; Chau, L. K.; Chavan, M. Y.; Lefoulon, F.; Thummel, R. P.; Kadish, K. M. *Inorg. Chem.* **1986**, 25(10), 1516-1518.

163. Norman, J. G. Jr.; Kolari, H. J. *J. Am. Chem. Soc.* **1978**, *100*, 791.

164. Cotton, F. A.; Walton, R. A. *In Multiple Bonds Between Metal Atoms*; Wiley-Interscience: New York, 1982.

165. Natkaniec, Leszek; Pruchnik, Florian P. *J. Chem. Soc., Dalton Trans.* **1994**, (22), 3261-3266.

166. Fairbairn, D. W.; Olive, P. L.; O'Neill, K. L. *Mutat. Res.* **1995**, *339*, 37.

167. Rojas, E.; Lopez, M. C.; Valverde, M. *J. Chromatogr., B: Biomed. Sci. Appl.* **1999**, *722*, 225.

168. Chiba, K.; Yoshizawa, K.; Makino, I.; Kawakami, K.; Onoue, M. *J. Biochem. Mol. Tox.* **2001**, 15, 150-158.

169. Egyeki, M.; Tóth, K.; Waldeck, W.; Schmezer, P.; Langowski, J.; Csík, G. *J. Photochem. Photobiol.: B Biology* **2006**, 84, 119-127.

170. Barnes, K. R.; Lippard, S. J. *Metal Ions in Biological Systems* **2004**, 42, 143-177.

171. Wang, D.; Lippard, S. J. *Nature Rev. Drug Discovery* **2005**, 4(4), 307-320.

172. Torchilin, V. P.; Trubetskoy, V. S.; Wolf, G. L. *Handbook of Targeted Delivery of Imaging Agents* **1995**, 403-413.

173. Arbab, A. S.; Liu, W.; Frank, J. A. *Exp. Rev. Med. Dev.* **2006**, 3(4), 427-439.

174. Bottrill, Melanie; Kwok, Lilian; Long, Nicholas J. *Chem. Soc. Rev.* **2006**, 35(6), 557-571.

175. Caravan, Peter. *Chem. Soc. Rev.* **2006**, 35(6), 512-523.

176. Zhang, C. X.; Lippard, S. J. *Curr. Opin. Chem. Biol.* **2003**, 7(4), 481-489.

177. Lippard, S. J. *Nature Chem. Biol.***2006**, 2(10), 504-507.

178. Farver, O. In *Textbook of Drug Design and Discovery* (3rd Edition); Taylor & Francis Ltd.: London, 2002; pp. 364-409.

179. Guo, Z.; Sadler, P. J. *Angew. Chem., Int. Ed.* **1999**, 38(11), 1512-1531.

180. Yam, V. W.-W.; Lo, K. K.-W.; Cheung, K.-K.; Kong, R. Y.-C. *J. Chem. Soc., Chem. Comm.* **1995**, 11, 1191-1193.

181. *CRC Handbook of Chemistry and Physics*, 81st ed.; Lide, D. R., Ed.; CRC Press: New York, 2001; Chapter 8, pp 46-47.

182. Reedijk, J. *Proc. Natl. Acad. Sci. U.S.A.* **2003**, 100(7), 3611-3616.

183. McAuliffe, C. A.; Sharma, H. L.; Tinker, N. D. *Cancer Chemotherapy Involving Platinum and Other Platinum Group Complexes*; 1991; Chapter 16, pp 546-593.

184. Monti, E.; Gariboldi, M.; Maiocchi, A.; Marengo, E.; Cassino, C.; Gabano, E.; Osella, D. *J. Med. Chem.* **2005**, 48(3), 857-866.

185. Macquet, J. P.; Butour, J. L. *J. Natl. Cancer Inst.* **1983**, 70(5), 899-905.

186. Cleare, M. J.; Hoeschele, J. D. *Bioinorg. Chem.* **1973**, 2(3), 187-210.

187. Farrell, N.; Kiley, D. M.; Schmidt, W.; Hacker, M. P. *Inorg. Chem.* **1990**, 29(3), 397-403.

188. Chifotides, H. T.; Hess, J. S.; Angeles-Boza, A. M.; Galán-Mascarós, J. R.; Sorasaenee, K.; Dunbar, K. R. *Dalton Transactions* **2003**, 4426-4430.

189. Daniels, M. A. M.; Mehmet, N.; Tocher, D. A. *J. Chem. Soc. Dalton Trans.* **1991**, 2601-2606.

190. Wilson, C.R.; Taube, H. *Inorg. Chem.* **1975**, 14, 405-411.

191. Roos, G. H. P.; McKervey, M. A. *Synth. Comm.* **1992**, 22(12), 1751-1756.

192. Bear, J. L.; Lifsey, R. S.; Chau, L. K.; Ahsan, M. Q.; Korp, J. D.; Chavan, M.; Kadish, K. M. *J. Chem. Soc., Dalton Trans.* **1989**, 93-100.

193. Pasternak, H.; Pruchnik, F. P. *Inorg. Nucl. Chem. Lett.* **1976**, 12, 591-598.

194. Turro, C. personal communication. Department of Chemistry, Ohio State University, Columbus, Ohio.

# VITA

Alfredo Milton Angeles Boza received his Bachelor of Sciences degree in chemistry from the Pontificia Universidad Católica del Perú in 2000. He took a position as an Inorganic Chemistry Instructor at the Universidad Peruana Cayetano Heredia, where he lectured for two semesters. He entered the Ph. D. program at Texas A&M University, where he joined the group directed by Prof. Dunbar, in January 2002. His research interests include the medicinal uses of compounds, in particular metal complexes as well as the photochemistry of molecules.

Mr. Angeles Boza may be reached at Matute Chalet 40-I, La Victoria (Lima13), Lima, Peru. His e-mail address is alfredo.angeles@gmail.com.